Master's Thesis

Characterization of Activator-dependent Differences in Platelet-derived Extracellular Vesicle Populations

Johanna M M Puutio

June 2020

Supervised by Docent Pia Siljander and Dr. Mari Palviainen

MASTERS PROGRAMME FOR GENETICS AND MOLECULAR BIOSCIENCES
FACULTY OF BIOLOGICAL AND ENVIRONMENTAL SCIENCES

HELSINGIN YLIOPISTO
HELSINGFORS UNIVERSITET
UNIVERSITY OF HELSINKI

Tiedekunta – Fakultet – Faculty Faculty of Biological and Environmental Sciences		Koulutusohjelma – Utbildingsprogram – Degree Programme Master's Programme in Genetics and Molecular Biosciences
Tekijä – Författare – Author Johanna Puutio		
Työn nimi – Arbetets titel – Title Characterization of activator-dependent differences in platelet-derived extracellular vesicle populations		
Oppiaine/Opintosuunta – Läroämne/Studieinriktning – Subject/Study track Molecular and Analytical Health Biosciences		
Työn laji – Arbetets art – Level Pro Gradu / Master's thesis	Aika – Datum – Month and year June 2020	Sivumäärä – Sidoantal – Number of pages 71

Tiivistelmä – Referat – Abstract

Extracellular vesicles (EVs) are phospholipid bilayer-enclosed nanoparticles that are secreted by eukaryotic and prokaryotic cells. EVs carry macromolecules and signalling molecules to adjacent cells and play an important role in intercellular communication under both pathologic and homeostatic conditions. Therefore, they have become of significant interest for their therapeutic, diagnostic and prognostic potential. EVs are small and highly heterogeneous in size, shape, cargo and membrane composition, posing several challenges for establishing analytical and clinical guidelines. Therefore, EV research requires standardized and robust methods for their separation and characterization.

In this study physical and immunochemical methods were employed to characterize human platelet-derived EVs (pEVs) generated from platelets activated with different external biochemical stimuli. The platelet-activating effect of the pro-inflammatory S100A8/A9 protein complex and a combination of thrombin and collagen were studied with nano flow cytometry. The size distribution of pEVs was studied with nanoparticle tracking analysis (NTA) and asymmetrical flow field-flow fractionation (AF4), which represents a newly emerging method on the EV field. Finally, fluorescent labelling and co-localization analysis were employed to characterize membrane marker composition of pEVs and assess its usefulness as an analytic tool for EV research.

We succeeded in providing new hints towards meaningful discoveries in platelet biology by characterizing the way platelets respond to inflammatory and hemostatic signals by shedding pEVs. When platelet activation markers are characterized with flow cytometry, the S100A8/A9 protein appeared to cause a shift in membrane activation markers when compared to the thrombin-collagen mix and the baseline control. Increased TLT-1 translocation and decreased integrin αIIbβ3 expression on pEV surfaces suggests that S100A8/A9 induced pEV secretion through differently packed platelet α-granules, rather than from the plasma membrane. An increase in TLT-1 expression compared to decreased P-selectin and αIIbβ3 suggests that S100A8/A9 stimulation shifts platelet phenotype towards secretion rather than aggregation. A protocol for small pEV separation with AF4-MALS was set up. With this method, subtle differences between small pEV populations were seen that were not distinguishable with NTA or flow cytometry. When investigated with AF4-MALS, S100A8/A9 induced pEVs appeared larger than those produced with thrombin-collagen activation. The mean particle sizes of the pEV populations obtained from activated platelets were generally also larger than those produced without an activator.

We tested novel methods to detect subtle differences in small EV population sizes that are easily missed with conventional methods due to their technical limitations. A well-optimised AF4 protocol can detect different pEV subpopulations and is a promising tool for EV. In the future, when AF4 is combined with a MALS detector and a fraction collector, nanoimaging of fluorescently labelled EVs could be combined with it as a downstream application to obtain information on their versatile biological functions.

Avainsanat – Nyckelord – Keywords
extracellular vesicles, platelets, platelet-derived extracellular vesicles, α-granules, S100A8/A9, nanoparticle tracking analysis, NTA, flow cytometry, nanoimaging, asymmetrical flow field-flow fractionation, AF4

Ohjaaja tai ohjaajat – Handledare – Supervisor or supervisors
Pia Siljander, Mari Palviainen

Säilytyspaikka – Förvaringställe – Where deposited

Helsingin yliopiston kirjasto, Helsingfors universitets bibliotek, Helsinki University Library

Muita tietoja – Övriga uppgifter – Additional information

HELSINGIN YLIOPISTO
HELSINGFORS UNIVERSITET
UNIVERSITY OF HELSINKI

Tiedekunta – Fakultet – Faculty	Koulutusohjelma – Utbildingsprogram – Degree Programme	
Bio ja Ympäristötieteellinen Tiedekunta	Genetiikan ja molekulaaristen biotieteiden maisteriohjelma	
Tekijä – Författare – Author Johanna Puutio		
Työn nimi – Arbetets titel – Title Verihiutaleperäisten solunulkoisten vesikkelipopulaatioiden aktivaattoririippuvaisten erojen karakterisointi		
Oppiaine/Opintosuunta – Läroämne/Studieinriktning – Subject/Study track Molekulaaristen ja analyyttisten terveyden biotieteiden opintosuunta		
Työn laji – Arbetets art – Level Pro Gradu -tutkielma	Aika – Datum – Month and year Kesäkuu 2020	Sivumäärä – Sidoantal – Number of pages 71

Tiivistelmä – Referat – Abstract

Solunulkoiset vesikkelit (Eng: extracellular vesicles, EV:s) ovat fosfolipimembraanin rajaamia nanopartikkeleja, joita erittävät eukaryootit ja prokaryootit. Solunulkoiset vesikkelit kantavat sisällään makromolekyylejä ja singalointimolekyylejä muihin soluihin, toimien näin tärkeinä solujen välisen kommunikaation välittäjinä sekä patologisissa että homeostaattisissa oloissa. Vesikkelit ovat lisäksi hyvin kiinnostavia niiden sovellusmahdollisuuksien vuoksi diagnostiikassa ja terapeuttisissa sovelluksissa. Solunulkoiset vesikkelit ovat pieniä ja heterogeenisiä kokonsa, sisältönsä sekä solukalvon koostumuksen puolesta. Tämän vuoksi niiden karakterisoinnissa sekä eristyksessä on yhä huomattavia haasteita, eikä selkeitä analyyttisiä ja kliinisiä ohjeistuksia ole kyetty muodostamaan. Tämän vuoksi vesikkelitutkimus kaipaa kipeästi standardoituja ja luotettavia menetelmiä niiden erotteluun ja karakterisointiin.

Tässä tutkielmassa fysikaalisia ja immunokemiallisia menetelmiä sovellettiin verihiutaleperäisten EV-populaatioiden tarkasteluun. Verihiutalevesikkelit tuotettiin aktivoimalla niitä erilaisilla biokemiallisilla aktivaatiosignaaleilla. Ihmisten verihiutaleita aktivoitiin trombiinilla ja kollageenilla, sekä kalsiumionoforilla. Uutena verihiutaleaktivaattorina tutkimukseen otettiin mukaan tulehdusreaktiota kiihdyttävä S100A8/A9 -proteiinikompleksi. Aktivaattorien vaikutusta verihiutaleisiin sekä niiden erittämiin vesikkeleihin tutkittiin nanovirtaussytometrialla. Tuottuneiden vesikkelien kokojakaumaa arvioitiin nanopartikkelien jäljitysanalyysillä (Eng: nanoparticle tracking analysis, NTA) sekä asymmetrisellä poikittaisvirtauskenttävirtausfraktioinnilla (Eng: asymmetric flow field-flow fractionation, AF4), joka on uusi menetelmä vesikkelitutkimuksessa. Viimeiseksi vesikkelien solukalvomarkkereita tarkasteltiin uudella nanopartikkelien kuvantamismenetelmällä, joka perustuu fluoresoivien leimojen lokalisaatioon vesikkelin kalvolla ja jonka hyödyllisyyttä vesikkelitutkimuksessa haluttiin arvioida.

Onnistuimme tuottamaan uusia vihjeitä tavoista, joilla verihiutaleet reagoivat solunulkoisiin tulehdus- ja kudosvauriosignaaleihin vesikkelien erityksen kautta. Kun verihiutaleiden aktivointimarkkereita tarkasteltiin virtaussytometrialla, S100A8/A9 proteiini aiheutti muutoksen kalvomarkkeriproteiinien jakautumisessa verihiutaleiden ja verihiutalevesikkelien pinnalla verrattuna trombiini-kollageeniaktivaatioon sekä aktivoimattomaan kontrolliin. Lisääntynyt TLT-1 markkerin pitoisuus yhdessä alentuneen integriini αIIbβ3-ekspression kanssa viittaa ilmiöön, jossa S100A8/A9 olisi saanut verihiutaleet tuottamaan vesikkelejä eri tavoin pakatuista α-jyväsistä, sen sijaan että niitä erittyisi suoraan verihiutaleen solukalvolta. TLT-1 ekspression kasvu verrattuna P-selektiinimarkkerin laskuun verihiutalevesikkelien pinnalla saattaa johtua S100A8/A9:n aiheuttamasta muutoksesta, jossa verihiutale erikoistuu aktivoituessaan vesikkelieritykseen aggregaation sijaan.

AF4 paljasti hienovaraisia, eri aktivaattoreiden aiheuttamia eroja verihiutalevesikkelien kokojakaumissa, joita ei kyetty erottamaan yhtä tarkasti jäljitysanalyysillä tai virtaussytometrialla. AF4-menetelmä optimoitiin pienten verihiutalevesikkelien tutkimukseen. Kun verihiutalevesikkelejä tarkasteltiin MALS-detektorilla, verihiutaleaktivaatio S100A8/A9-proteiinilla tuotti suurempia vesikkelejä, kuin trombiinilla ja kollageenilla aktivoidut verihiutaleet. AF4 on hellä ja monipuolinen menetelmä, jolla voidaan erotella verihiutalevesikkelien alapopulaatioita hyvin tarkasti ja on näin ollen erittäin lupaava menetelmä vesikkelien karakterisointiin ja fraktiointiin. Tulevaisuudessa AF4-MALS –menetelmä voitaisiin yhdistää fraktionkeräimeen, jolloin erotellut vesikkelipopulaatiot voidaan kerätä jatkokäsittelyä varten. Eräs jatkokäsittelymenetelmä voi tulevaisuudessa olla hyvin optimoitu nanokuvantaminen. Nämä menetelmät yhdistämällä saadaan tarkkaa tietoa vesikkelien monimuotoisista biologisista ominaisuuksista.

Avainsanat – Nyckelord – Keywords
solunulkoiset vesikkelit, verihiutaleet, verihiutalevesikkelit, α-jyväset, S100A8/A9, nanopartikkelien jäljitysanalyysi, NTA, virtaussytometria, asymmetrinen poikittaisvirtauskenttävirtausfraktiointi, AF4

Ohjaaja tai ohjaajat – Handledare – Supervisor or supervisors
Pia Siljander, Mari Palviainen

Säilytyspaikka – Förvaringställe – Where deposited

Helsingin yliopiston kirjasto, Helsingfors universitets bibliotek, Helsinki University Library

Muita tietoja – Övriga uppgifter – Additional information

ABSTRACT

Extracellular vesicles (EVs) are phospholipid bilayer-enclosed nanoparticles that are secreted by eukaryotic and prokaryotic cells. EVs carry macromolecules and signalling molecules to adjacent cells and play an important role in intercellular communication under both pathologic and homeostatic conditions. Therefore, they have become of significant interest for their therapeutic, diagnostic and prognostic potential. EVs are small and highly heterogeneous in size, shape, cargo and membrane composition, posing several challenges for establishing analytical and clinical guidelines. Therefore, EV research requires standardized and robust methods for their separation and characterization.

In this study physical and immunochemical methods were employed to characterize human platelet-derived EVs (pEVs) generated from platelets activated with different external biochemical stimuli. The platelet-activating effect of the pro-inflammatory S100A8/A9 protein complex and a combination of thrombin and collagen were studied with nano flow cytometry. The size distribution of pEVs was studied with nanoparticle tracking analysis (NTA) and asymmetrical flow field-flow fractionation (AF4), which represents a newly emerging method on the EV field. Finally, fluorescent labelling and co-localization analysis were employed to characterize membrane marker composition of pEVs and assess its usefulness as an analytic tool for EV research.

We succeeded in providing new hints towards meaningful discoveries in platelet biology by characterizing the way platelets respond to inflammatory and hemostatic signals by shedding pEVs. When platelet activation markers are characterized with flow cytometry, the S100A8/A9 protein appeared to cause a shift in membrane activation markers when compared to the thrombin-collagen mix and the baseline control. Increased TLT-1 translocation and decreased integrin αIIbβ3 expression on pEV surfaces suggests that S100A8/A9 induced pEV secretion through differently packed platelet α-granules, rather than from the plasma membrane. An increase in TLT-1 expression compared to decreased P-selectin and αIIbβ3 suggests that S100A8/A9 stimulation shifts platelet phenotype towards secretion rather than aggregation. A protocol for small pEV separation with AF4-MALS was set up. With this method, subtle differences between small pEV populations were seen that were not distinguishable with NTA or flow cytometry. When investigated with AF4-MALS, S100A8/A9 induced pEVs appeared larger than those produced with thrombin-collagen activation. The mean particle sizes of the pEV populations obtained from activated platelets were generally also larger than those produced without an activator.

We tested novel methods to detect subtle differences in small EV population sizes that are easily missed with conventional methods due to their technical limitations. A well-optimised AF4 protocol can detect different pEV subpopulations and is a promising tool for EV. In the future, when AF4 is combined with a MALS detector and a fraction collector, nanoimaging of fluorescently labelled EVs could be combined with it as a downstream application to obtain information on their versatile biological functions.

TABLE OF CONTENTS

ABBREVIATIONS

AF4	Asymmetrical flow field-flow fractionation
ACD	Acid citrate dextrose
BSA	Bovine serum albumin
CMRD	Cell mask deep red
DLS	Dynamic light scattering
DPBS	Dulbecco's phosphate buffered saline
ELISA	Enzyme-linked immunosorbent assay
EM	Electron microscopy
EV	Extracellular vesicle
FACS	Fluorescence-activated cell sorting
FITC	Fluorescein isothiocyanate
GP	Glycoprotein
IEX	Ion exchange
IPTG	Isopropyl β-D-1-thiogalactopyranoside
ISEV	International Society for Extracellular Vesicles
MALS	Multi-angle light scattering
miRNA	micro-RNA
MISEV	Minimal Information for Studies of Extracellular Vesicles
mRNA	messenger-RNA
MVB	Multivesicular body
MWCO	Molecular weight cut-off
NMR	Nuclear magnetic resonance
NTA	Nanoparticle tracking analysis
PAGE	Polyacrylamide gel electrophoresis
PBS	Phosphate buffered saline
PCR	Polymerase chain reaction
PE	Phycoerythrin
PEI	Polyethylenimin
pEV	Platelet-derived extracellular vesicle
PGE1	Prostaglandin E1
PS	Phosphatidylserine
R_g	Radius of gyration
R_h	Hydrodynamic radius
RI	Refractive index
R_r	Geometric radius
SDS	Sodium dodecyl sulphate
SEC	Size exclusion chromatography
STORM	Stochastic optical reconstruction microscopy

TC	Thrombin and collagen
TEM	Transmission electron microscopy
THB	Tyrode's Hepes buffer
TLR	Toll-like receptor
TLT-1	TREM-like transcript-1-like transcript
TREM	Triggering receptor expressed on myeloid cells
UC	Ultracentrifugation
V_c	Crossflow
V_{out}	Channel flow

1. INTRODUCTION

1.1 Extracellular vesicles

Extracellular vesicles (EVs) are small, membrane-enclosed particles consisting of a lipid bilayer membrane and they are secreted by both eukaryotes and prokaryotes (Yáñez-Mó et al., 2015). The International Society for Extracellular Vesicles (ISEV) defines EVs as "*particles naturally released from cells that are delimited by a lipid bilayer and cannot replicate*" (Théry *et al.,* 2018). In humans, they are found in plasma, serum, urine, feces, saliva, amniotic and cerebrospinal fluid, semen, and breast milk (Yáñez-Mó et al., 2015). EVs are able to influence the function of their recipient cells upon releasing their cargo. This takes place through receptor-mediated endocytosis, phagocytosis or direct fusion (Raposo & Sahl, 2019), serving as a fourth strategy for cellular communication in addition to the classical autocrine, paracrine and endocrine signaling (Yáñez-Mó et al., 2015, Raposo & Sahl, 2019). EVs have shown to be able to carry and transfer signaling molecules such as proteins, nucleic acids, sugars and lipid mediators between the parent cell and an adjacent recipient cell (Raposo & Sahl, 2019). The packing of molecular cargo into EVs is not a random process, and reflects the pathophysiological state of the mother cell (Yáñez-Mó et al., 2015). Consequently, they play a role in physiological processes under both homeostatic and pathological conditions. EVs have the ability to alter the function of the recipient cell in the long term by introducing mRNA, miRNA and siRNA strands to their targets (Momen-Heravi *et al.,* 2019). This suggests that EVs can not only affect short term events such as receptor-mediated signaling, protein production and transcription events, but also permanently alter the way certain genes are interpreted within the target cell (Villa et al. 2019).

EVs are have historically been classified according to how they are separated by centrifugation, larger vesicles sedimenting at lower g forces than smaller ones (Petgel & Gould, 2019). This separation created EV classes where smaller particles comprise exosomes and larger ones microvesicles (also known as ectosomes and microparticles) (Gould & Raposo, 2013, Petgel & Gould, 2019). Exsomes are approximately 30-150 nm in diameter whereas microvesicles are 100-1000 nm in diameter (Momen-Heravi et al., 2018). However, clear markers for the identification of exosomes and microvesicles have not yet been established (Yáñez-Mó et al., 2015). EVs are still commonly divided into the "exosome" and "microvesicle" categories based on their biogenesis (Figure 1). For the sake of clarity, EVs within the exosome size range that originate from the endosomal network are recommended by ISEV to be called small EVs, whereas larger microvesicles that bud directly from the plasma membrane are called medium or large EVs (Théry *et al.,* 2018).

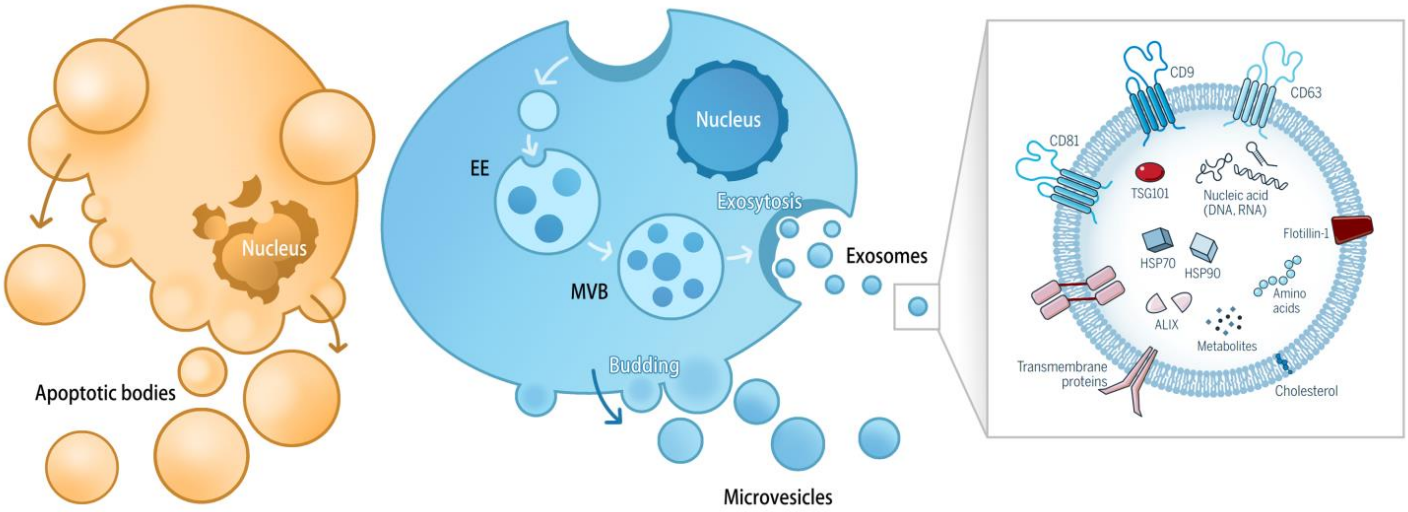

Figure 1. Biogenesis and structure of EVs. *Apoptotic bodies are remnants of dying cells and are not secreted by healthy cells. Exosomes are born within the endosomal network and accumulate inside early endosomes (EE). Later they are packed in multivesicular bodies (MVBs) and are eventually released into the extracellular space as exosomes. Microvesicles are thought to form around specific plasma membrane microenvironments and bud directly out of the plasma membrane. EVs are enclosed by a lipid bilayer and contain tetraspanins (e.g. CD81, CD9 and CD63), Flotillin 1 and other transmembrane proteins enriched on their surfaces. EVs transport bioactive cargo that comprises nucleic acids, lipid mediators, signalling proteins, amino acids and other metabolites to target cells to influence their function. Recreated and compiled from Yáñez-Mó et al., (2015) and Kalluri & LeBleu (2020).*

Exosomes are formed within the endocytic network when their precursors, intraluminal vesicles (ILVs), bud inwards from the membranes of the endosomal network into multivesicular bodies (MVBs) (Yáñez-Mó et al., 2015) (figure 1). MVBs are then transported to the cell surface and fuse with the plasma membrane to release their exosome cargo through exocytosis (Yáñez-Mó et al., 2015). The fusion process takes place under homeostatic conditions in a resting cell, but can also be triggered by an appropriate stimulus, such as cAMP- and Ca^{2+}-mediated signals (Meldolesi, 2018). Before fusion with the plasma membrane, MVBs have an additional purpose of acting as exosome storage within the mother cell (Meldolesi, 2018).

Microvesicles are directly formed at the surface of the plasma membrane (Figure 1). Microvesicles are usually considered to be in the medium size EV category, but the smallest plasma membrane derived EVs overlap with the small EV size generally attributed to exosomes (Yáñez-Mó et al., 2015, Momen-Heravi et al., 2018). Microvesicle cargo is assembled at the cytosolic side of the plasma membrane in designated microdomains and sorted into budding vesicles that are released into the extracellular matrix (Meldolesi 2018). Additionally, it has been observed that the membrane protein and lipid composition differs from that of the surrounding plasma membrane the microvesicle is released from. This finding suggests that the budding is a regulated process (Yáñez-Mó et al. 2015, Meldolesi 2018). Unlike in exosomes, microvesicles are not stored within the cell after their biogenesis, and are promptly released into the extracellular matrix upon budding (Meldolesi 2018). A third class of EVs is also formed upon the fragmentation of a dying cell (Figure 1). These EVs are called apoptotic bodies and they encompass large membrane

structures that are secreted from a disintegrating, apoptotic cells. Apoptotic bodies contain lipid fragments, leftover organelles and proteins of the dying cell as their cargo. Apoptotic bodies are generally not thought to be involved in active cellular communication and are not secreted under normal conditions (Yáñez-Mó et al., 2015).

EVs have become of significant interest for therapeutic applications for their ability to navigate the extracellular matrix to find and release a payload inside specific target cells (Villa *et al.,* 2019). EVs also serve as potential diagnostic markers as they are involved in several pathophysiological processes such as immune responses, tumor biology, angiogenesis, neurodegenerative diseases, wound healing and cardiovascular diseases (Kalluri LeBleu, 2020). EVs could potentially be used for liquid biopsies as they are readily available in body fluids. In addition to diagnostics, they also have potential in monitoring several conditions such as pregnancy, progression of a disease or the effectiveness of a treatment (Kalluri LeBleu, 2020). Additionally, therapeutic small EVs have the potential to pass through inter-endothelial junctions and even smallest blood vessels to reach their intended target (Villa *et al.,* 2019*)*, as well as the blood-brain-barrier (Zhuang *et al.,* 2011) to access the brain.

1.2 Platelets

Platelets are small anucleated blood cells that are mostly known for their involvement in blood clotting and wound healing. In addition to these functions, they are involved in immunity and inflammation, nervous system diseases and tumor biology (Kouprenova *et al.,* 2019, Mejden & Heemskerk, 2019). Platelets are approximately 2-4 μm in size and circulate in the blood for 7-10 days until they are eliminated via the spleen and liver (Kouprenova *et al.,* 2019). Platelets are derived from pluripotent hematopoietic stem cells through fragmentation of megakaryocytes in a process called thrombopoiesis. Thrombopoiesis is triggered via the binding of thrombopoietin to its receptors on the surfaces of megakaryocytes when blood platelet count is low (Mejden & Heemskerk, 2019). The fragmentation of megakaryocytes is driven by a series of cytoskeletal rearrangements that result in the shedding of proplatelets from its surface. During these rearrangements, cell organelles are distributed evenly inside proplatelets that then further elongate, fragmentate and mature into heterogeneous platelet populations (Machlus & Italiano, 2013). These populations may differ in size, granule and membrane structure density and glycoprotein expression profiles. As a result, platelets express heterogeneity in both structure and responses to extracellular stimuli (Mejden & Heemskerk, 2019).

Platelets do not have a nucleus, but contain cell organelles such as mitochondria, lysosomes and granule structures (Kouprenova *et al.,* 2019). Platelet granules can be divided into α-granules and δ- granules which also known as dense granules. Lysosomes, α-granules and dense granules originate from the megakaryocyte endosomal network, where lysosomes and dense granules bud directly from late endosomes and α-granules from MVBs (Ambrosio & Di Pietro, 2017, Flaumenhaft & Sharda 2019). Platelets also contain a membrane structure network called the

open canalicular system which acts as a membrane reserve and transports platelet cargo into the extracellular space (Selvadurai & Hamilton, 2018). The open canalicular system also assists in takin up material from the surrounding plasma (Selvadurai & Hamilton, 2018). When platelets are activated, their granules translocate and fuse with the platelet surface to release their biologically active cargo (Chen *et al.,* 2018). Platelet granule contents play a crucial role in the upregulation of platelet activation as well as their adhesion and aggregation. This mechanism will be detailed further in the context of hemostasis in the following chapter.

Despite having similar origins, α-granules and dense granules have different contents. Dense granules contain small molecular species such as ADP, ATP and polyphosphates, calcium, thromboxane A_2 and serotonin capable of activating other platelets and promoting coagulation (Chen *et al.,* 2018). α-granules contain most of the coagulation and growth factors platelets release upon their activation. These include coagulation-promoting fibrinogen and von Willebrand factor (Chen *et al.,* 2018) and chemokines and interleukins (Flaumenhart & Sharda, 2019) that participate in inflammation and immunity. α-granules also contain platelet plasma membrane proteins such as several integrins (particularly the αIIbβ3 receptor for aggregation), immunoglobulin family receptors such as glycoprotein VI (GPVI), tetraspanins such as CD9, P-selectin and TREM-like transcript-1 (TLT-1) (Chen *et al.* 2018).

1.2.1 Platelet activation and hemostasis

Platelets are versatile and heterogeneous cells that are unique in their ability to dramatically transform their morphology and function upon activation. Platelets are involved in complex signaling events under both normal hemostasis and pathophysiological conditions. Despite lacking a nucleus and therefore possessing a limited capacity for *de novo* protein production, platelets contain RNA cargo that they are able to process into limited amount of proteins required in platelet signaling (Mejden & Heemskerk, 2019). Platelets contain enzymes, cytokines and growth factors that are derived from their megakaryocyte origins and play a part in their function (Machlus & Italiano, 2013). As a part of their function, platelets are able to undergo activation upon biochemical or physical stimulation (Siljander *et al.,* 1996). Upon vascular injury, various stimuli like collagen and tissue factor are exposed from the walls of the ruptured blood vessel and induce platelet aggregation to prevent blood loss (Figure 2). The resulting platelet aggregate is referred to as a thrombus, and the formation process under homeostatic conditions is known as hemostasis. When vascular thrombus formation occurs under pathologic conditions such as stroke or the rupture of an atherosclerotic plaque, it is referred to as thrombosis (Sharf, 2018).

Platelets can be activated by a large variety of agonists, but also as a result of shear force stress of blood circulation or *ex vivo* through for instance changes in temperature. Agonist-mediated activation takes place when platelet surface receptors bind their target, triggering several downstream signaling events depending on the receptor in question (Tomaiuolo *et al.,* 2017, Mejden & Heemskerk, 2019).

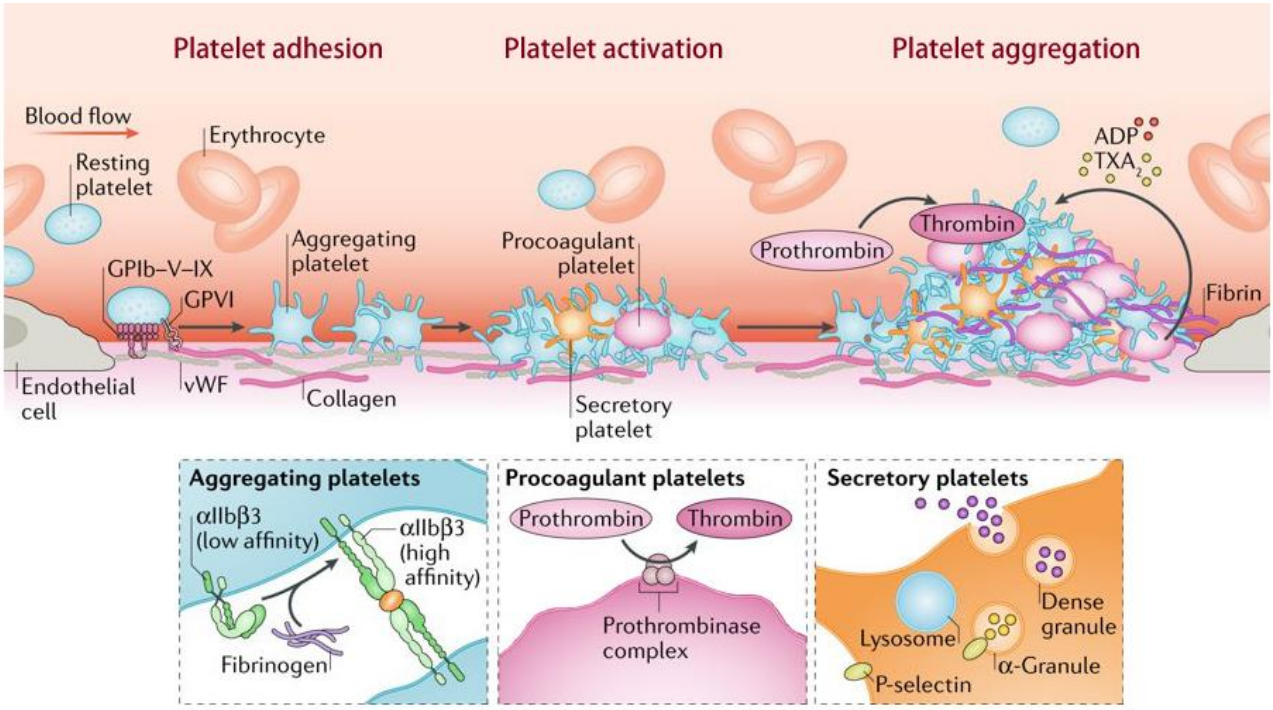

Figure 2. Stages of classical hemostasis and platelet activation. *Platelets are recruited upon vascular injury when vWF and collagen are exposed from the ruptured endothelial wall. Platelets adhere to them through GPIb-V-IX and GPVI and begin to aggregate in the presence of fibrinogen with activated fibrinogen receptor αIIbβ3. Activated platelets have different phenotypes: they aggregate or display procoagulant or secretory functions. Procoagulant platelets recruit prothrombinase complex on their surfaces and amplify coagulation by converting prothrombin into thrombin. Secretory platelets release bioactive molecules from their granules, express P-selectin on their surfaces or generate EVs. Aggregating platelets start to secrete signals such as ADP and thromboxane A_2 (TXA_2) to attract more platelets at the site of the growing thrombus. As platelets aggregate further, they form a stable plug complete with a fibrin network. Adapted from Mejden & Heemskerk (2019).*

These signaling events often (but not always) culminate in the triggering of an influx of Ca^{2+} ions into the platelet cytosol. The rise of the cytosolic Ca^{2+} concentration triggers downstream signaling events that trigger platelet responses (Tomaiuolo *et al.,* 2017). These responses depend on the agonist in question and include pseudopod formation, platelet adhesion, granule secretion and platelet aggregation but also membrane ballooning and the formation of EVs, previously also called microparticles in platelet research (Mejden & Heemskerk, 2019). Common platelet-activating agonists are, thromboxane A_2, ADP, serotonin and thrombin (Tomaiuolo *et al.,* 2017, Battinelli & Loscalzo, 2019). Additionally, fibrillar collagens (types I and III) found in the endothelium of blood vessels are among the most potent platelet activators (Swieringa *et al.* 2018).

In classical hemostasis, platelet activation leads to thrombus formation in various steps (Figure 2). These stages are platelet recruitment and adhesion, activation and aggregation and finally stabilization of the formed aggregate (Mejden & Heemskerk., 2019). The major trigger for platelet

recruitment and adhesion is a ruptured endothelial wall, which will expose several platelet-activating molecules. Upon vascular injury, the vessel walls constrict and circulating platelets are captured by exposed vWF that is immobilized to collagen. Platelets bind vWF with a protein complex consisting of glycoproteins Ib, V and IX (GPIb-V-IX) that is found on the surfaces of resting platelets. When deep subendothelial damage has occurred, the initial platelet adhesion is further stabilized by platelet interaction with exposed fibrillar collagen. Platelets bind collagen via integrin $\alpha 2\beta 1$ and the subsequent activation by GPVI induces signaling leading to the activation of integrin $\alpha IIb\beta 3$ (Figure 2). After initial recruitment of platelets, they are activated and start to aggregate with each other in a critical step of hemostasis. Platelet-platelet interaction is mediated via the activated integrin $\alpha IIb\beta 3$ (also referred to as CD41/CD61 or GPIIb/IIIa), which assumes its high-affinity conformation and binds fibrinogen. Fibrinogen bridges platelets together and is ultimately converted into fibrin by the action of thrombin at the end of the coagulation cascade (Tomaiuolo et al., 2017, Mejden & Heemskerk., 2019., Battinelli & Loscalzo, 2019). Platelet-platelet interaction leads to further platelet recruitment in a positive feedback loop, where the release of soluble agonists such as ADP and thromboxane A_2 from platelets amplifies their activation (Battinelli & Loscalzo, 2019).

When platelets are activated with appropriate stimulus, intracellular Ca^{2+} increases at least one order of magnitude (from to approximately 50 nM to 0.2-1 μM) and is released from dense granules or from the surrounding extracellular space (Agbani *et al.,* 2017). During activation, a subpopulation of procoagulant platelets undergo lipid rearrangements, exposing negatively charged phosphatidylserine (PS) and phosphatidylethanolamine (PE) on their surfaces as a response to an increase in the cytosolic Ca^{2+} - level. This lipid scrambling creates docking sites for prothrombinase and tenase complexes of the coagulation cascade that recruit coagulation factors and ultimately synthetize thrombin, creating a positive feedback loop to upregulate coagulation (Battinelli & Loscalzo, 2019). Platelets also undergo cytoskeletal rearrangements and morphological changes. Platelets lose their discoid shape and exhibit membrane ballooning and form pseudopods. These processes further increase the adhesive capacity of platelets and expand the area of docking sites for prothrombinase recruitment (Mejden & Heemskerk, 2019).

When no pathologies are involved, hemostasis is under careful feedback regulation as procoagulant and suppressing signals converse to maintain appropriate levels of platelet activation (Tomaiuolo et al., 2017). Under homeostatic conditions, premature activation of resting platelets is also constantly suppressed by the surrounding environment. The vascular endothelium secretes nitric oxide, ATP and ADP-degrading ectonucleotidases, thrombin-inactivating thrombomodulin and prostaglandins to suppress platelet activation (Tomaiuolo et al., 2017, Mejden & Heemskerk, 2019). As platelet activation is upregulated during later stages of hemostasis, procoagulant platelets also themselves secrete anti-coagulative and fibrinolytic molecules to form a negative feedback loop to prevent excessive thrombus formation, allowing platelet activation to take place only when it is required (Tomaiuolo et al., 2017) (Figure 2).

1.2.2 Platelets in inflammation and immunity

Platelets also participate in the regulation of inflammation and interact with the immune system in both innate and adaptive immune responses (Semple *et al.,* 2011). Due to the ability of platelets to influence blood flow and endothelial barriers, they play a role in the development of sings of acute inflammation such as swelling, redness and tenderness of the affected area (Rondina & Zimmerman, 2019). As a response to inflammation platelets secrete cytokines, chemokines and soluble agonists with proangiogenic and antimicrobial properties.

Platelets have the ability to synthetize human Toll-like receptors (TLRs) from their mRNA contents and express them on their plasma membrane (Semple *et al.,* 2011). Immune cells use TLRs to recognize patterns on pathogen surfaces. In platelets, TLR-mediated signaling is able to induce platelet activation (D'Atri & Schattner, 2017). As a result, platelets adhere to bacterial pathogens and trap them within an aggregate. Platelets can be directly involved in the destruction of the bacteria by secreting antimicrobial thrombocidins or through recruitment of neutrophils. (Semple *et al.,* 2011). Patelets activate neutrophils by secreting inflammatory chemokines and cytokines and recruit them by directly adhering to them at inflammation sites (Rainger *et al.* 2015). Doing so, platelets detect and contribute to defense against microbes in a coordinated vascular coagulation response known as immunothrombosis, where the pathogen is trapped within an aggregate and destroyed by leukocytes (Semple *et al.,* 2011). These interactions are mediated through CD154, CD40 and P-selectin on the platelet surfaces (D'Atri & Schattner, 2017).

Platelets are also able to interact with dendritic cells with the same receptors and activate them. Therefore, through dendritic cells, platelets are able to increase their antigen presentation to T-cells which activates a response from the adaptive immune system (Semple *et al.,* 2011). Additionally, platelets can also directly present antigens to CD8 positive T-cells to initiate a response from the adaptive immune system (Semple & Kapur, 2020). When platelets are activated to initiate an immune reaction they release granule content that further promotes differentiation of B-cells, maturation of monocytes and dendritic cells and further activation of neutrophils (Koupenova *et al.,* 2019).

1.3 pEVs

pEVs comprise a variety of EVs secreted by platelets upon activation by external stimuli. They were first reported in 1946 by Charglaff and West as an agent able to induce blood clotting (Chargaff & West, 1946). In 1967 they were visualized with electron microscopy by Wolf and dubbed "platelet dust" as the first discovered lipid-enclosed EVs (Wolf, 1967). Therefore, it was established that these particles have properties that are reminiscent of the function of their parent cell (Wolf, 1967). Together with EVs derived from red blood cells, they are the most abundant EVs in human blood under homeostatic conditions (Arraud *et al.,* 2014, Antwi-Baffour *et*

al., 2015). Like other EVs, pEVs are commonly 30-1000 nm in diameter and spherical in shape, but approximately 5% of them are tubular and range from 1 to 5 μm in length (Gasecka *et al.,* 2019).

Resting platelets are suspected to secrete a low amount of spherical EVs under homeostatic conditions in healthy individuals (Gasecka *et al.,* 2019). The rate in which pEVs are shed increases dramatically when platelets are activated (Aatonen *et al.,* 2014, Antwi-Baffour *et al.,* 2015). Activated platelets secrete platelet-derived EVs that massively amplify the coagulation capacity of platelets (Agbani *et al.,* 2017). This activation can be caused by platelet agonists such as cytokines, ADP, thrombin and collagen or by second messengers mimicked by chemicals such as Ca^{2+} ionophore and phorbol esters (Antwi-Baffour *et al.,* 2015). Platelets also release pEVs when they encounter physical activation such as shear stress in the circulation (Antwi-Baffour *et al.,* 2015). Additionally, aging platelets also release platelet microparticles in a process similar to apoptosis that are thought to be the platelet equivalent of apoptotic bodies (Vasina *et al.,* 2011).

The other pEVs consist of large microvesicles that bud directly from the platelet surface following cytoskeleton remodeling and small exosome-like pEVs that are thought to originate from platelet α-granules (Gasecka *et al.,* 2019). With the combination of western blotting and electron microscopy, platelets were shown to secrete previously elusive small pEVs in addition to larger microvesicles (Heijnen *et al.,* 1999). These vesicles could be labelled with the vesicle marker CD63, which is also a marker found within MVBs and α-granules. Since this vesicle population carries this endocytic marker and because α-granules have similar origins to MVBs, the pEVs secreted from platelet granules can be thought as platelet exosomes (Heijnen *et al.,* 1999, Antwi-Baffour *et al.,* 2015). It was recently shown that platelets do secrete small EVs in the exosomal size range and that separate subpopulations of small pEVs exist within the exosome population itself (Multia *et al.,* 2019). Proteomic analysis has also showed that small pEVs are enriched in α-granule proteins, whereas large pEVs contain mostly lipid mediators and occasionally mitochondrial proteins (Dean *et al*., 2009). Therefore, small and large pEVs are likely to be functionally different populations with different mean size distributions (Dean *et al.,* 2009).

Like other EVs, pEVs express surface proteins and lipids on their membranes that correspond to their cell of origin. pEV surfaces contain adhesive platelet proteins such as the activation marker P-selectin, GPIb and integrin αIIbβ3 (Garcia *et al.,* 2005, Boillard *et al.,* 2017, Gasecka *et al.,* 2019). pEVs also contain common EV markers such as CD9, CD63, CD81 and heat shock protein HSP70 (Melki *et al.,* 2017, Gasecka *et al.,* 2019).

pEVs also express PS and PE on their surfaces. Out of these PS especially is characteristic to activated procoagulant platelets and the pEVs shed by them, as lipid rearrangements of the platelet surface play a crucial role in pEV budding (Zwaal & Schroit, 1997, Wei *et al.,* 2018). However, not all pEVs express PS (Gasecka *et al.,* 2019). The dynamic cargo of pEVs also varies based on the EV type and the stimulation their parent platelets have encountered (Aatonen *et al.,* 2014). Proteomic analyses of pEV proteomes have confirmed that pEVs carry several types of cytokines, chemokines and growth factors (Garcia *et al.,* 2005). They also carry transcription factors (Lannan *et al.,* 2015) and nucleic acids such as mRNAs and miRNAs (Plé *et al.,* 2012).

Additionally, platelets transport functional mitochondria packed in large pEVs, which due to the size of mitochondria are a separate population from small pEVs and most microvesicles (Boudreau *et al.,* 2014).

Stimulation of platelets different receptor-specific agonists can be utilized in platelet and pEV research. Commonly used platelet activators are agonists that mimic the initiation of platelet aggregation in hemostasis like thrombin and collagen and their co-stimulation, which has been shown to achieve the most potent pEV generating stimulus. (Siljander *et al.,* 1996, Aatonen *et al.,* 2014, De Witt *et al.,* 2014). The platelet-activating rise in cytosolic Ca^{2+} levels can also be directly induced with Ca^{2+} ionophore, which produces large quantities of non-physiological pEVs (Siljander e*t al.,* 1996)*,* that seem to be unselectively packed and poorer in protein content when compared to pEVs generated by physiologically relevant activators (Aatonen *et al.,* 2014).

1.3.1 pEVs in health and disease

Like other EVs, pEVs are thought to interact with cellular targets and influence their function through the release of their cargo inside their target cell (Gasecka *et al.,* 2019). Therefore, due to their cargo and surface proteins, pEVs have the potential to influence a variety of physiological and pathological processes. The expression of PS, PE and receptors for procoagulant agonists on pEV surfaces define their procoagulant properties. PS and PE also give pEVs a negative charge. PS exposing pEVs serve an extension of activated aggregating platelets, offering platforms for procoagulant reactions to occur (Wei *et al.,* 2018). Aberrant pEV formation and pEV counts in circulation contribute to the mechanism of multiple diseases (Castaman *et al.,* 1996, Satta *et al.,* 1997, Hugel *et al.,* 1999). As such pEVs have potential in the development of diagnostic and therapeutic approaches. Additionally, it has been shown that many therapeutic hemostatic effects of platelets are achieved at least partly through pEVs in patients with hemorrhage or trauma, which supports the hypothesis that functional pEVs – either engineered or naturally produced – could be used as a hemostatic drug (Lopez *et al.,* 2019).

In addition to hemostasis and thrombosis, pEVs serve as an extension of platelets in inflammation and immunity. They are able to interact with neutrophils, T and B lymphocytes and macrophages to trigger B-cell maturation and immunoglobulin production as well as activation of neutrophils (Gasecka *et al.,* 2019), further cementing the importance of platelets and pEVs in the immune system. pEVs are also able to induce the maturation monocytes into macrophages and guide their phenotype through the release of pEV miRNA cargo (Sadallah *et al.,* 2011).

Despite their abundance and versatile roles as mediators of cellular communication, the physiological roles of pEVs are still not fully understood. The fact that pEVs play a role in hemostasis has been established, but all the mechanisms in which they contribute to thrombosis or coagulation defects are still not fully uncovered. In addition to physiological coagulation and tissue repair, pEVs also contribute to multiple other pathological events such as autoimmune disorders, angiogenesis, tumor biology and cardiovascular diseases (Melki *et al.,* 2017, Gasecka *et al.,* 2019). More investigation is required to uncover the mechanisms in which pEVs influence the

pathogenesis of these conditions, as well as the mechanisms in which they participate in the maintenance of homeostasis. In the future, as pEVs can perhaps also be utilized in diagnostic and therapeutic applications for cancer (Dovizio *et al.,* 2018), bleeding disorders (Lopez *et al.,* 2019), cardiovascular diseases (Zaldivia *et al.,* 2017) and wound healing (Guo *et al.,* 2017).

1.4 S100A8/A9 as a novel platelet agonist

The S100A8/A9 protein, also known as calprotectin or myeloid-related protein 8/14 (MRP-8/MRP-14), is a low molecular weight heterodimeric metal ion binding complex belonging to the S100 superfamily. First discovered by Moore *et al.* in 1965 from bovine brain tissue, the S100 family has a unique solubility to 100% saturated ammonium sulphate at neutral pH, which lent the family its name (Moore & McGregor, 1965). This feature is still exploited in purification strategies for S100 proteins (Futami *et al.* 2016). The S100A8/A9 mostly exists as a heterodimer, where monomers spontaneously assemble into their heterodimeric conformation and held together with electrostatic attraction. The S100A8/A9 heterodimer binds both Zn^{2+} and Ca^{2+} ions, which regulate their oligomerization and the stability of the ensuing heterodimer. The binding of Zn^{2+} has a structural function, whereas the binding of the Ca^{2+} ions with EF-hand domains triggers a conformational change that allows the dimer to interact with other signaling proteins (Vogl *et al.,* 2012).

S100A8/A9 is expressed abundantly in myeloid cells such as neutrophils, keratinocytes, monocytes and macrophages. In neutrophils, The S100A8/A9 can make up to 45% of all the cytoplasmic proteins (Wang *et al.,* 2018). In granulocytes, it is released upon their activation into the extracellular space (Shabani *et al.,* 2018). In resting cells, it and acts as a calcium sensor and participates in arachidonic acid metabolism and cytoskeleton rearrangements. During inflammation, S100A8/A9 induces cytokine secretion and leukocyte recruitment and is heavily upregulated (Wang *et al.,* 2018).

S100A8/A9 interacts with several cell surface receptors on the membranes of immune and endothelial cells, but all of its targets are not yet known. Like other immune cells, activated platelets also express S100A8/A9, where it is found in both in α-granules and the cell surface. This indicates that platelets store S100A8/A9 in membrane-enclosed vesicles where they are among the soluble agonists platelets secrete to participate in cell-to-cell signaling (Lood *et al.,* 2016). Additionally, it has been observed that platelets aggregate and secrete soluble P-selectin when they are stimulated with S100A8/A9 in patients with coronary artery disease (Larsen *et al.,* 2015). Therefore, in addition to its proinflammatory properties, S100A8/A9 also has a prothrombotic effect. In order to further study platelets as immune cells, their relationship with the proinflammatory S100A8/A9 and its potential as a platelet activating agonist warrants further investigation.

1.5. Separation and characterization of EVs

Despite the excitement and promise surrounding EVs, it is a very young field of study and as such still suffers from the lack of internationally standardized and precise methods in EV isolation, detection and characterization (Coumans *et al.,* 2017, Gasecka *et al.,* 2019). Despite some methods, such as ultracentrifugation (UC) having been adopted as gold standards, they have been proven to not be optimal for the purpose of EV separation (Gasecka *et al.,* 2019). In order to study the normal functions of EVs and the cells that secrete them, including their therapeutic and diagnostic potential, accurate characterization of their biophysical and biochemical properties is necessary. However, it is difficult to differentiate between different EV types, as they are heterogeneous, often possessing similar physical size distributions and membrane proteins used as EV markers. In terms of platelet research, it is especially challenging to separate pEVs from complex body fluids such as blood and to tell the difference between EVs and contaminating lipoproteins, protein aggregates, cell organelles and platelet remains (Coumans *et al.,* 2017, Zarà *et al.,* 2019). It is also important to consider that parent cells may release different EV subpopulations based on the present activating stimulus (Aatonen *et al.,* 2014). When isolating the total EV population from complex starting material, their subpopulation size range is often unknown. Therefore the identification of all the EV populations present in an unknown sample is difficult (Gasecka *et al.,* 2019). In 2018, ISEV updated their guidelines for minimal information for studies of EVs (MISEV) (Théry *et al.,* 2018) and stated that complete isolation of EVs from contaminants from complex biological fluids is an unrealistic goal. Therefore terms like EV "separation" and "concentration" should be used instead of "purification" or "isolation" (Théry *et al.,* 2018). On top of the difficulties caused by the complexity of the starting material, technical limitations regarding separation and detection have hindered the EV field as no currently available method is able to isolate or detect all EVs from complex biofluids (Coumans *et al.,* 2017).

1.5.1. EV separation

Different methods can be employed for EV separation and characterization based on the size, shape, mass density, charge and surface protein composition of the studied EV population. An overview of the common methods for EV separation are collected in table I. EVs are most commonly isolated from, plasma, serum or cell culture media in bulk by differential centrifugation utilizing stepwise increase in centrifugation speed. Contaminating cells and cell debris (10 min at <1500 x g), microvesicles (30 min at 10 000-20 000 x g) and exosomes (90-120 min at >100 000 x g), can be crudely separated from contaminating proteins in the final supernatant (Momen-Heravi *et al.,* 2013, Coumans *et al.,* 2017). Different chemical gradients can also be employed in density gradient centrifugation to sediment EVs and contaminants based on their density equilibrium within a matrix commonly made of sucrose or iodixanol (Momen-Heravi *et al.,* 2013). Other common, straight-forward methods to isolate EVs based on their diameter are size exclusion chromatography (SEC) and ultrafiltration (Coumans *et al.,* 2017). SEC separates particles based on their mobility in a porous gel matrix based on their geometric size and shape, large molecules eluting faster than small ones (Böing *et al.* 2014). Ultrafiltration, on the other hand, forces sample

components or contaminants to enter through a membrane with a desired cutoff with centrifugation, which can also be used for sample concentration and buffer exchange. These methods are often best applied in tandem with other EV enrichment methods, as they are not able to yield EVs with high purity (Coumans e*t al.,* 2017, Brennan *et al.,* 2020). When studying small EVs on the exosome size range, their small size makes their separation even more difficult. As exosomes have recently gained a lot of pharmaceutical interest, demand for fast isolation methods has increased. With increased interest, commercial kits are also rapidly emerging as available methods for their collection. Numerous methods have been tried for improved EV isolation and novel ones are being urgently developed to meet the needs of the growing EV field.

Table I. An overview of common techniques in EV isolation.

Type of EVs	Method
Microvesicles (100-1000nm)	UC, Density gradient, SEC, Ultrafiltration, Immunocapture, Immunoprecipitation, Co-precipitation, Density Gradient
Exosomes (30-150 nm)	UC, Immunocapture, Immunoprecipitation, Co-precipitation, Density gradient, Ultrafiltration, Commercial kits, SEC, AF4
Apoptotic bodies (500nm-4000 nm)	Centrifugation, Filtration, FACS

Abbreviations: UC: ultracentrifugation, SEC: size exclusion chromatography, AF4: asymmetrical field flow-field fractionation, FACS: fluorescence activated cell-sorting. Adapted and compiled from Coumans et al., (*2017), Shao* et al., (*2018),* Zarà *et al., (*2019) and *Brennan* et al., (*2020).*

1.5.2. EV characterization

As EVs exhibit heterogeneity in both their size populations and marker profile, a single method cannot differentiate between exosomes, microvesicles, apoptotic bodies and contaminants effectively (Coumans *et al.,* 2017, Gasecka *et al.,* 2019). Common strategies for assessing the origin of EV populations of either small or large EV origin include characterization of their size profile, detection of membrane markers and characterization of their cargo. According to the MISEV (2018) guidelines, the enriched presence of at least three protein markers typical for the studied EV subtype together with the absence of at least one negative marker need to be confirmed to make a claim about exosome or microvesicle detection (Théry *et al.,* 2018).

As optical microscopy techniques often fail to detect EVs properly due to the similarity of their diffraction limit and the size of a single EV, the EV field has adopted electron microscopy to study their size and morphology (Coumans *et al.,* 2017). Scanning electron microscopy, transmission electron microscopy and cryo-electron microscopy are all high-resolution techniques that employ a beam of electrons to obtain topological information on the sample surface and have all been

used to characterize EVs (Shao *et al.,* 2018). Techniques based on nanoparticle behavior in the surrounding solution have also been widely adopted for the purposes of EV research. Dynamic light scattering (DLS) and nanoparticle tracking analysis (NTA) are popular techniques relying on tracking the Brownian motion of EVs in a known suspension to determine their size and concentration (Shao *et al.,* 2018). Similar measurements can be also carried out with resistive pulse sensing techniques that utilize the Coulter principle to detect changes in ionic current when particles pass through a pore (Coumans *et al.,* 2017, Shao *et al.,* 2018). Out of these, NTA is perhaps the most widely used method for EV characterization. In NTA and its derivatives, a laser is shined through the sample and scattered light is detected and captured on video. The hydrodynamic radius (R_h) of individual particles is mathematically determined through the Stokes-Einstein equation based on their different diffusion movement. Lastly particle concentration is estimated based on the detected particle amount in the field of view (Shao *t al.,* 2018). When correctly optimized, NTA is widely used for rapid concentration and size profile measurements with a detection limit of 70 nm (Gasecka *et al.,* 2019). However, it is unable to differentiate between EVs and contaminants and different EV subtypes and is best to be used in tandem with microscopy to confirm the presence of EVs (Théry *et al.,* 2018). Additionally, the smallest EV populations below the detection limit are not seen with NTA (Gasecka *et al.,* 2019).

EV surface markers can be characterized to obtain information on the origin of the EV and to obtain information on the pathophysiological state of the mother cell. As platelet activation markers (such as P-selectin and the conformation state of integrin αIIbβ3) are also found on pEV surfaces they reveal information on the activation state of the platelets that shed them. Conventional methods such as enzyme-linked immunosorbent assay (ELISA) and western blotting can be used to show the presence of a protein within an EV sample and are widely used within the EV community. While ELISA is scalable and modifiable to be a part of specific protein assesments, mass spectrometry remains a popular choice for high-throughput shotgun proteomic approaches in both membrane marker and cargo studies (Kreimer *et al.*¸2015).

Flow cytometry can detect single particles based on how they scatter laser light or emit fluorescence signal as particles pass through a laser beam (Coumans *et al.,* 2017). As the detection limit of conventional flow cytometry is approximately 300 nm it is not able to detect most EVs. Recently EV-dedicated small particle flow cytometry techniques (>100 nm) have been developed to enumerate fluorescently stained or unstained EVs (Shao e*t al.,* 2018). When particles are fluorescently labelled a system with multiple lasers can simultaneously detect the presence of several labels on different measurement channels (Coumans *et al.,* 2017). Therefore, when correctly calibrated with appropriate reference material, small particle flow cytometry has the advantage of being able to measure the concentration of EV populations and detect the presence of fluorescent markers in a single run. However even the EV-dedicated flow cytometers have trouble detecting the small EV population. Particles in the exosome size range are missed in flow cytometry data and results are skewed to favour larger particles that are more readily captured by light scatter detectors (Shao *et al.,* 2018, Gasecka *et al.,* 2019).

Emerging fluorescence imaging techniques are an alternative to flow cytometry for EV concentration measurement and characterization of labelled markers on EV surfaces. Fluorescently labelled particles can be detected by nanoimaging techniques with a resolution of 20-50 nm which is enough to visualize single small EVs of this size (Chen *et al.,* 2016). Instruments with multiple lasers set at different wavelengths can excite multiple fluorophores simultaneously. Techniques such as stochastic optical reconstruction microscopy (STORM) or photoactivated localization (PALM) are super-resolution microscopy techniques where individual fluorophores are activated in a random order, causing the fluorophores to blink during their analysis. Image reconstruction from the registered blinks allows for high resolution imaging while avoiding premature fluorophore bleaching. In these methods, particles are stained and fixed on a surface, allowing co-localization studies and visualization of how EVs interact with surrounding tissues (Chen *et al.,* 2016). In addition to this, some nanoimaging techniques are also able to perform live imaging and therefore produce size distribution data based on particle tracking with the same principle as NTA does for EV preparations or track EV movement in living tissue (Panagopoulou *et al.,* 2020). Methods to characterize EV size and membrane markers are collected in table II.

Table II. Conventional and emerging techniques in EV detection and characterization.

Target	Method
Size distribution and concentration	Flow cytometry, NTA, Electron microscopy, DLS, AFM, RPS, SPR, Micro-NMR, Raman spectroscopy, AF4
Membrane markers	ELISA, Western blot, Flow cytometry, Immunofluorescence microscopy, Nanoimaging, Mass spectrometry, SPR, Micro-NMR
Cargo	Proteins, lipids and metabolites: Mass spectrometry, Western Blot, ELISA, SPR, NMR Nucleic acids: Nucleic acid precipitation, PCR, Real time PCR, high-throughput sequencing

Abbreviations: UC: ultracentrifugation, SEC: size exclusion chromatography, AFM: atomic force microscopy, RPS: resistive pulse sensing, SPR: surface plasmon resonance, NMR: nuclear magnetic resonance, AF4: asymmetrical field flow-field fractionation, FACS: fluorescence activated cell-sorting, NTA: nanoparticle tracking analysis, DLS: dynamic light scattering, ELISA: enzyme-linked immunosorbent assay, PCR: polymerase chain reaction. This table is adapted and compiled from Coumans et al., (*2017), Shao* et al., (*2018),* Zarà et al., *(2019)* and *Brennan* et al., (*2020).*

1.5.3. AF4 in EV characterization

Asymmetrical flow field-flow fractionation, also known as AFFFF or AF4, is an emerging technology for EV characterization and shows promise for both analytical and preparative applications (Zhang & Lyden 2019). The method separates nanoparticle subpopulations based on their hydrodynamic radius (R_h), which provides information about the size and shape of the particle. R_h describes the mass and size of the particle, but also provides additional information on how mass is distributed around the axis of gyration in aqueous conditions (Figure 3). Therefore, hydrodynamic radius is useful in describing the shape of the particle in addition to separation. As a distinguishing factor from chromatographic methods, flow field-flow fractionation techniques do not feature a solid phase for the sample particles to interact with (Wahlund & Giddings, 1987). Instead, particles are resolved as they are guided by carefully applied buffer flows to traverse a separation channel. The R_h of a particle can be mathematically determined, much like in NTA and other applications that rely on predictions of particle movement based on size in suspension (Giebel & Helmbrecht, 2017).

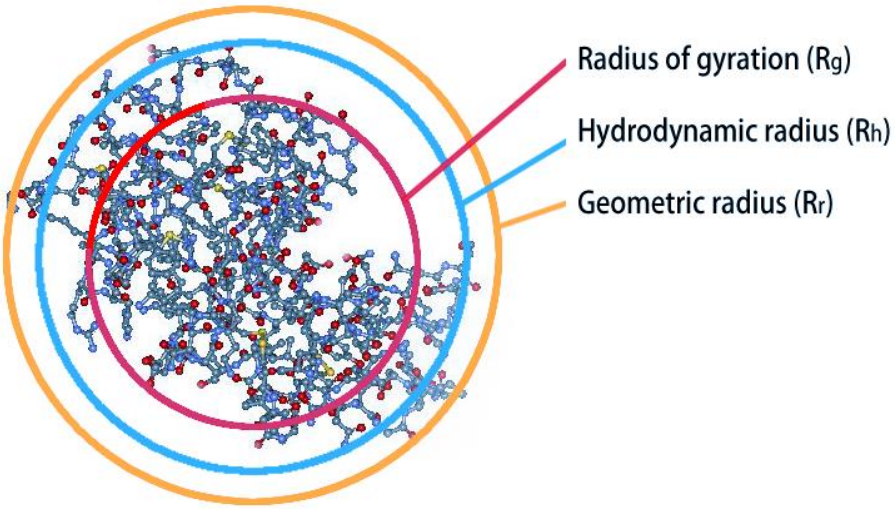

Figure 3. ***Different radii of an asymmetrical particle can be determined by flow fractionation techniques combined with a light scatter detector.*** *Radius of gyration (R_g), hydrodynamic radius (R_h) and geometric radius (R_r) are different from each other and can be determined with different field flow techniques. Constructed and recreated based on Primavera et al., (2014).*

The AF4 system contains a separation channel equipped with a porous semi-permeable membrane with a desired cut off. During the run, the sample particles are pushed against the membrane, separated and then detected and eluted (Figure 4). The sample is first injected and concentrated on a narrow zone in a focusing step. After this, the channel flow (V_{out}) separates sample components in the channel based on their R_h, smaller particles eluting faster than large ones. Crossflow (V_c) is the driving force of the flow field that enables sample separation and is applied perpendicular to V_{out}. V_c and sample diffusion are opposing forces and determine how far the particle cloud will travel from the membrane, smaller particles diffusing further away from the

walls than larger ones. After separation has occurred, V_{out} will carry the separated particles towards the detector (Wahlund & Giddings, 1987).

The AF4 system can be equipped with different detectors and a fraction collector for the purpose of harvesting separated subpopulations for downstream analysis (Zhang *et al.,* 2019). The most common detectors are ultraviolet (UV) and refractive index (RI) detectors, and light scatter detectors such as multi-angle light scattering (MALS) detector and dynamic light scattering detector (DLS). UV and RI detectors are suitable for fluorescent sample detection and concentration measurements whereas MALS and DLS detectors are used to determine the R_g (MALS) and R_h (DLS) of the sample particles. When MALS and DLS detectors are combined, shape factor and polydispersity index can also be determined. The UV detector can also be combined with a light scatter detector to obtain the molecular weight distribution of the analysed sample (Eskelin *et al.,* 2019).

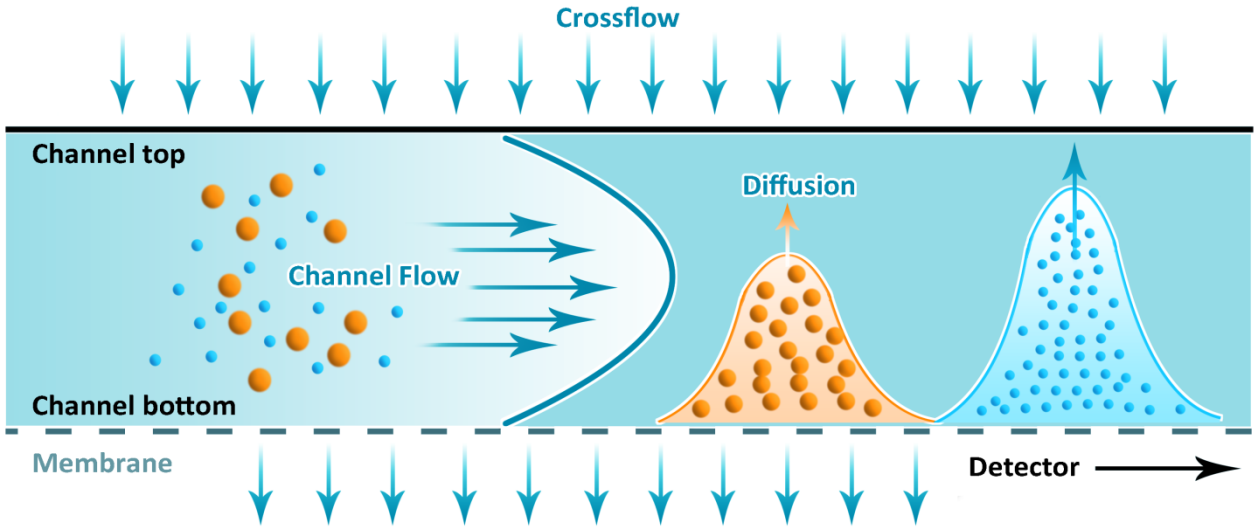

Figure 4. ***Principle of sample separation in an AF4 channel.*** *Parabolic channel flow (V_{out}) carries sample forward in the channel towards the detector. Smaller particles diffuse faster towards the centre of the channel where V_{out} is the strongest and thereby elute first. Crossflow (V_c) flows through the channel and exits through the membrane at the channel bottom. V_c pushes the sample cloud against the membrane against diffusion and acts as the primary force driving separation. Finally particles elute based on their hydrodynamic size and are registered by a detector at the end of the channel. Compiled and recreated from Eskelin et al.¸(2019) and Giebel & Helmbrecht, (2017).*

Separation can be controlled by changing the flow parameters, out of which the most notable ones are V_c and V_{out} and their subsequent ratio (Eskelin *et al.,* 2019, Zhang *et al.,* 2019). By changing these parameters with separation time, separation resolution can be optimized for each sample composition. Commonly a linearly decreasing V_c gradient is imposed over the particle size range of interest, until desired subpopulations have separated. Generally, V_c and the length of the

separation gradient are the most important parameters that affect separation quality (Eskelin *et al*., 2019). After separation, a fractogram displays the subpopulations with different hydrodynamic radii based on different retention times.

AF4 is able to separate particles between 2nm to 1µm in size (Eskelin *et al.,* 2019) and serves as a separation tool between HPLC and other flow cytometric applications in terms of the acceptable size range of the analysed particles. AF4 was first developed to study polymer behaviour in liquids, but has since been routinely applied for separation of proteins and nanoparticles such as liposomes and viruses which bear a significant resemblance to EVs in terms of size and many biophysical properties. Therefore AF4 has potential to become a method to study small EVs in the exosome size range that are at the moment elusive to other nanoparticle characterization techniques.

2. AIMS

Platelets have versatile functions in the human body and secrete pEVs as a response to a variety of stimuli. The role of platelets beyond classical hemostasis is currently being unraveled, their participation in inflammation and immunity being under rigorous investigation. One of the significant contributors to platelet function is the pEVs that they secrete as strategy for intercellular communication. However, the way platelets extend their function to their pEVs is still not fully understood. This project aimed to characterize pEV subpopulations secreted by human platelets when they are stimulated with different agonists relevant for hemostasis and inflammation to study whether the agonists produce different pEV populations. The size profile, particle concentration and surface markers of pEV populations produced with different agonists were characterized to study potential activator-dependent differences.

The EV field has long suffered from the lack of a single method that would be able to gently separate and detect the vastly heterogeneous EV populations in both the small and large EV size ranges. A novel AF4 system was set up at the Faculty of Biological and Environmental Sciences at the University of Helsinki for pEV characterization and separation as the second aim of this work. The ability of the AF4 technique to detect EV subpopulations was evaluated together with its potential for downstream applications.

The aims of this project can therefore be summarized as follows:

1. Characterization of pEV subpopulations secreted by human platelets as a response to different platelet-activating agonists.

2. Establishing a method for the separation and characterization of small pEV size and marker profiles with AF4 and nanoimaging and to assess their usefulness in EV research.

3. MATERIALS AND METHODS

3.1. Expression and purification of S100A8/A9

S100A8/A9 was produced in a separate project pertaining this thesis work, with a focus on setting up a protein expression and purification system for the S100A8/A9 dimer. Two plasmids containing the S100 A8 and A9 monomers were a kind gift from associate professor Junichiro Futami from the Okayama University, Japan. Both plasmids were successfully transformed and coexpressed in competent BL21(DE3) *E. coli* cells (C23271 Lot number: 0491404, New England Biolabs Inc., Ipswich, USA) according to the manufacturer's instructions. Bacterial cells were grown in the presence of 100µg/ml of ampicillin and protein production was induced with 0.5mM of isopropyl β-D-1-thiogalactopyranoside (IPTG).

Cells were collected by centrifugation (2700 x g for 12 minutes) and resuspended in 20 ml of 50 mM TRIS-HCl (50 mM NaCl, 5 mM $MgSO_4$, pH 7.5). Cells membranes were dirsupted with 30 10s sonication cycles on ice using a B-30 Branson Sonifier (Branson Ultrasonics Corporation, Danbury, USA), with a 50 second cooling step between each cycle. Nucleic acids were digested with 0.25 µl (7.15 U) of Novagen Benzonase (Merck KGaA, Darmstadt, Germany) for 30 minutes on ice and precipitated with dropwise addition of polyethylenimin (PEI, average MW 600, Wako Chemical). and removed by centrifugation (2700 x g for 10 minutes) and soluble proteins were collected from the supernatant by precipitation by adding 11.3 g of ammonium sulphate (Mallinckrodt Baker, Deventer, The Netherlands) up to 80% saturation while mixing vigorously. Precipitated proteins were harvested by centrifugation at 2700 x g for 15 minutes and pellet was resuspended in 2 ml of 20 mM TRIS-HCl with 30 mM dithiothreitol (DTT) to reduce disulphide bonds for 1.5h at +37 °C. Sample buffer was exchanged by filtering the buffer through a 3 kDa molecular weight cut (MWCO) Millipore Amicon Ultra 4 ml ultrafiltration device (Sigma-Aldrich Inc.) at 3000 x g until less than 100 µl of original sample volume was left. Sample volume was filled back up to 2 ml with 50 mM sodium phosphate buffer (ph 6.0).

The S100A8/A9 monomers were purified with ion exchange chromatography with HiTrap SP HP 1ml commercial columns (GE Healthcare Life Sciences). Protein purification was done in three steps, where the first step was using a stepwise NaCl gradient 0.15M to 0.6M for elution. During the second purification step, the sample from the first step was run through another clean HiTrap column and eluted with 0.2 M NaCl. During IEX purification, pressure was manually applied with a 10 ml plastic syringe so that flow rate of 1 ml/min was maintained. Finally, as a third step remaining contaminating proteins were removed by ultrafiltration with 1 ml Amicon Ultra 30 kDa MWCO filtration devices (Sigma-Aldrich Inc.) at 2700 x g for 60 minutes. The protein expression and purification protocols developed for this study were modified from a method previously described by Futami *et al.* (2016).

The final concentration of the purified S100A8/A9 was determined to be 0.29 mg/ml with a modified Lowry protein assay (DC protein assay, Bio-Rad Laboratories Inc., Hercules, USA) where absorbance was measured at 750 nm from technical triplicates. Bovine serum albumin (BSA) (Bio-Rad Laboratories Inc.) was used as a standard. Protein purity was verified with SDS-PAGE. A picture of the gel is shown in supplemental figure S1 in the "Supplement" section of this thesis with a detailed description of the SDS-PAGE run conditions.

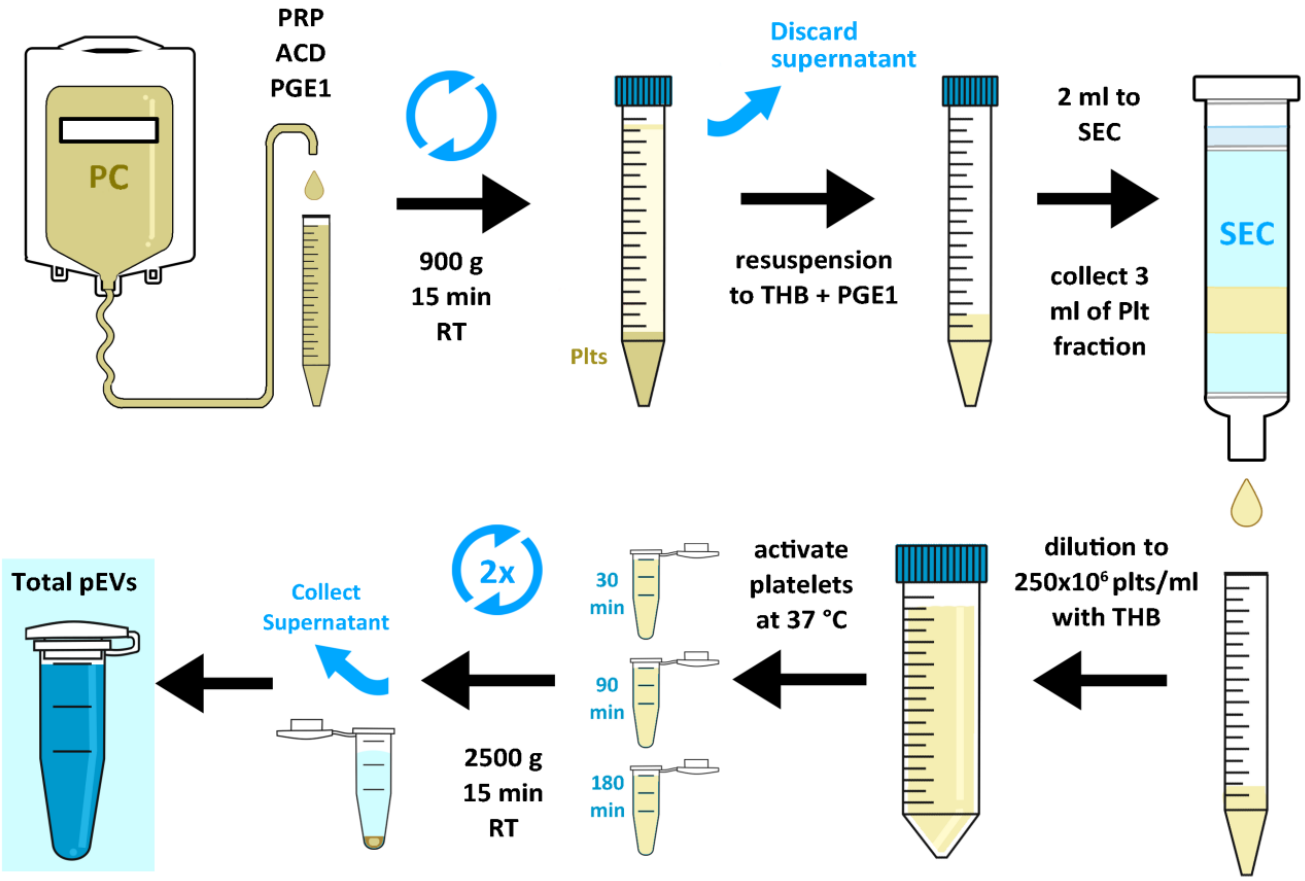

Figure 5. ***Flow chart of the standard platelet and crude pEV isolation process.*** *Platelets are first collected by centrifugation. Platelets are purified with SEC and their concentration is adjusted. Isolated platelets are then ready to be activated under different conditions. Activator and activation time can be varied at this step. Platelets and cell debris are removed by centrifugation two times. Each time the supernatant containing pEVs is collected and moved to a new tube. The final product is the tube containing total pEVs, which is highlighted with a blue background at the end of the flow chart. From this crude pEV sample, pEVs can be further isolated with ultracentrifugation to remove further contaminants for downstream analysis. Centrifugation steps are indicated with circular double arrows. PC = platelet concentrate, ACD = acid citrate dextrose, PGE1 = Prostaglandin E1, RBC = red blood cell, Plt = platelet, THB = Tyrode's Hepes buffer, SEC = size exclusion chromatography, RT = room temperature (22 °C).*

3.2 Platelet isolation

Platelet concentrate bags containing concentrated platelets from four ABO and Rh(D) -matched healthy volunteer blood donors were prepared and provided by the Finnish Red Cross Blood service. 13.5 ml of platelet concentrate was first pelleted by centrifugation at 900 x g for 15 minutes with soft brake in the presence of acid citrate dextrose (ACD; 39 mM citric acid, 75 mM sodium citrate and 135 mM D-glucose, pH 4.5) as a preservative. Pellets containing platelets were carefully resuspended in 1ml pf Ca^{2+} -free, filtered Tyrode's Hepes buffer (THB) (137 mM NaCl, 0.3 mM NaH_2PO_4, 3.5 mM Hepes and 5.5 mM D-glucose, pH 7.35) in the presence of prostaglandin E1 (PGE1) (Sigma-Aldrich Inc., St. Louis, USA) to the final concentration of 100 ng/ml to prevent premature platelet activation during the isolation process. Platelets were separated from protein contaminants with size exclusion chromatography (SEC), using 10 ml TELOS columns (Kinesis Inc., Berlin Township, USA) hand-packed with CL-2B sepharose matrix (GE Healthcare Life Sciences, Chigago, USA). The sepharose was washed three times with TBH prior to column packing by changing the buffer each time after three rounds of centrifugation at 150 x g for 5 minutes. 2 ml of platelet pellet was used for each column and approximately 3 ml of platelets were collected after the eluent had turned milky. Platelet concentration was determined with a Beckman Coulter T-540 (Beckman Coulter Inc.) blood analyzer and adjusted to $250*10^6$ platelets/ml, which has previously been shown to be an optimal concentration for platelet activation (Aatonen *et al.,* 2014). A schematic representation of the different steps in both platelet isolation and the subsequent pEV isolation are illustrated in Figure 5. Any deviations from this procedure are noted separately in the following sections.

3.3 Platelet activation

3.3.1 Platelet activation with Ca^{2+} ionophore

Contents of a 7 day old PC bag were divided into 50 ml Falcon tubes, where PGE1 was added to the final concentration of 100 ng/ml. Platelets were collected by centrifugation as previously described, yielding approximately 120 ml of platelets adjusted to $250x10^6$ platelets/ml. Platelets were divided to 50 ml Falcon tubes, each containing 25 ml of platelet solution and incubated in 10 µM of Ca^{2+} ionophore A23187 (Merck KGaA, Darmstadt, Germany) in the presence of with 1 mM $MgCl_2$, 2mM $CaCl_2$ and 3 mM KCl_2 for 60 minutes at +37°C.

3.3.2 Platelet activation with S100A8/A9 and thrombin-collagen

Batch A. Determination of activation conditions with S100A8/A9. Platelets were activated with the S100A8/A9 protein in three different concentrations by activating 1 ml of platelets at 1:10, 1:100 and 1:250 (v/v) dilutions where each activation mix respectively contained 0.029 mg/ml, 0.0029 mg/ml and 0.00116 mg/ml of purified protein in the presence of 1 mM $MgCl_2$, 2mM $CaCl_2$ and 3 mM KCl_2. 0.2 U/ml of thrombin and 2 µg/ml of collagen were carefully pipetted separately

on the walls of the Eppendorf tube and only simultaneously mixed with platelets as incubation was started. The activation was carried out together with a control sample where no activator was present. Platelets were incubated for 40 minutes at +37°C.

500 µl of platelets were activated with 0.029 mg/ml of S100A8/A9 for 30, 90 and 180 minutes with a non-activated control in technical duplicates. A thrombin-collagen co-activation was to be included for all time points, but due to time constraints it could not be prepared as planned. A pEV sample from thrombin-collagen activated platelets was obtained from Dr. Mari Palviainen (EV-group, Faculty of Pharmacy, University of Helsinki, Finland) for the 30-minute time point.

Batch B. Sample preparation for AF4. Large-scale platelet activation with the S100A8/A9 (10 ml), thrombin-collagen (50 ml) and unstimulated control (50 ml) was carried out. Platelets were incubated with their activators for 60 minutes at +37°C.

Batch C. Sample preparation for nanoimaging. Material constraints, 400 µl of purified (2 x IEX purification) S100A8/A9 and 3 ml of less pure (1 x IEX purification) S100A8/A9 were combined to activate 20 ml of platelets for 120 minutes. Unstimulated control (340 ml) and thrombin-collagen (50 ml) activations were carried out for 30 minutes at + 37 °C. For live imaging, 100 ml of thrombin-collagen and 400 ml of unstimulated control activations were carried out. Platelets were incubated with thrombin and collagen for 60 minutes at +37°C.

3.4 Isolation of pEVs

3.4.1 Crude pEV extraction

Platelets and cell debris was removed by centrifugation at 2500 x g two times in room temperature (Figure 5). Each time the supernatant containing pEVs was collected and moved to a new tube. This method was employed for downstream applications where pEVs were further identified from other contaminants by fluorescent labels and population gating or SEC. Supernatants were stored at +4°C in LoBind Eppendorf tubes (Eppendorf Co., Hamburg, Germany).

3.4.2 UC

Platelets were removed by centrifugation twice at 2500 x g for 15 minutes at room temperature. Total pEVs were isolated by ultracentrifugation at 110 000 x g for 120 minutes at +4°C with a Beckman Coulter Optima LE-80K ultracentrifuge (Beckman Coulter Inc., Brea, USA) and a Ti50.2 rotor (Beckman Coulter Inc.). Supernatant containing protein contaminants was discarded and the remaining pEV pellet was resuspended by vigorous vortexing in 100-200 µl of calcium-free Gibgo Dulbecco's phosphate buffered saline (DPBS, pH=7.1) (Thermo Fisher Scientific Inc. Waltham, USA), depending on the required starting volume for downstream applications.

3.5 Flow cytometry

25 µl of platelets were labelled with fluorescently tagged monoclonal antibodies against human platelet surface markers. Labelling was carried out with 5 µl of anti-human P-selectin conjugated with R-phycoerythrin (PE) (clone AK4, BD Biosciences, Franklin Lakes, USA), 0.95 µl of PAC1 conjugated with fluorescein isothiocyanate (FITC) (BioLegend, San Diego, USA) and 7.5 µl of rat anti-human TLT-1 (R&D Systems Inc., Minneapolis, USA) conjugated with Alexa Fluor 488 (Alexa488) (Table III). Isotype controls conjugated with the appropriate fluorescent markers for each label were also prepared. In the same reaction volume, 5 µl of mouse IgG1 κ isotype control (BD Biosciences) was used for PE, 0.95 µl of mouse IgM κ isotype control (BioLegend) was used for FITC and 5 µl of rat IgG2B (R&D Systems Inc.) was used as an isotype control for Alexa488. Labelling was carried out for 20 minutes at +37 °C in the dark in technical duplicates. After that, the labelling reaction was stopped through dilution by adding 200 µl of THB to the reaction tubes.

25 µl of pEV supernatants were labelled for flow cytometry with the same antibodies as platelets (Table III). 25 µl of pEV supernatants were labelled with 4 µl of anti-P-selectin and 5 µl of anti-TLT-1 antibodies for 60 minutes in room temperature, in the dark. Isotype controls for PE and Alexa488 were prepared from the S100A8/A9 180 time point sample with 0.5 µl of mouse IgG1 κ isotype control for PE and 3.5 µl of rat IgG2B for Alexa-488, each conjugated with their appropriate fluorescent labels. Labelling reactions were stopped with 200 µl of TBH and samples were again prepared in technical duplicates.

Table III. Fluorescently tagged antibodies used in platelet and pEV flow cytometry

Antibody type	Binding target	Label	Clone	Lot number	Channel	Amount (µl) plts/pEVs
mouse anti-human IgG_1 κ	P-selectin	PE	AK4	5167967	Orange	5 / 4
mouse anti-human IgM κ	αIIbβ3	FITC	PAC1	B209384	Green	0.95 / -
rat anti-human IgG_{2B}	TLT-1	Alexa488	268420	AFEQ0118111	Green	7.5 / 5
mouse IgG_1 κ	isotype	PE	MOPC-21	6077643	Orange	5 / 0.5
mouse IgM κ	isotype	FITC	MM-30	B207138	Green	0.95 / -
rat IgG_{2B}	isotype	Alexa488	141945	ABWA0317101	Green	5 / 3.5

Platelets and pEVs were analysed with the Apogee A50 Micro Flow Cytometer (Apogee Flow Systems Ltd., Hemel Hempstead, United Kingdom). Platelet and pEV populations were identified

and picked for analysis based on small- and large angle light scatter (SALS/LALS) signal with previously determined gating. Fluorescent signal was filtered at 525 and 575 nm for the detection of FITC (green), Alexa Fluor 488 (green) and PE (orange) labels. Gates for green and orange channels were determined individually for each experiment from isotype controls and unlabeled samples for each label. A maximum of 1% of fluorescent events out of all observed events on the SALS/LALS channel was considered an acceptable background.

70µl of sample was diluted to 200µl of buffer on a 96-well microtiter plate and measurements were performed for 90 seconds with a flow rate of 1.5 µl/min with 150 mbar pressure and gain value at 1. For platelet detection threshold of 14 and a voltage of 280V were used for SALS and 31 and 200 for LALS. For pEV measurements, a detection threshold for SALS was set at 15 and 56 for LALS. Voltages for SALS and LALS were set to 320V and 295V, respectively. Population gating, instrument control and scattergram data analysis was carried out with the Histogram software (version 255.0.0.148, Apogee Flow Systems Ltd.). Statistical evaluation was done with a two-tailed, paired Student's T-test for Microsoft Excel 2010. A p-value of 0.05 was considered significant.

3.6 NTA

pEV concentration and particle size was measured with the Nanosight LM14C NTA instrument (Malvern Panalytical Ltd., Malvern, United Kingdom) with a violet (405 nm 70 mA) diode laser (Hamamatsu Photonics K.K., Hamamatsu City, Japan) and a SCMOS camera. Samples were manually injected with a 1ml plastic syringe (Terumo Medical Corporation, Tokyo, Japan) diluted to appropriate measuring concentration with filtered particle-free DPBS. Measuring chamber was washed with 70% ethanol and MilliQ water between each measurement. 5 30-second videos with 40-100 particles per frame were taken for each sample, with camera level at 14, screen gain at 1.0 and detection threshold at 4. Shutter slider and slider gain were 1000 and 400 and videos were recorded with a 25 FPS framerate. Automatic settings for the maximum jump distance between frames for each tracked particle, temperature change and blur correction were employed. The device was controlled and the results analysed with the NanoSight NTA 3.0 software (Malvern Panalytical Ltd).

3.7 AF4

Characterization of pEV subpopulations with an online UV detector was carried out with the Postnova AF2000 MultiFlow AF4 instrument (Postnova Analytics, Landsberg, Germany). Online UV-Vis detector (PN3211; wavelength 190-600 nm) coupled with a preparative flow cell (Shimadzu SPD-20A, Shimadzu, Kyoto, Japan) was used and absorbance measured at 280 nm with detector sensitivity at 0.001. Solvent organizer (PN7140) and degasser (PN7520) were used to control buffer flow, a syringe pump (Kloehn v6, Norgen Inc., Littleton, USA) was used for controlling cross-flow and a purging port (PN1610) was used for rinsing. Analytical channel (Postnova CHA-612) in a temperature controlled channel oven (PN4020) was used with a 350 µm channel spacer and a 10 kDa MWCO regenerated cellulose membrane (Postnova 2-AF4-MEM-612). Sample was injected manually with a 100 µl Hamilton glass syringe (Hamilton Company, Reno, USA) into a manual

injection valve (Rheodyne 9725i, Sigma-Aldrich Inc.) coupled with a 100 µl injection loop. Samples were prepared in filtered phosphate buffered saline (PBS) (137 mM NaCl, 2.7 mM KCl, 8 mM Na2HPO4, and 2 mM KH2PO4, pH 7.4), which also served as the mobile phase. Fractions were collected with a PN8050 fraction collector at +10°C. The instrument was controlled and data collected with the Postnova AF2000 software. Method development was based on a modified version of the a protocol previously described by Multia *et al.* (2019). Sample was injected at 0.1 ml/min flowrate over 5 minutes. After a 1 minute transition step, elution was started with a constant V_c of 2.5 ml/min for 15 minutes, followed by a gradient from 2.5 ml/min to 0.1 ml/min for 5 minutes and then to zero within 5 minutes (Table IV A) with V_{out} at 1 ml/min.

Table IV. Crossflow parameters for pEV characterization with AF4.

A. *Initial parameters for UV-AF4.*

Start time (min)	End time (min)	Duration (min)	Mode	V_c start (ml/min)	V_c end (ml/min)
0	5	5	Injection + focus	2.5	2.5
5	6	1	Transition	2.5	2.5
6	16	15	Elution	2.5	2.5
16	21	5	Elution	2.5	0.1
21	26	5	Elution	0.1	0.1
26	31	5	Elution	0.1	0

B. *Modified parameters for UV-AF4.*

Start time (min)	End time (min)	Duration (min)	Mode	V_c start (ml/min)	V_c end (ml/min)
0	5	5	Injection + Focus	0.5	0.5
5	6	1	Transition	0.5	0.5
6	11	5	Elution	0.5	0.5
11	36	25	Elution	0.5	0
36	45	9	Elution	0	0

C. *Optimized parameters for UV-AF4 and MALS.*

Start time (min)	End time (min)	Duration (min)	Mode	V_c start (ml/min)	V_c end (ml/min)
0	2	2	Elution	0.5	0.5
2	3	1	Focus	-	-
3	5	2	Focus + injection	-	-
5	50	45	Elution	0.5	0
50	60	5	Elution	0	0

20 µg of BSA (Bio-Rad) was injected as a size standard to evaluate the size range these flow parameters were able to separate. As a result, it was discovered that mostly particles in the protein size range were analysed and the method required further optimization. New parameters for pEV separation were derived from a method previously described by Zhang *et al.,* (2018). For the new method, V_{out} was set to 0.3 ml/min and V_c was applied as a constant 0.5 ml/min for 5 minutes after the start of elution, followed by a V_c gradient over 25 minutes from 0.5 ml/min to zero (Table IV B). $5.0*10^{10}$ PFU/ml of ϕX174 (r=25 nm) and $1.0*10^{11}$ PFU/ml of ϕ6 (r=70 nm) viruses were obtained from Dr. Katri Eskelin (Molecular and Translational Virology group, Faculty of Biological and Environmental Sciences, University of Helsinki, Finland) and analysed as size standards to determine separation range of the updated parameters.

Techical duplicates of pEV samples were sent to Wyatt Technology GmbH (Dernbach, Germany) for AF4-MALS. For pEVs obtained from Ca^{2+} ionophore activation, S100A8/A9 activation and unstimulated platelets samples were analysed without duplicates. This choice had to be made due to the scarcity of S100A8/A9 pEV material and due to the fact that the duplicate for control was lost during transportation. 10 µl of ionophore pEV sample was injected, whereas 50 µl of S100A8/A9 and control samples were used due to lower particle concentration. AF4 method development and sample measurements were carried out by Head of Analytical Service Dr. Roger Scherrers based on the parameters described by Zhang *et al.,* (2018).

At Wyatt Technology, measurements were carried out with the Wyatt Eclipse flow system with a built in degasser, quaternary pump and autosampler. The Eclipse AF4 module was coupled with a Wyatt UV online detector at 280 nm and an online DAWN 18 angle light scattering MALS detector equipped with a 658 nm emission wavelength laser. UV absorbance signal was recorded at 280 nm and MALS signal at a 90° angle. The final AF4 method for both UV and MALS measurements was optimized for the system with the ASTRA Software tool for the acquisition and analysis of MALS data (Table IV C). Abnormally behaving large aggregates and proteins were eluted out of the sample with an additional elution step with a constant V_c of 0.5 ml/min over 2 minutes to minimise void volume. Sample injection and focusing was carried out for 2 minutes without V_c with injection flow set to 0.2 ml/min. Elution was carried out in a single step for 45 minutes as a gradient from 0.5 to zero. After V_c reached 0 ml/min, elution was continued for an additional 5 minutes with only V_{out} present to ensure that all sample had left the channel. V_{out} was maintained constant at 1ml/min for the entire duration and filtered particle-free PBS (pH 7.4) was used as the mobile phase. UV and MALS data were processed with the ASTRA software tool.

3.8 Nanoimaging

Collected pEVs were concentrated by ultrafiltration with 20 ml Stratorius Vivaspin ultrafiltration devices with a 10 kDa MWCO Polyethersulfone (PES) membrane (Stratorius AG., Göttingen, Germany). Samples were labelled for nanoimaging with conjugated antibodies and 1:1000 CellMask Deep Red (CMDR) (Invitrogen, Thermo Fisher Scientific) lipid dye to a final concentration

of 0.5 µg/ml. Sample was filled to 500 µl with PBS and incubated with CMDR for 60 minutes in the dark at room temperature. Samples were prepared with an unlabelled control with no dye. Excess dye and contaminating proteins were removed with SEC using a commercial IZON qEV 70 nm column (Izon Science Ltd., Oxford, United Kingdom). Column was washed with 3 column volumes of PBS between each sample and 500 µl fractions were collected manually. Fractions were analysed with NTA and 3-5 fractions with the highest concentrations were pooled and concentrated with 50 µl 10 kDa MWCO PES Omega membrane Nanosep filtration devices (Pall Corporation, Port Washington, USA) at 14000 x g for 20 minutes and resuspended to 50 µl of DPBS.

pEVs were immobilized on small wells on top of a coverslip for nanoimaging. Coverslips were first sonicated in MilliQ purified water and 50 ml of 1M KOH FOR for 30 minutes in 50 ml falcon tubes. The wells were washed twice with MilliQ water and left to dry, after which they were coated with 10 µl of Poly-L-Lysine for 2 hours at +37 °C in a humidifying chamber. 10 µl of pEVs were immobilized in +4 °C overnight. The following morning 10 µl of pEVs were again added on the wells and left to bind the coverslip for 2 hours in +4 °C. Additional S100A8/A9 could not be added due to shortage of sample. Wells were blocked with 9 µl of blocking buffer (5% EV-depleted BSA in ⌀ 0.1 µm filtered PBS) for 30 minutes in room temperature. EV-depleted BSA was obtained from Dr. Katariina Maaninka (EV-Group, Faculty of Biological and Environmental Sciences, University of Helsinki). 1 µl of anti-human CD61 (BD Biosciences) conjugated with fluorescent Atto-488 label (Expedeon Ltd., Heidelberg, Germany) was added to the final concentration of 50 ng/µl in each sample well. Lightning Link Atto 488 Labeling Kit was used for the antibody conjugation according to manufacturer's instructions for the Lightning Link Rapid Conjugation Systems (Expedeon Ltd., product #350-0005), with the exception that 10 times more Atto-488 label was used. Immunostaining of pEVs was carried out overnight at +4°C in the dark. Excess dye and buffer was removed by gently washing the well 3 times with 10 µl of PBS. Due to the fact that the method had never been tried before in our laboratory and that studies that employ ONI imaging to study pEVs are extremely scarce, dye concentrations had to be picked based on unpublished recommendations by the manufacturer for this experiment.

pEVs were imaged using the dSTORM technique on the ONI Nanoimager S system at the Light Microscopy Unit at Institute of Biotechnology, University of Helsinki in 10 µl of BCubed ONI imaging buffer (ONI BCubed Reagent kit,ONI Ltd., Oxford, United Kingdom), equipped with 4 lasers at 405 nm (violet), 488 (blue), 561 (green) and 640 (red), each with a 1000 mW maximum output power. A sCmos camera with a 50µm x 80µm field of view per channel and a 1.6 electron rms read noise was used, coupled with a 100 x 1.49 NA oil immersion objective. CMDR (red) and anti-CD61-Atto488 (green) were imaged simultaneously on two different channels with an average laser power of 10% at appropriate excitation wavelengths at 50 Hz and 20 ms exposure for 1000 frames. Samples were imaged through the coverslip with a droplet of immersion oil positioned between the coverslip surface and objective lens.

Image acquisition and processing was performed using the NimOS software version 1.6.1.9898 (ONI Ltd.). Co-localization analysis was performed with open source ImageJ software, developed by Wayne Rasband (2012) (Version 1.52a: Available at https://imagej.nih.gov/ij/download.html). Statistical analysis was performed with the JACoP plugin for ImageJ, developed by Cordelières & Bolte (2006), (version 1.0, Available at https://imagej.nih.gov/ij/plugins/track/jacop2.html). Pearson's and Manders' overlap coefficients were calculated with the JACoP plugin by setting detection threshold at 55 for CMDR and 51 for CD61-Atto488 with a vertical shift value of 20.

pEVs were concentrated by ultrafiltration with 15 ml Amicon Ultra filtration devices with a 10 kDa MWCO regenerated cellulose membrane. pEVs were labelled with a 1:10000 dilution of anti-human CD61 conjugated with Atto488 and a 1:5000 dilution of CMDR to a final concentration of 0.25 µg/ml. Triple labeling was carried out with the same concentrations of CMDR and anti-CD61-Atto488, with added 1:200 dilution of mouse anti-human CD9 (HansaBioMed Life Sciences, Tallinn, Estonia) conjugated with Atto594 (Atto594 Conjugation kit, Innova Biosciences Ltd., Cambridge, United Kingdom) (Table V). Sample volume was filled to 500 µl with PBS incubated with anti-CD9 and anti-CD61 for 2 hours in the dark at room temperature. Incubation time for CMDR was 30 minutes. Samples were again prepared alongside unlabelled controls.

Table V. Fluorescent antibodies used in pEV nanoimaging

Antibody type	Binding target	Label	Lot number	Channel	Dilution
mouse anti-human	CD61	Atto-488	8290738	Green	1:10000
mouse anti-human IgG_1	CD9	Atto-594	160418	Red	1:200
-	lipids	CMDR-640	2127436	Red	1:5000

EVs were separated and excess dye and contaminating proteins were removed with SEC using a commercial Izon qEV 70 nm column and an automatic fraction collector (AFC) (Izon Science Ltd.) with a 1ml/min flowrate. Column was washed with 3 column volumes (CVs) of PBS between each sample and 500 µl fractions were collected. Fractions were analysed with NTA and 3 fractions with the highest particle concentrations were pooled and concentrated with 50 µl Nanosep filtration devices as previously drescribed. 10 µl of each sample was pipetted on coverslip wells and imaged in live tracking mode with the ONI Nanoimager S system with the same parameters. Automatic drift correction and focusing were employed during the analysis and a minimum track length of 5 frames with a maximum jump distance between frames of 0.5 mm was allowed for localization tracking analysis. A minimum of 1000 frames were acquired with an average laser power set at 5% to avoid fluorophore bleaching. Acquisition was stopped when fluorophores were fully bleached. Image acquisition and processing was performed using the NimOS software.

4. RESULTS

4.1 Assesment of platelet activation

Platelets that had been activated with the S100A8/A9 protein complex were analysed using nanoparticle flow cytometry to assess the protein's potential as a novel platelet activator. Platelets activated by S100A8/A9 were compared to platelets that had not received activation stimuli as a baseline control for platelet vesiculation. Both platelet mixtures were stained with PAC1 that binds the active conformation of αIIbβ3, anti-P-selectin and anti-TLT-1 to detetct platelet activation through different activation routes. As the activating effect of the S100A8/A9 protein has not been previously determined in pEV studies, different activation times (30, 90 and 180 minutes) (Figure 6) and concentrations (1:10, 1:100 and 1:250 dilutions) were compared in stimulated and unstimulated as effective activation conditions needed to be established. Samples were analysed with flow cytometry in duplicates. Preliminary studies on optimal activation concentration for the S100A8/A9 revealed revealed the highest activator concentration at 0.029 mg/ml produced the most potent effect and was therefore chosen for all further activations (data not shown). Typical representatives of the flow cytometry scattergrams and their gatings are shown in supplemental figure S2.

Based on the abundance of platelet activation markers detected in this study, increased incubation time did not seem to markedly affect the level of the three marker proteins. When the stimulated platelets were compared to the un-stimulated control, a trend for decreased platelet activation is observed when S100A8/A9 is used as an activator based on P-selectin abundance when incubation time is 30 ($p = 0.019$, $n = 2$) and 90 minutes ($p = 0.049$, $n = 2$). For PAC1, less than 10 events are detected for each microliter analysed at all time points (Figure 6).

Next, the total populations of pEVs derived from the same platelet samples were collected by centrifugation and labelled against P-selectin and TLT-1 to check whether these markers could be found on the pEV surfaces. To additionally compare the effect of the S100A8/A9 protein on overall platelet vesiculation with a known strong activation, pEVs isolated from thrombin-collagen co-activated platelets (30 min) were added to the analysis as a positive control (figure 7). Typical representations of the flow cytometry scattergrams and their gatings are shown in supplemental figure S3 for labelled and unlabelled pEVs at the end of this thesis.

The marker profile and event counts shown in figure 7 above show a trend for increased platelet vesiculation as activation time increases between the 30 minute and 90 minute time points, whereas control sample vesiculation only marginally increases as a function of time. However, platelet activation by S100A8/A9 does not seem to increase between 90 and 180 minutes. Therefore an incubation time between 60 to 90 minutes time seemed to be optimal for activation with S100A8/A9 and was used for subsequent platelet activations in this study. Activation by S100A8/A9 decreased the number of P-selectin –positive pEVs when compared to the strong

thrombin-collagen co-stimulation (30 minute activation, p = 0.055). Additionally, S100A8/A9 seemed to increase the amount of TLT-1 -expressing pEVs when compared to pEVs obtained with the unstimulated control (180 minute activation, p = 0.050). Based on this platelet activation study with flow cytometry, it was decided that the S100A8/A9 protein could be a potential platelet activator.

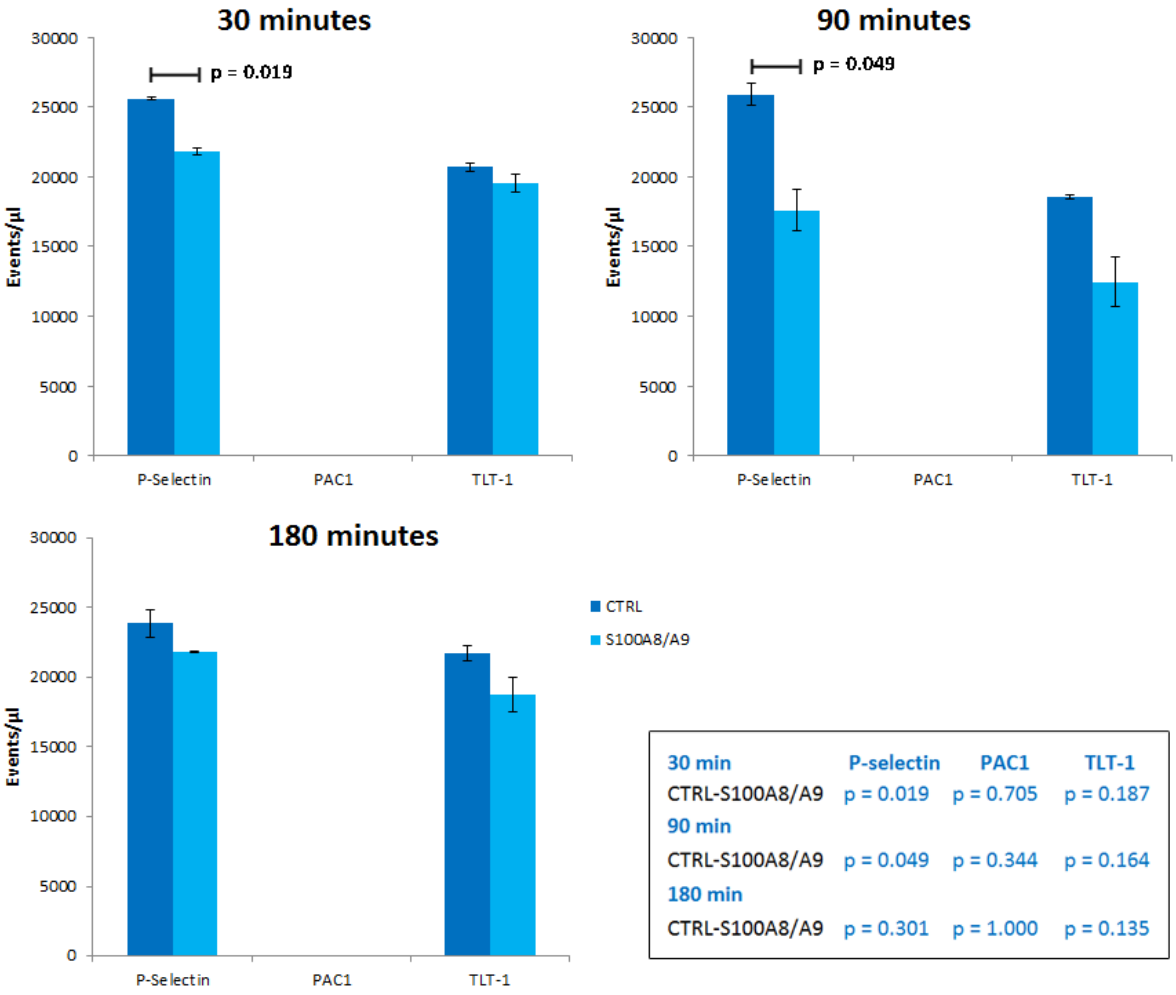

Figure 6. ***Platelet activation with S100A8/A9.*** *Platelets were activated for 30 minutes, 90 minutes and 180 minutes with 0.0029 mg/ml of S100A8/A9 and labelled against P-selectin, TLT-1 and the activated αIIbβ3 (PAC1). The samples were analysed with the Apogee A50 Micro Flow Cytometer system. Results were compared to un-stimulated control (CTRL). Experiments were gated for the full platelet population based on all scattered light that arrived to the SALS and LALS detectors. For the visualization of P-selectin (orange), PAC1 and TLT-1 (green), filters for these wavelengths were gated separately based on unlabelled controls and antibody isotypes. For these filtered gatings, only the platelet population region determined by the first gating was considered. Detected events per microliter analysed are shown for each marker as bars and reported as an average of two technical duplicates. P-values were determined by a paired student's T-test. Differences between samples that are considered significant are marked above their respective bars.*

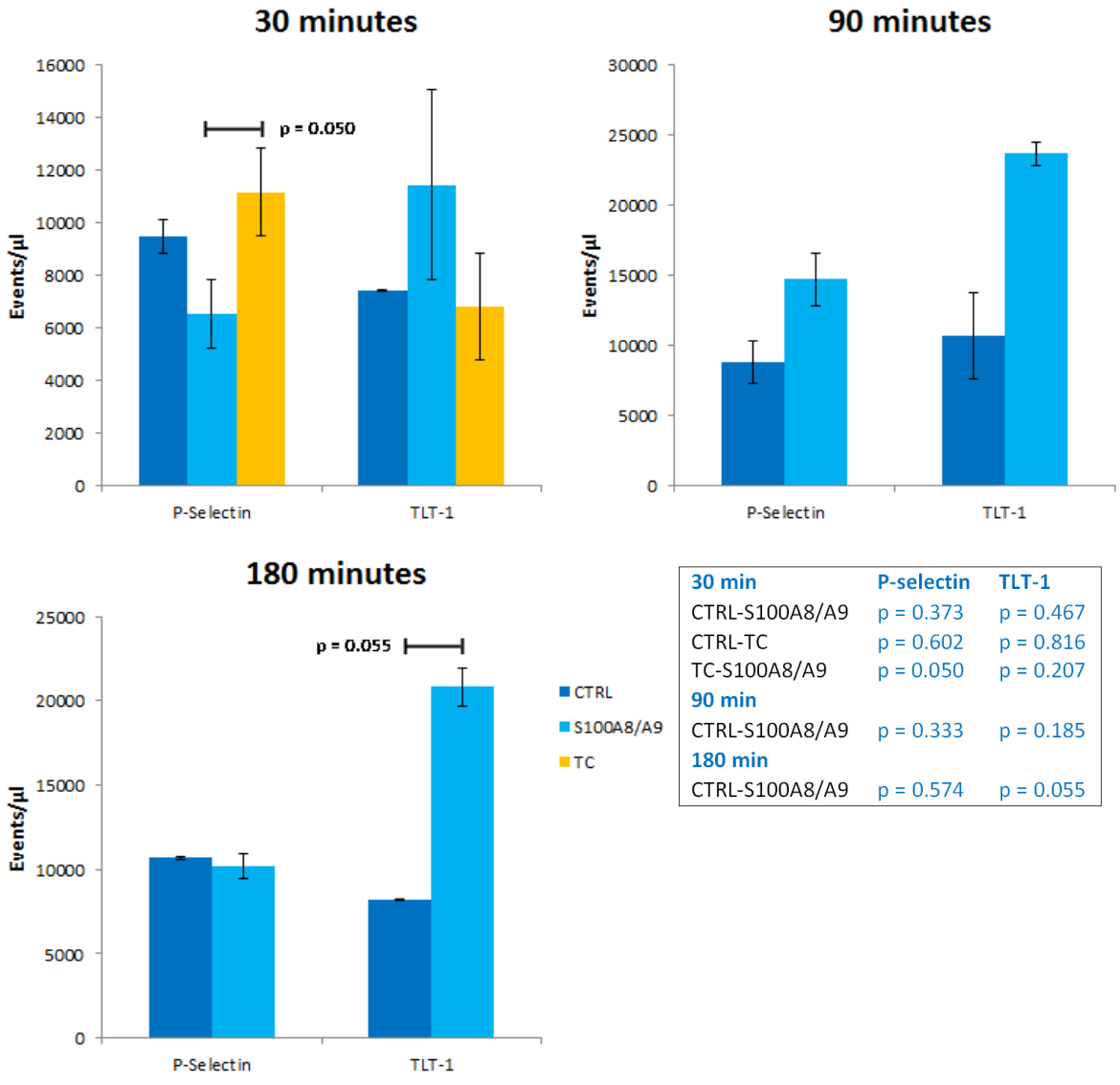

Figure 7. ***Assessment of pEV surface markers with Apogee A50 Micro Flow Cytometer system.*** *pEVs that were collected from platelets activated for 30 minutes, 90 minutes and 180 minutes with the S100A8/A9 protein were labelled against P-selectin and TLT-1 and analysed with flow cytometry to detect the presence of platelet activation markers. Experiments were gated for the full pEV population based on all scattered light that arrived to the SALS and LALS detectors. For the visualization of P-selectin (orange), and TLT-1 (green), filters for these wavelengths were gated separately based on unlabelled controls and antibody isotypes. For these filtered gatings, only the population region determined by the first gating was considered. Results were compared to an un-stimulated control (CTRL) and co-activation with a mix of thrombin and collagen (TC). The detected event counts are reported as an average of two technical duplicates. . P-values were determined by a paired student's T-test. Differences between samples that are considered significant are marked above their respective bars.*

4.2 Measurement of pEV concentration and size

In order to further characterize the pEV profiles produced with the S100A8/A9 and thrombin-collagen activations, new platelet activations were carried out to produce pEVs for the determination of their concentration and size. These pEVs were then compared to pEVs from an unstimulated control, as previously described. In addition to these activators, large-scale platelet stimulation was conducted with Ca^{2+} ionophore AS3187 to produce larger quantities of pEV material for subsequent AF4 method optimization. Ionophore stimulation was carried out for 60 minutes, after which the released pEVs were collected and purified with ultracentrifugation for the small EV size range. pEVs were divided into six tubes and characterized with NTA to determine their size distribution and particle concentration (figure 8A). Ionophore activation produced a sufficient amount of particles for future method optimization, as a particle count to the power of 11 is considered sufficient for most downstream applications. The six samples possess a very uniform size distribution with most particles falling within the 120-135 nm region.

Next, the particle concentrations and size distribution profiles of pEVs from the new activations with S100A8/A9 and thrombin-collagen were analysed with NTA (Figure 8B). A slight decrease in mean and mode particle size was seen when compared to the particles obtained from platelet stimulation with Ca^{2+} ionophore. In all samples, most particles are distributed around the main peaks around 110-130 nm with smaller populations observed around 300-400 nm. Some forking of the first peak is observed in the thrombin-collagen and the control samples which may suggest the presence of two small EV populations. Nothing was seen below 70 nm, which is the detection limit of NTA. Additionally, the samples seemed to display larger variance between duplicates than the ionophore samples. Lastly, when the size distribution profiles for the ionophore particle material and the S100A8/A9 and TC activation material are compared, it can be noted that they all are sufficiently similar and have a high enough particle concentration for downstream analysis. Therefore method optimisation with the ionophore material is justified in order to study the other samples.

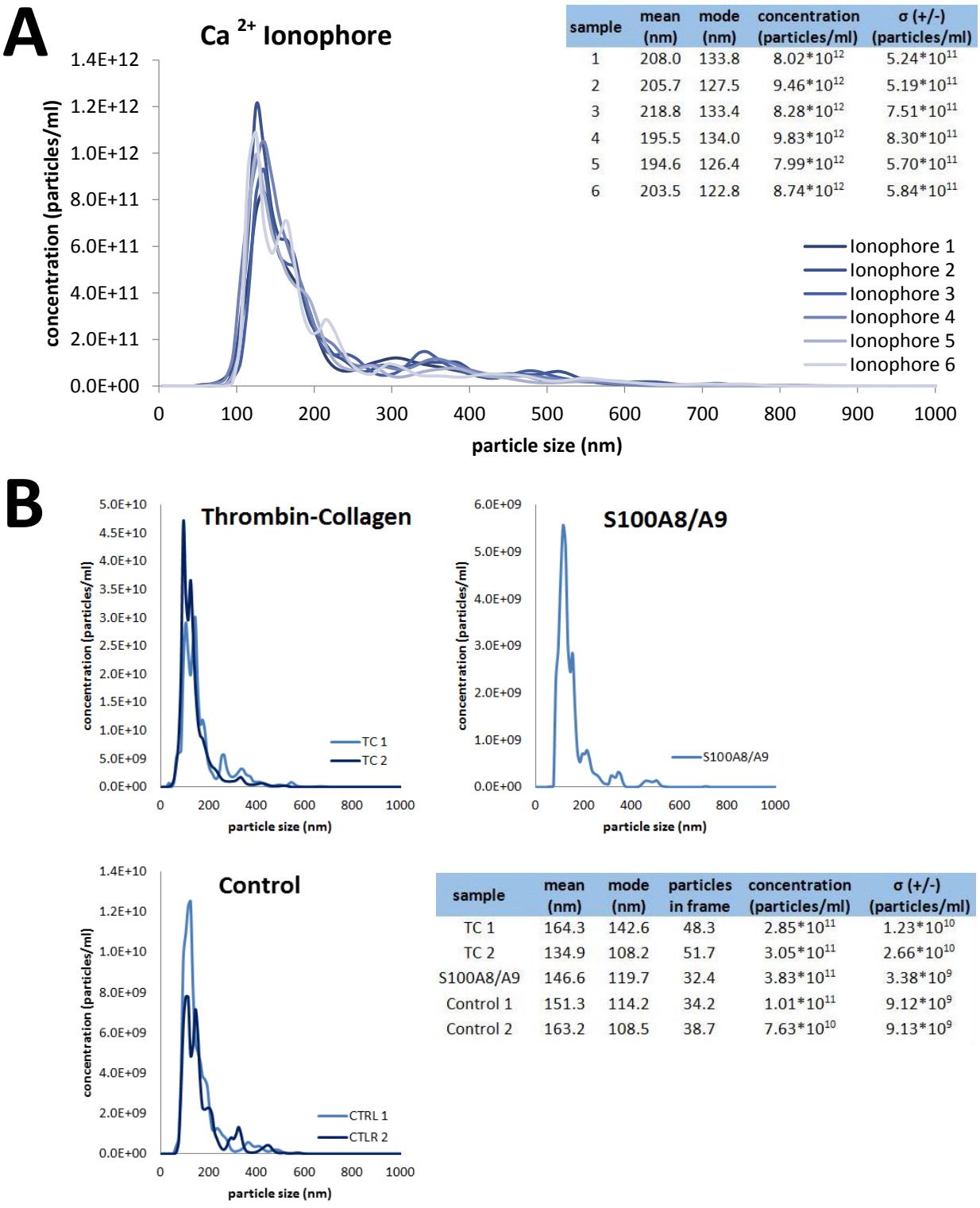

sample	mean (nm)	mode (nm)	concentration (particles/ml)	σ (+/-) (particles/ml)
1	208.0	133.8	$8.02*10^{12}$	$5.24*10^{11}$
2	205.7	127.5	$9.46*10^{12}$	$5.19*10^{11}$
3	218.8	133.4	$8.28*10^{12}$	$7.51*10^{11}$
4	195.5	134.0	$9.83*10^{12}$	$8.30*10^{11}$
5	194.6	126.4	$7.99*10^{12}$	$5.70*10^{11}$
6	203.5	122.8	$8.74*10^{12}$	$5.84*10^{11}$

sample	mean (nm)	mode (nm)	particles in frame	concentration (particles/ml)	σ (+/-) (particles/ml)
TC 1	164.3	142.6	48.3	$2.85*10^{11}$	$1.23*10^{10}$
TC 2	134.9	108.2	51.7	$3.05*10^{11}$	$2.66*10^{10}$
S100A8/A9	146.6	119.7	32.4	$3.83*10^{11}$	$3.38*10^{9}$
Control 1	151.3	114.2	34.2	$1.01*10^{11}$	$9.12*10^{9}$
Control 2	163.2	108.5	38.7	$7.63*10^{10}$	$9.13*10^{9}$

Figure 8. ***Size distribution and concentration of pEVs from platelets stimulated with Ca2+ ionophore, thrombin-collagen and S100A8/A9.*** *The concentration of pEVs from* ***A)*** *Ca2+ ionophore-stimulated platelets and* ***B)*** *un-stimulated (CTRL) platelets, thrombin-collagen co-stimulated platelets (TC) and S100A8/A9 –stimulated platelets was measured with NTA and visualized as a function of particle size. Each distribution represents an average calculated from five 30-second videos. Duplicates were prepared for all samples except for pEVs produced with 100A8/A9. Mean and mode particle sizes and sample concentrations are tabulated in the bottom right corner. Particles analysed in each frame is also shown, if less than 40 analysed particles in each frame may lead to errors in the analysis.*

4.3 Characterization of pEVs with AF4

4.3.1 Method optimization

AF4 is an emerging method in the EV field and has not been previously employed on pEV study at the Faculty of Biological and Environmental Sciences at the Viikki campus of the Unversity of Helsinki. Due to the flow cytometric analysis of platelet and pEV marker populations, differences in their abundance was seen when different platelet agonists were used. NTA was used to obtain preliminary information on the size distribution of pEVs, but it failed to detect the smallest pEVs that may be present in the samples. To investigate how the differences in platelet activation marker distribution would translate to the formation of subpopulations of different pEVs, an AF4 method was set up for the separation and characterization of pEV samples. AF4 method development was started by following previously developed AF4 parameters published by Multia *et al. (*2019).

The AF4 experiments were started with a system equipped with a UV detector. The lower and upper detection limits with decreasing and increasing amounts of pEVs procued with Ca^{2+} ionophore were tested. Different V_C/V_{out} ratios were also experimented with to obtain the best separation of emerging subpopulations. The measurements were conducted with the UV detector range set at 0.001 and the lower detection limit was reached when particle concentration was 10^{10} particles/ml. When sample dilution was increased from this magnitude, the UV signal was not anymore distinguishable from background to signal noise. This detection limit remained the same when detector sensitivity range was adjusted to 0.0001, because this change also amplified noise to the same degree (data not shown). The fractogram of a typical optimisation run produced four distinct subpopulation peaks can be seen (P1-4, figure 9). Since the four subpopulations seemed to be present across all ionophore pEV runs, the potential of the AF4 system as a preparative step in EV separation was evaluated by collecting 300 µl fractions from five different runs. The fractions that contained peaks 1-4 (Figure 9) were pooled and concentrated by ultrafiltration. The particle concentration of the pooled fractions for each peak was measured with NTA. However, NTA could only detect less than 10 particles in each analysed frame for these samples. Data is not shown, as NTA analysis could not be completed with so little material.

Due to the absence of EV-like particles in the AF4 fractions, we next evaluated sample stickiness to rule out strong membrane interactions that could lead to sample loss or abnormal elution. The AF4 method was calibrated for a quantitative measurement of the particles that pass through the separation channel. The experiment was carried out by injecting a known amount of pEV sample five times to determine if the obtained signal intensity corresponded to the injected sample amount when no V_c was present. The “protein content” of the ionophore sample was determined by a photometric measurement, where absorbance was measured at 280 nm from an average of two measurements. Based on these measurements, it was determined that 39.6 µg of sample was injected each time. As the peak intensity slowly rose with each injection (ROI 1-5), it looked like the sample was slightly sticking to the membrane during the analysis (figure 10).

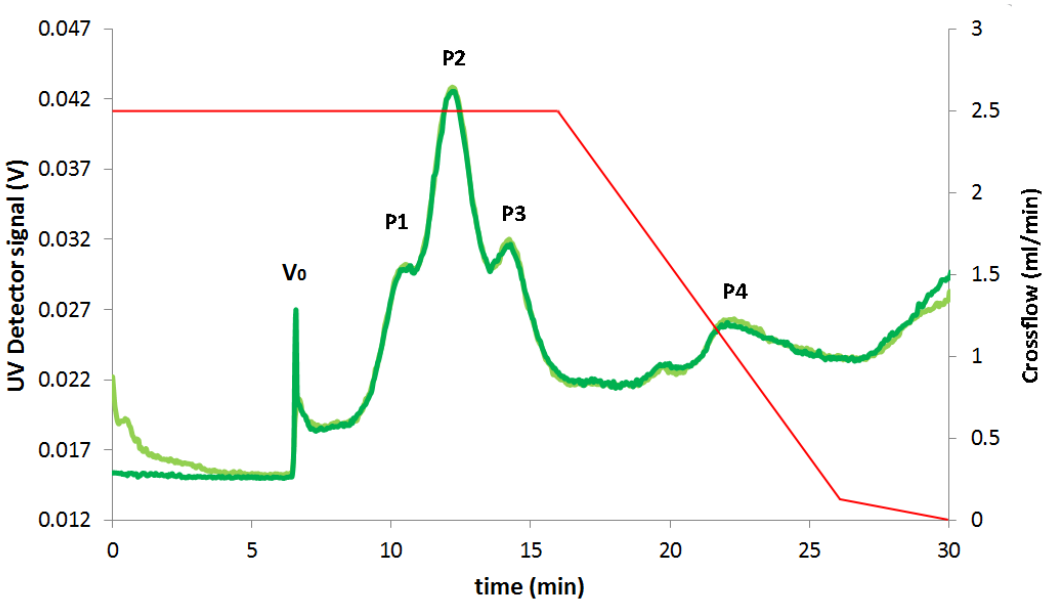

Figure 9. ***UV-AF4 fractogram of Ca^{2+} ionophore activated pEVs.*** *pEVs produced with Ca^{2+} ionophore were used for method optimization for AF4. 10 µl of pEVs were analysed twice and technical replicates shown in green. UV detector signal is plotted as a function of time. V_c was decreased from 2.5 ml/min to 0.1 ml/min in a linear within 10 minutes. After that V_c was dropped to 0 within the span of 5 minutes and separation was stopped. Absorbance was measured at 280 nm with detector sensitivity at 0.001. V_c is marked with a red line in the figure. V_0 marks the peak for void volume at sample injection, after which four subpopulation peaks can be seen (P1-4).*

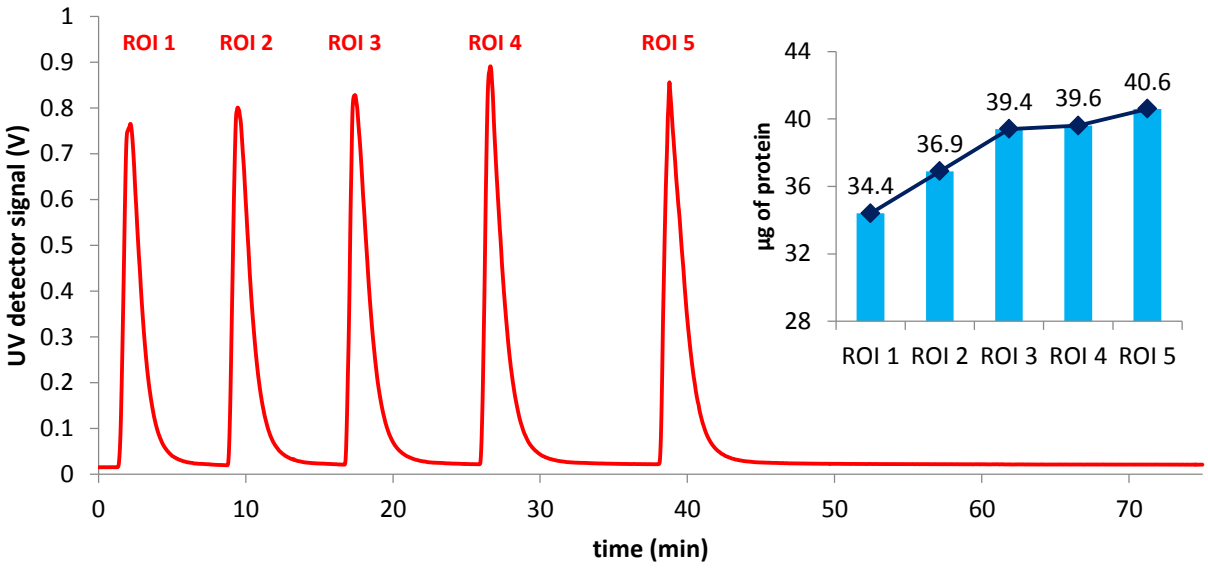

Figure 10. ***Investigation of EV stickiness with direct sample injection.*** *Sample stickiness was investigated by repeatedly injecting the same amount of Ca2+ ionophore-induced pEVs into the AF4 separation channel to check for changes in peak intensity. Each injection was previously determined to contain 39.6 µg of sample material. Channel and injector flow rates were set to 0.3 ml/min and no V_c was used. Absorbance was measured at 280 nm and detector sensitivity was set to 0.001, as before.The UV signal intensity for each injection is shown as a function of time. The area under the curve for each peak was calculated and plotted to show a trend line of increasing particle concentration with each region of interest (ROI 1-5).*

4.3.2 UV-AF4

After initial run parameters for pEV samples were established, pEVs from S100A8/A9, thrombin-collagen and control activations were separated and detected with UV-AF4. Preliminary size distribution and EV concentration profiles were determined with NTA as previously described (figure 8). To determine the lower size range for the analysis, 20 µg of bovine serum albumin (BSA) was injected into the channel to test where its monomer (R_h 3.88 nm), dimer (R_h = 5.32 nm) and trimer (R_h = 6.69 nm) would fall within the separation range achieved with the current parameters.

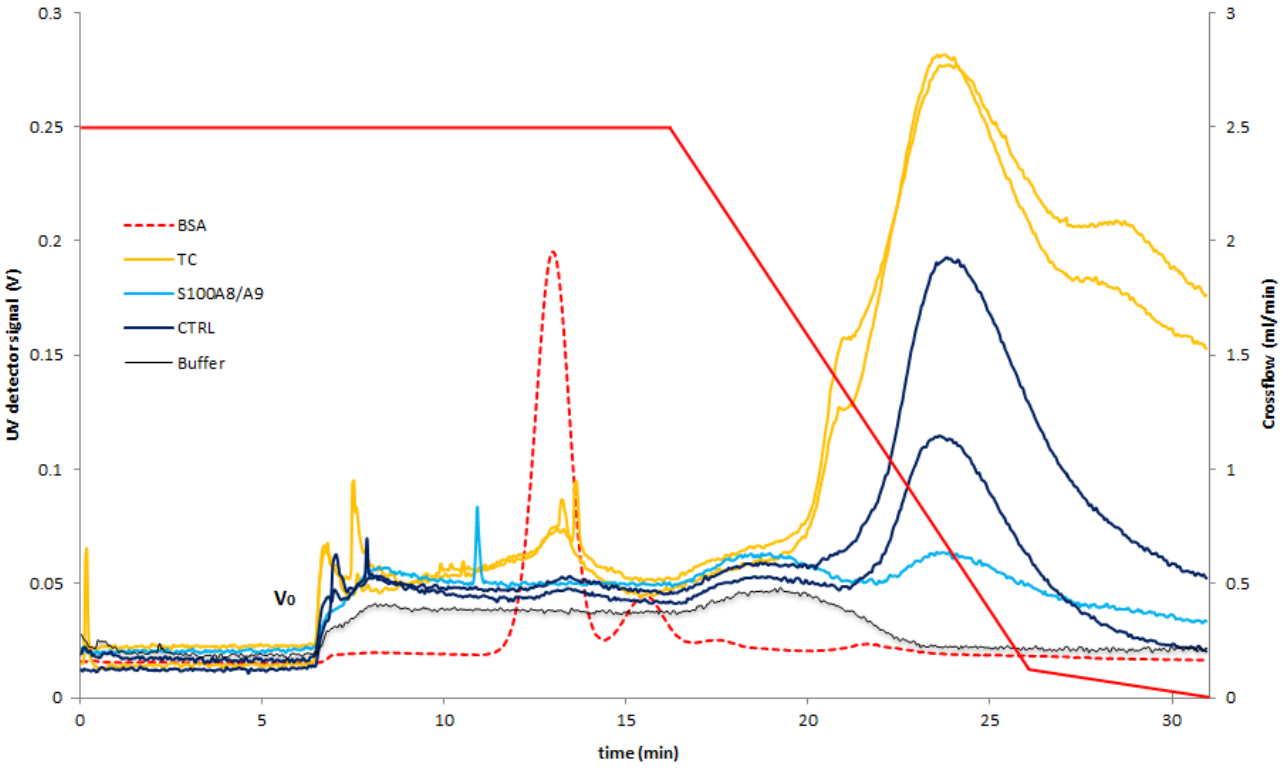

Figure 11. ***Characterization of thrombin-collagen, S100A8/A9 and control pEV subpopulations with UV-AF4.*** *pEVs produced with thrombin-collagen (TC) and S100A8/A9 activations were analysed with UV-AF4 along with an unstimulated control (CTRL). 100 µl of undiluted sample was injected into the channel each time. The baseline of a buffer run is shown in grey. Bovine serum albumin (BSA) was included as a size standard and is shown as a red dotted line. V_c was decreased from 2.5 ml/min to 0.1 ml/min in a linear within 10 minutes. After that V_c was dropped to 0 within the span of 5 minutes and separation was stopped. Absorbance was measured at 280 nm with detector sensitivity at 0.001. V_c is marked with a red line in the figure. V_0 marks the peak for void volume at sample injection.*

The subpopulations that were previously seen in the pEVs produced with Ca^{2+} ionophore (figure 9) were now absent from the fractogram (Figure 11). Only in the case of thrombin-collagen, peaks at 14, 22 and 26 minutes that could be indicative of pEV subpopulations were observed. S100A8/A9 and control activations seem to not have produced any pEV subpopulations within the analysed region and their signal is hardly distinguishable from the buffer baseline.However, a large and very

intense population of large particles is starting to separate at the end of the V_c gradient with retention times above 26 minutes. BSA monomer and dimer are seen as clearly separated peaks around 13 and 16 minutes of separation. The parameters used in the analysis seemed to separate mostly proteins, and further method adjustment was required to extend the separation power further into the small EV size region.

Therefore, the AF4 method was further optimised with the ionophore pEV batch. In a similar paper about the separation EVs with AF4, Zhang *et al.,* published a working protocol for the separation of small EVs along with their discovery of a novel nanoparticle subclass exomeres (Zhang *et al.,* 2018). This publication was used as the starting point for the next step in our pEV analysis. More pEVs produced with a Ca^{2+} ionophore activation were analysed to evaluate sample subpopulation separation with these new parameters. Flow parameters developed by Zhang *et al.,* 2018 were utilized where linear V_c decay from 0.5 ml/min to 0 over 25 minutes of separation was employed. pEV sample was injected without additional dilution and analysed alongside viruses of known size to give an estimate of the analysed region (Figure 12). A virus mix containing $5.0*10^{10}$ PFU/ml of bacteriophage ϕX174 (r=25 nm) and $1.0*10^{11}$ PFU/ml of ϕ6 (r=70 nm) was used for this experiment.

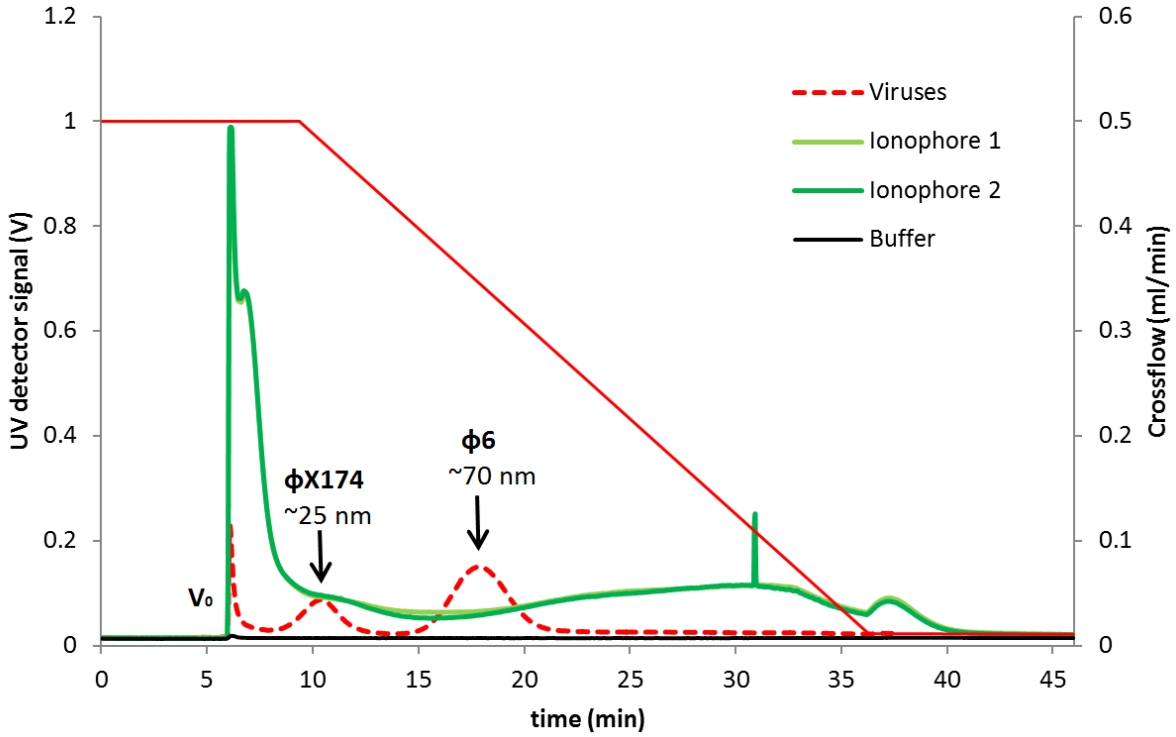

Figure 12. ***Analysis of Ca^{2+} ionophore induced pEVs and virus controls with an updated UV-AF4 protocol.*** *Undiluted ionophore sample 5 was analysed alongside a bacteriophage mix of 5.0*1010 PFU/ml of φX174 (r=25 nm) and 1.0*1011 PFU/ml of φ6 (r=70 nm) used to estimate the size range of EV separation with the updated flow parameters. Two technical replicates of the ionophore pEV sample were analysed with absorbance measured at 280 nm and detector sensitivity at 0.001.* V_c *was set to 0.5 with a linear decay to zero within the span of 25 minutes of sample separation.* V_c *is shown as an overlay with a red line with void volume marked with* V_0 *at the start of elution. Virus standards are marked with a dashed red line and buffer baseline shown in black.*

A change in the observed sample profile was observed (figure 12). Immediately after injection, a large void volume peak containing material smaller than 25 nm in diameter was present in the fractogram. The initial peak is followed by no distinct separated subpopulations. However, from the way that the viruses are separated with these parameters, it appears that a size range from approximately 30 to 250 nm size is analysed with these parameters, corresponding to the size of small EVs. Additionally, in contrast to previous experiments, all the signals recorded from the Ca^{2+} ionophore and virus samples are well above the detection limit and clearly distinguishable from the buffer baseline.

4.3.3 AF4-MALS

After the new AF4 parameters were briefly tested (figure 12), it was deemed necessary to also re-analyse the pEVs produced with thrombin-collagen and S100A8/A9 stimulation with the new protocol. pEVs produced with S100A8/A9, thrombin-collagen and ionophore stimulation were sent sent to be kindly analysed by Dr. Roger Scherrers at Wyatt Technology with their AF4 system that also contains a multi-angle light scattering (MALS) detector in addition to a UV detector. Samples were again analysed together with a unstimulated baseline control.

Before the MALS analysis, the samples were characterized once again with a UV detector in order to see if any differences to the pEV behaviour when the AF4 method was adjusted (figure 13) according to the protocol developed by Zhang and colleagues (2018). 10 µl of ionophore-stimulated pEVs, 10 µl of each thrombin-collagen duplicate pEV samples and 50 µl of S100A8/A9 and control pEV samples were injected into the system and analysed with an online UV detector in technical replicates. Channel dimensions and the membrane used in this experiment were kept the same as the ones used in the previous AF4 experiments conducted at the Faculty of Biological and Environmental Sciences in the University of Helsinki. For this analysis, V_c gradient duration was increased to 45 minutes for longer separation, as described in the reference publication.

A marked improvement in subpopulation separation was present for all samples in the fractogram (figure 13). Characteristic peaks for pEVs from platelets stimulated with Ca^{2+} ionophore at 10-20 minutes (P1-4, figure 9) were observed again with these parameters. When V_c decay length is increased, both TC duplicates also now produce a signal with a main peak at 21 minutes and a shoulder at 25 minutes with good replicability between the two samples. Two populations are also seen in the control and S100A8/A9 samples around the same retention time at 20 and 23 minutes, even when the latter signal remains very faint due to a possibly low particle concentration. Overall, the separation power of the AF4 system is increased as V_c gradient is extended over a longer time period. To further compare the physical dimensions of the pEVs obtained with different platelet activators and Ca^{2+} ionophore MALS data was collected from the same samples to obtain additional information on the size and relative abundance of the analysed particles by measuring their R_g (figure 14).

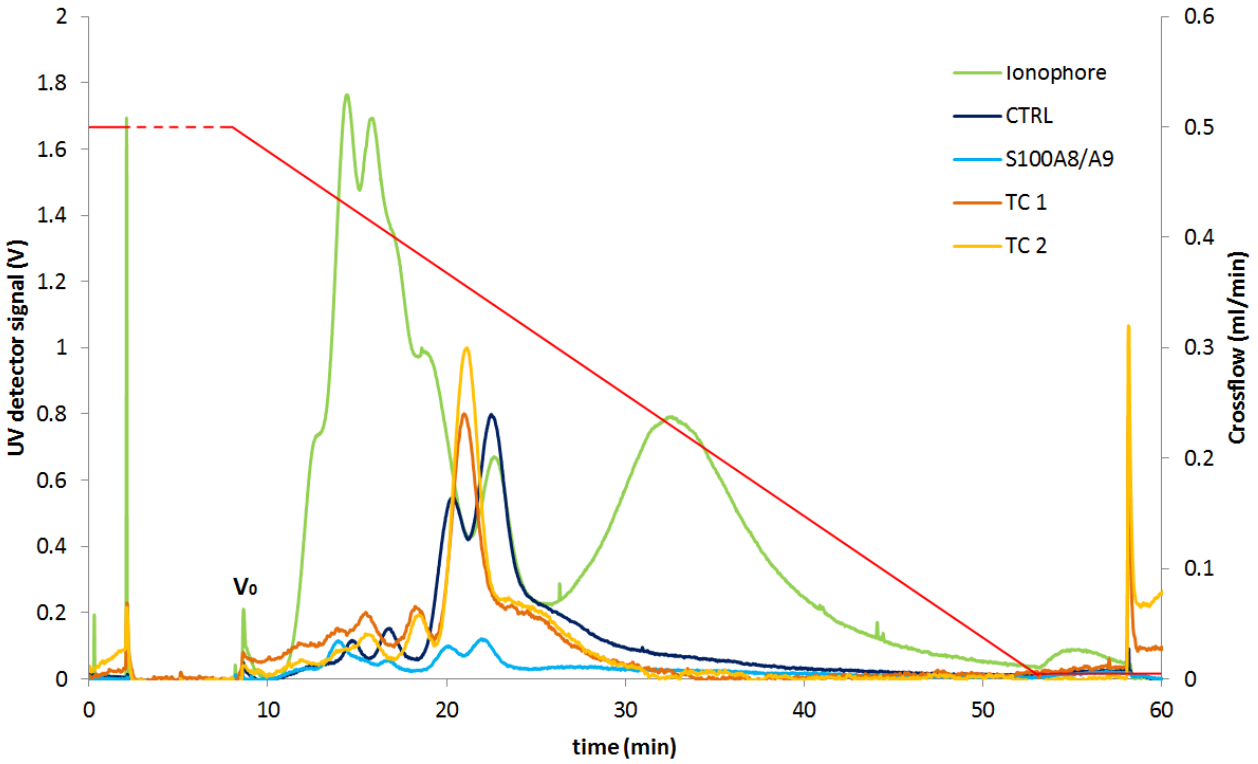

Figure 13. Characterization of TC, S100A8/A9 and Ca^{2+} ionophore pEV subpopulations with updated UV-AF4 parameters. *Platelet EVs produced with thrombin-collagen (TC) and S100A8/A9 activations were analysed with AF4 and a UV detector along with an unstimulated control (CTRL). Duplicates of the TC samples were analysed, whereas S100A8/A9, CTRL and Ionophore samples were analysed alone. 10 µl of ionophore sample, 10 µl of each TC sample and 50 µl of S100A8/A9 and CTRL samples were injected. Absorbance was measured at 280 nm. V_c was set to 0.5 ml/min with a linear decay to zero within the span of 45 minutes. V_c is shown as an overlay with a red line with void volume marked with V_0 at the start of elution. At the dashed portion of the line* V_c *was briefly dropped to 0 ml/min before resuming at 0.5 ml/min again. Two replicate runs were performed to obtain the result at Wyatt Technology GmbH, Dernbach, Germany.*

With AF4-MALS, differences between the differently produced pEVs were observed in particle retention times and subsequent R_g. pEVs obtained with thrombin and collagen activation eluted first, after which un-stimulated pEVs, Ca^{2+} ionophore and S100A8/A9–stimulated pEVs are eluted close to each other (Figure 14). The unstimulated control pEVs produced a large main preak at 34 minutes with smaller subpopulations that elute faster than the main peak at approximately 20, 24 and 28 minutes (Figure 14 B). The main particle distribution peaks for Ca^{2+} ionophore, S100A8/A9 and control all appeared after the 30 minute time point (marked in figure 13 with a grey line), and their main retention times were very similar, with a main peak at 35 minutes. The main fractions of both thrombin-collagen samples eluted before the 30 minute mark at approximately 28 minutes (figure 14 A). This observation suggested that TC co-stimulation produces pEVs with a smaller main population than those produced with the other agonists. pEVs from unstimulated platelets also produce a shoulder around the same retention time as the main peak for TC pEVs.

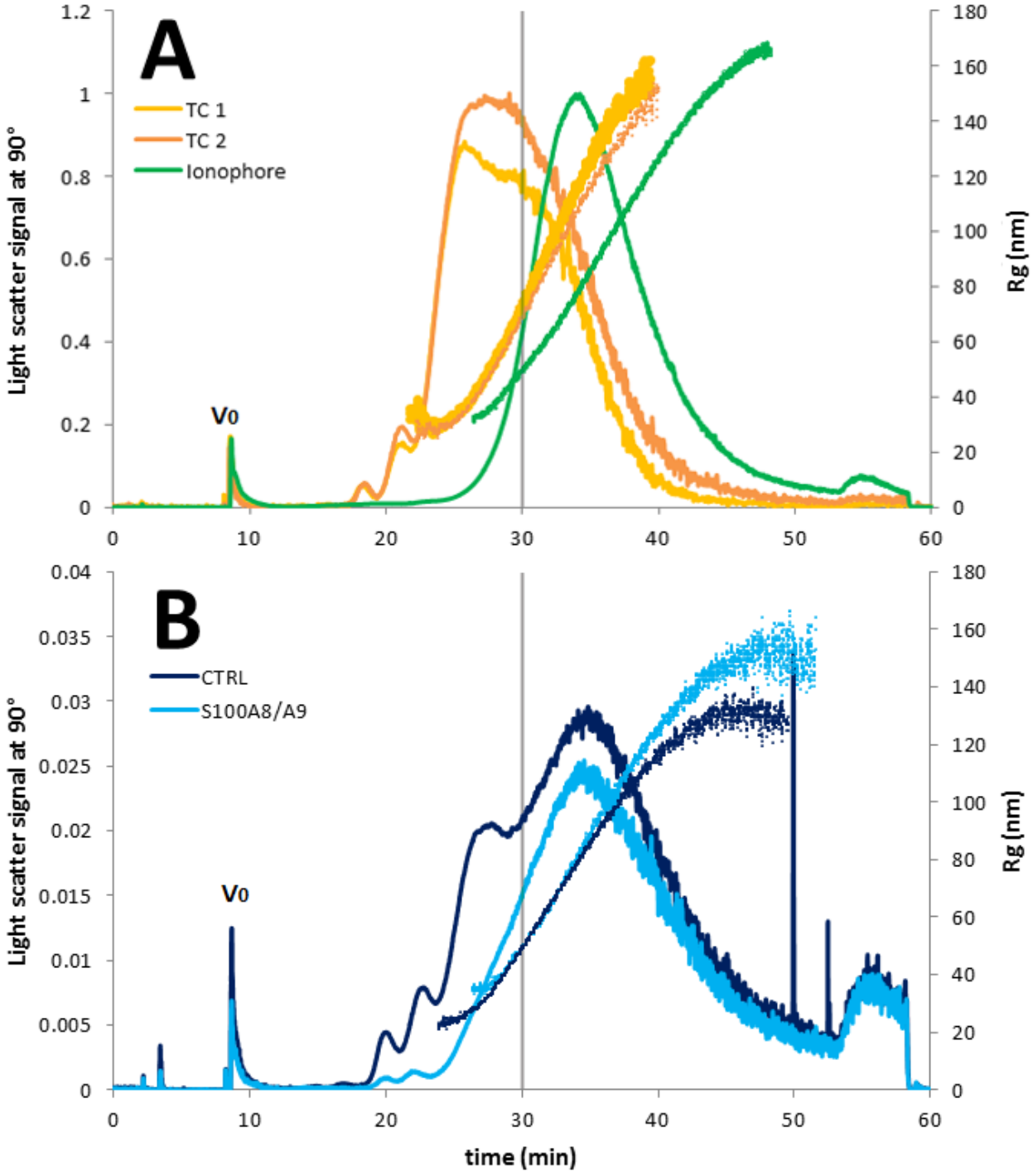

Figure 14. ***Characterization of pEV subpopulations generated with TC, S100A8/A9 and Ca^{2+} ionophore stimulation with AF4-MALS.*** *10 µl of TC 1, TC2 and ionophore pEV samples were analysed together with 50 ul of S100A8/A9 and CTRL samples with AF4-MALS equipped with a Dawn 18 angle MALS detector, mesauring light scatter at 90°. V_c was set to 0.5 ml/min with a linear decay to zero within the span of 45 minutes. TC duplicates (TC1 and TC2) and ionophore sample runs (panel A) are plotted separately from CTRL and S100A8/A9 runs (picture B) to better visualize the signal distributions for all samples despite different amounts of injected sample and the subsequent differences in signal intensity. To provide a reference point between the graphs, the 30 minute time point has been marked with a grey line. V_0 marks the beginning of elution. R_g is plotted as dots on the 2nd y-axis. Two replicate runs were performed to obtain the result at Wyatt Technology GmbH, Dernbach, Germany.*

Geometric radius was plotted on the second axis at the right hand side of the graph. R_g for both of the thrombin-collagen sample ranged from 20 nm to approximately 150 nm whereas the ionophore sample displayed a slightly larger R_g distribution between 30 and 170 nm (figure 14, panel A). pEV R_g range for S100A8/A9 stimulated platelets spread from 38 nm to 160 nm, while the unstimulated control displays a smaller range from 20 nm to 138 nm (figure 14, panel B). A vast majority of all observed particles were within the small EV size range below 200 nm.

When particle distributions were weighted with the number fraction, particles of different sizes are equally represented in the graph similarly to NTA data for easier visual comparison (figure 15 A). Differences in average R_g were observed when different activators had been used, with the unstimulated control having produced the most particles with the smallest mean size. The R_g of the pEVs obtained from unstimulated platelets was increased in pEVs from thrombin-collagen activation. Lastly, pEVs produced with S100A8/A9 and Ionophore produced the largest pEVs. Ionophore pEVs displayed the widest size R_g range (figure 15 A).

From the MALS scattering signal and the estimated R_g distribution, an estimation of the total particle concentration and geometric radius (R_r) can be calculated (figure 15 B). R_r corresponds to the R_g values measured for each sample, where control has the smallest mean geometric radius, followed by TC 1 and 2, S100A8/A9 and finally Ionophore with the largest radius, respectively. Significant sample loss is observed when the particle concentration measured by AF4-MALS and the initial concentration obtained with NTA are compared.

A

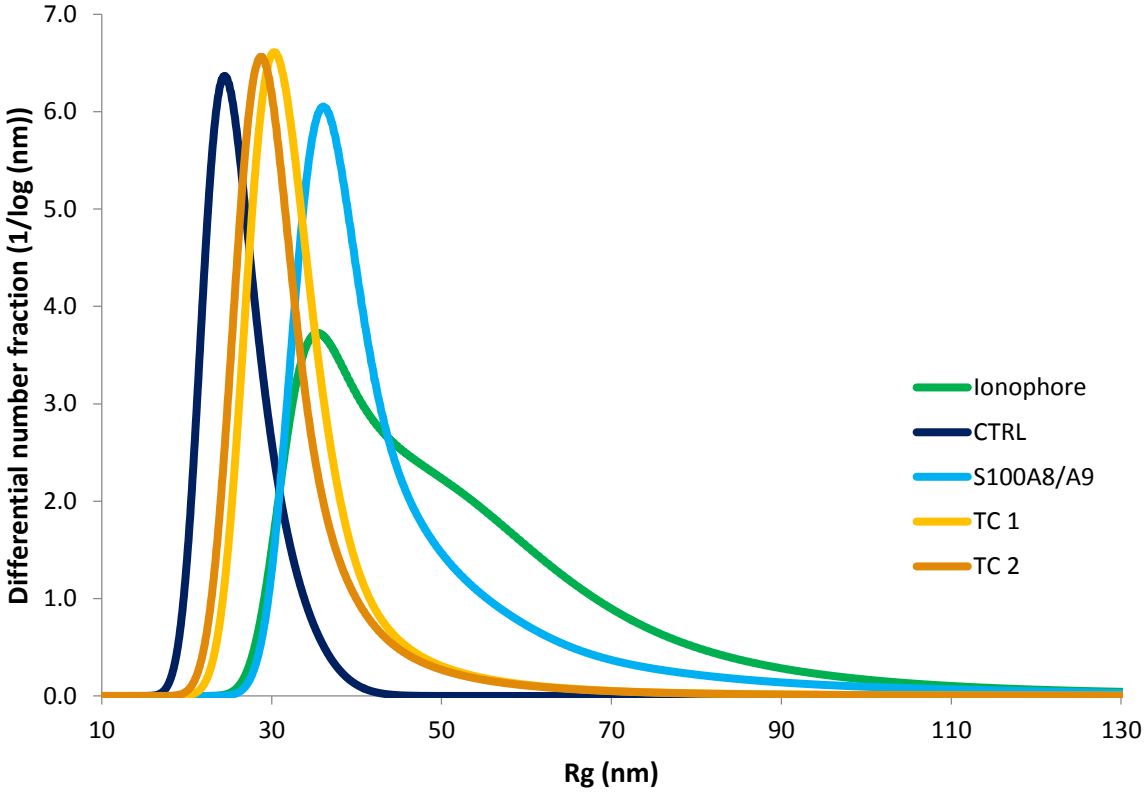

B

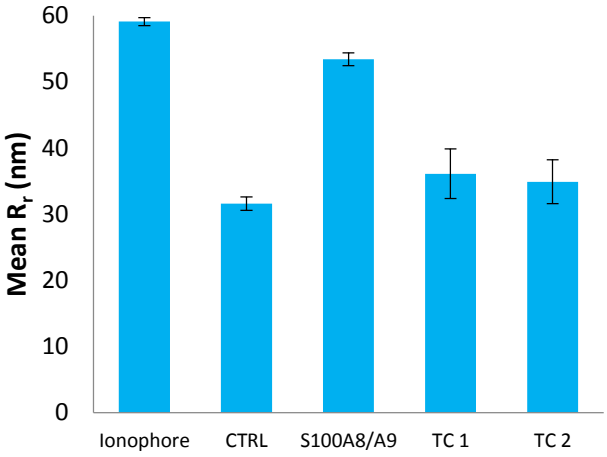

Sample	C NTA (particles/ml)	C AF4 (particles/ml)	R_r (nm)
Ionophore	$8.02*10^{12}$	$4.96*10^{9}$	59.1
CTRL	$7.63*10^{10}$	$7.80*10^{8}$	31.6
S100A8/A9	$3.83*10^{10}$	$5.28*10^{7}$	53.4
TC 1	$2.85*10^{11}$	$9.79*10^{8}$	36.1
TC 2	$3.05*10^{11}$	$1.35*10^{9}$	34.9

Figure 15. ***Total particle distribution, concentration and mean geometric radius determined with AF4-MALS. A)*** *R_g was determined for the particles analysed with AF4-MALS and plotted against the differential number fraction for the visualization of the relative abundance of particles of each size.* ***B)*** *Total particle concentration and mean R_r were determined with AF4-MALS for pEVs from Ca^{2+} ionophore, S100A8/A9, and thrombin-collagen stimulated platelets. A visual representation of the mean R_r size for each sample is shown on the left, while particle concentrations from MALS and NTA analysis are shown in the table on the right. MALS data of two runs for each sample was analysed with the Astra software tool for the Wyatt Eclipse AF4 syste by Rodger Scherrers at Wyatt Technology GmbH, Dernbach, Germany.*

4.4 Nanoimaging

In addition to AF4, nanoimaging is also an emerging method for EV characterization. The original purpose of this experiment was to stain EV markers on the surfaces of pEV subpopulation fractions obtained from preparative AF4 separation. However, as fractions could not be collected from the MALS analysis, the preparative potential of AF4 could not be investigated further. In order to separately test the novel nanoimaging thechique for pEVs, samples were imaged with the ONI Nanoimager S system. Platelets were stimulated with S100A8/A9 and thrombin-collagen and were prepared alongside a unstimulated platelet sample as previously described. The obtained pEVs were concentrated with ultrafiltration and labelled for the detection of the platelet marker CD61 that is part of the integrin αIIbβ3 complex and a fluorescent lipid dye (CMDR). Excess dye was removed with SEC and the fractions with highest concentration were pooled and immobilized on coverslips wells with poly-L-lysine for imaging.

All samples were imaged with the dSTORM technique on the ONI Nanoimager S system on two different channels (green for PE-labelled anti-CD61 and red for cell mask deep red) with laser pulses given at their respective wavelengths. Nothing could be seen in the unlabelled samples and all images came out blank (data not shown), as expected. However, out of the labelled wells on the coverslip, only the control sample had an EV concentration high enough to be imaged properly. The S100A8/A9 and TC-activated pEV samples appeared blank or nearly blank, similarly to the unlabelled controls. In other words, these samples could not produce a signal that would surpass the background noise threshold for the experiment. To further evaluate the CD61 and CMDR labelling and the degree of co-localization, the obtained image was subjected to statistical image analysis with the JACoP plugin for ImageJ software (Figure 16).

The imaging of lipid particles seems to be possible with the CMDR lipid dye. Spherical and tubular EV-like particles were imaged with CMDR staining (Figure 16 A). However, very few fluorophores were detected on the green channel for CD61-positive particles. Pearson's coefficient and Mander's coefficients were calculated for the overlapping green and red pixels (shown as yellow) to give an estimate of co-localization. Additionally, M1 and M2 coefficients were derived from the Mander's coefficient to evaluate the overlapping percentages for each dye in relation to the other's prevalence. M1 describes the amount of red pixels that are also overlapping with green pixels, whereas M2 describes the amount of green pixels that are also red. From this, one may estimate that M1 represents the amount of particles stained with CMDR that were also positive for CD61, whereas M2 represents the amount of particles stained with CD61 that were also stained with CMDR. When transformed to percentages, these values are 66.8% and 0.6% for M1 and M2, respectively. This means that 66.8% of EVs stained with CD61 were also positive for the lipid dye, but only 0.6 % of particles stained with CMDR were CD61-positive. Additionally, live imaging was also attempted with triple labelled pEVs. However, less than 4 tracks were recorded for each particle due to immediate fluorophore bleaching even when minimum laser power was used. This was not enough to achieve any meaningful analysis on particle movement and data could not be recorded (data not shown).

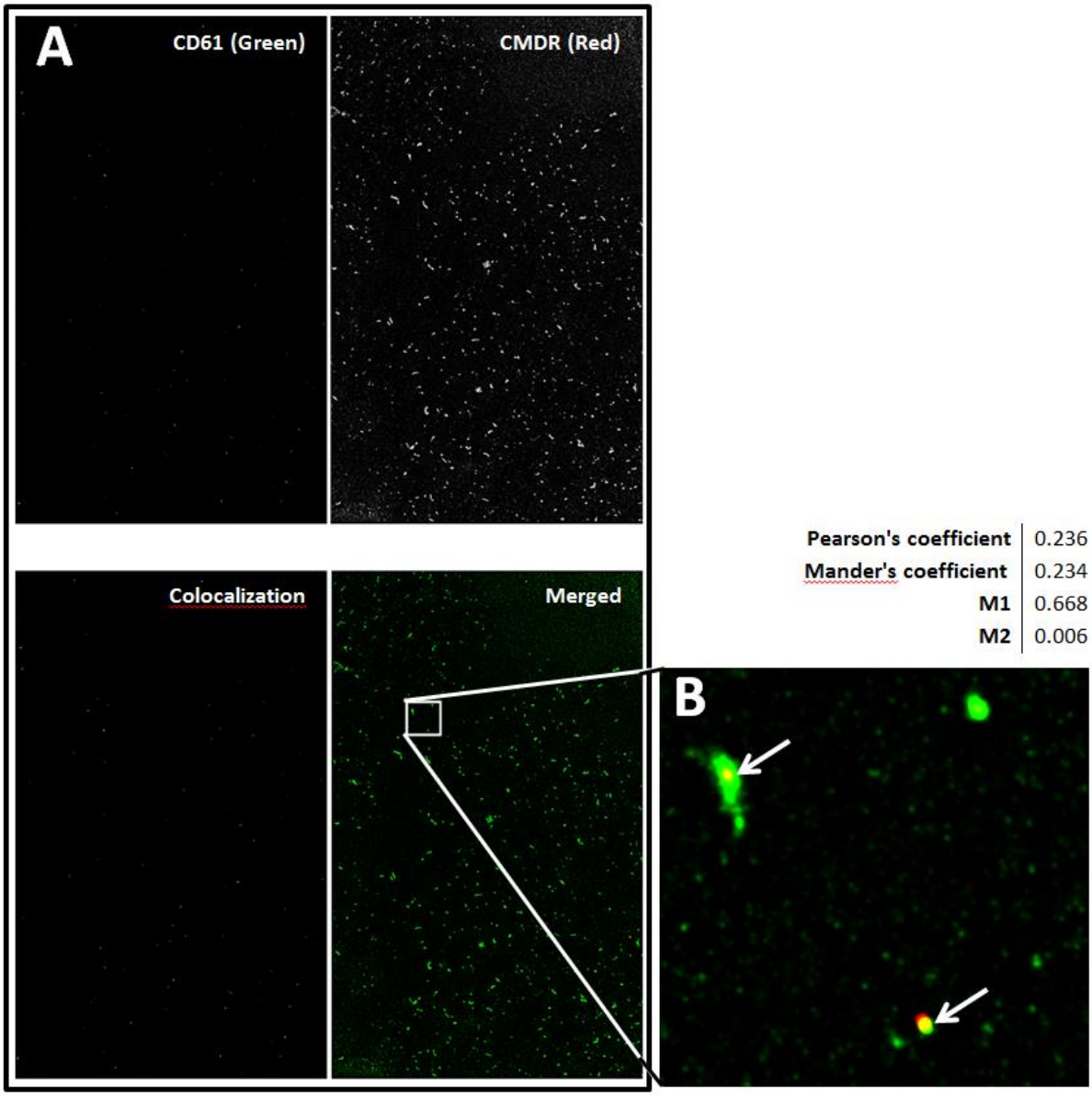

Figure 16. ***Nanoimaging and co-localization analysis of pEVs.*** *Platelet EVs were double labelled with anti-CD61-Alexa488 and Cell Mask Deep Red (CMDR) lipid dye to stain EV membrane lipids and the platelet specific marker CD61 on the EV surfaces to visualize them with the ONI Nanoimager.* ***A)*** *CD61 is visible on the green channel and CMDR on the red channel. Below them co-localization and merged images with both channels visible are shown. Pearson's and Mander's coefficients with its derivatives M1 and M2 were calculated using the JACoP plugin on the ImageJ software. Pearson's and Mander's coefficients describe the statistical significance of the co-occurrence of both red and green signals on the same pixel, whereas M1 and M2 are derived from Mander's coefficient and represent the proportion of red pixels that were also green (proportion of pixels emitting green CD61 signal that were also positive for CMDR) and vice versa (proportion of pixels stained with CMDR that were also stained with CD61), respectively.* ***B)*** *A close up of the merged image where co-localization is visible. Co-localization is shown in yellow and marked with white arrows.*

5.1 Determination of the activation state of stimulated platelets

To investigate the ability of different platelet-activating agents to generate pEVs, human platelets were stimulated with the S100A8/A9 protein and thrombin-collagen and prepared together with an unstimulated control to determine a baseline vesiculation level. Activated platelets were stained against P-selectin, TLT-1 and the fibrinogen-activated αIIbβ3 integrin complex to assess their activation state. Stained samples were analysed with nanoparticle flow cytometry. P-selectin represented a conventional marker for pEV secretion from α-granules (Gasecka *et al.,* 2019), whereas the presence of αIIbβ3 complex served as an indicator for platelet aggregation (Bennett 2005). TLT-1 was included as an additional novel marker that has ties to platelet activation through inflammation-related pathways (Schmoker *et al.,* 2020). Out of these, the components of αIIbβ3 permanently resides on platelet surfaces and is detected in its active conformation by the binding of PAC1, whereas TLT-1 and P-selectin are α-granule proteins and translocate to the surface upon platelet activation (Gasecka *et al.,* 2019, Schmoker *et al.,* 2020).

A decrease in P-selectin and TLT-1 expression was seen when unstimulated platelets were compared to ones activated with S100A8/A9, and this difference was statistically significant when incubation time is 30 or 90 minutes. Platelets lose their P-selectin decoration rapidly *in vivo* after being stimulated (Michelson *et al.,* 1996), and a drop in P-selectin level is not commonly observed in *in vitro* studies where activation stimulus is continuously present throughout the experiment (Michelson *et al.,* 1994). This suggests that platelets stimulation with S100A8/A9 could downregulate P-selectin expression on platelet surfaces as it is not likely to be caused by natural internalization. Platelet activation markers can also be either transferred to the surfaces of budding microvesicles or secreted as soluble proteins, which could also explain the decrease in P-selectin on platelet surfaces.

Additionally, no PAC1 binding was detected on the control platelets nor the ones stimulated with S100A8/A9. This confirms that platelets were also not activated through the activation of αIIbβ3 required for platelet aggregation. Considerable increase in PAC1 binding has been observed when platelets are stimulated with thrombin and collagen in similar studies in our laboratory (Palviainen *et al.*, unpublished data) and with collagen and ADP elsewhere (Morel *et al.,* 2017, Lu & Malinauskas, 2011, respectively). This suggests that our data where no αIIbβ3 formation was detected may indeed be a real observation and platelet aggregation is indeed not present in platelets stimulated by the S100A8/A9 protein. Further studies where platelet aggregation is measured with an aggregometer would confirm this finding.

TLT-1 is present in platelets in higher copy numbers than P-selectin and is upregulated and translocated to the platelet surfaces more rapidly than P-selectin (Smith *et al.,* 2018). TLT-1 is

translocated to platelet surfaces as a response to stimulation with collagen and when hemostasis is initiated through immunological stimulus (Schmoker et al 2020). Therefore TLT-1 is expected to be found on platelet surfaces when they are activated through both thrombin-collagen stimulation and potentially S100A8/A9. Therefore, even though a significant decrease in TLT-1 translocation to platelet surfaces was not present in this data, a clear abundance of TLT-1 compared to P-selectin was not seen either as would have been expected based on the literature. Therefore, it seems that S100A8/A9 may have an effect on platelet activation as shown by the low copy numbers of TLT-1 – positive platelets, but clear inhibition is not observed. A more comprehensive study with flow cytometry samples prepared in triplicates is required to confirm the platelet-inhibiting trend to investigate this claim further to obtain results that hold up when inspected for statistical significance.

5.2 The effect of different platelet activators on pEV marker profiles

To investigate the relationship between platelet activation with different agonists and pEV secretion, P-selectin and TLT-1 expression was measured on pEV surfaces with nanoparticle flow cytometry. Total pEVs secreted by platelets activated with S100A8/A9 and a mix of thrombin and collagen were isolated from the stimulated platelet samples and analyzed with flow cytometry.

A significant decrease in P-selectin expression was seen when pEVs produced with thrombin-collagen were compared to those produced with S100A8/A9. A similar change in the expression of TLT-1 was not observed when incubation time was 30 minutes. The upregulation of P-selectin expression was expected, as P-selectin is found on pEV surfaces when they are secreted by activated platelets (Heijnen *et al.,* 1999). When incubation time was increased to 180 minutes, a growing increase in TLT-1 -positive pEVs was observed when S100A8/A9 stimulated platelets were compared with unstimulated platelets. A similar difference in the expression of P-selectin was not observed. The observed upregulation of TLT-1 in the pEVs generated with S100A8/A9 stimulation is supported by the previous flow cytometry data, where differences in platelet marker profiles were seen upon S100A8/A9 stimulation. These data suggest that S100A8/A9 may act as a weak activator that mostly affects α-granule trafficking and the subsequent release of pEVs. This result adds to the growing information on interactions between S100A8/A9 and platelets and is in accordance with an earlier study where weak platelet activation was reported in the presence of S100A8/A9 (Larsen *et al.,* 2015). Additionally, earlier this year it was shown that platelets operating in an environment with elevated levels of S100A8/A9 secrete pEVs that were enriched in mRNA involved in platelet physiology and immunity (Saenz-Pipaon *et al.,* 2020). Among these mRNAs were transcripts for the S100A9 monomer (Saenz-Pipaon *et al.,* 2020), which supports our idea that the presence of S100A8/A9 gears platelets towards an immunological response where immunomodulators could be packed inside the released pEVs.

As the results were not sufficiently repeated and could have been better controlled, it is difficult to draw definite conclusions, making it hard to offer possible explanations for the differences between P-selectin and TLT-1 expression. It can, however, be speculated that the pro-inflammatory S100A8/A9 could gear platelets toward a secretory phenotype as a response to inflammation instead of platelet adhesion and aggregation. Even though both TLT-1 and P-selectin are both stored inside α-granules, TLT-1 does not completely co-localize with P-selectin in α-granules (Smith *et al.,* 2018). Indeed, it is known that different pathophysiological conditions mediated by different platelet agonists prompt the secretion of differently packed α-granule subclasses (Italiano & Battinelli, 2009). Therefore, our findings give further support to the idea of α-granule subpopulations that are differentially enriched in TLT-1 and P-selectin and are mobilized in different quantities upon platelet activation with pro-inflammatory and hemostatic stimuli. Therefore, platelets stimulated with different agonists do release different subpopulations of pEVs that may be influenced by the different α-granule subopulations as a source for cargo of pEV origin (Antwi-Baffour *et al.,* 2015). Even though it is possible that the detected TLT-1 and P-selectin positive pEVs were indeed from α-granules, pEVs enriched endocytic markers could also have been secreted directly from the platelet surface after an α-granule has fused with that specific microenvironment in the plasma membrane. However, the observed different subpopulations are likely to carry pEVs with different functions. It would be exciting to see whether a similar difference between TLT-1 and P-selectin expression is observed when platelets are stimulated with different pro-inflammatory agonists such as lipopolysaccharide (Lopes Pires *et al.,* 2917) to further investigate the possibility of differently mobilized α-granules.

The combination of the flow cytometry data from both platelet and pEV surface marker studies points towards the formulation of a new hypothesis. As it is confirmed that different agonists are able to activate platelets in different ways, it is also beneficial to use multiple activation markers to confirm the presence or absence of platelet activation. The novel S100A8/A9 agonist has ties to inflammation, whereas thrombin and collagen represent well-established activators for the initiation of platelet aggregation under conditions that mimic vascular injury. Our data shows that although both P-selectin and TLT-1 are both stored within α-granules, they are not simultaneously present on platelet or pEV surfaces in a consistent way. TLT-1 expression on platelet surfaces is observed both during platelet aggregation (Morales *et al.,* 2010) and platelet activation that is related to inflammation stimuli (Schmoker *et al.,* 2020). Therefore, stimulation through inflammation modulators such as S100A8/A9 may be seen in increased TLT-1 expression on pEV surfaces and this signal would otherwise have been missed when platelet activation were only inspected through conventional platelet activation markers such as P-selectin and PAC1.

As the observed differences between different platelet agonist point towards a possible change in α-granule mobilization and pEV secretion, it would be important to inspect all pEVs on the small EV size range. It is possible that a population of small pEVs originate from α-granules as they are enriched in α-granule proteins (Dean *et al.,* 2009). However, the same platelet may have already undergone several instances of α-granule fusion with the plasma membrane. Therefore, the TLT-1

and P-selectin positive pEVs may also originate directly from the plasma membrane where α-granule proteins were already present. Due to limitations in detection limit in the small EV size range, the flow cytometry results would have to be reproduced with a system that is able to detect the total EV population. With the current detection limit at 150 nm for the system used in this study, it is possible that a large population of small EVs were not present in this data.

5.3 The effect of platelet activators on pEV size distribution

As activator-dependent differences were observed in flow cytometry studies of platelet activation and vesiculation, we continued the characterization of pEVs produced by S100A8/A9 and a combination of thrombin and collagen. The pEVs produced with these activators were again compared to a unstimulated control and to pEVs produced through Ca^{2+} ionophore stimulation. In NTA, all samples displayed a similar size profile with a main peak around 100-130 nm, which is below the lower detection limit of nanoparticle flow cytometry. Smaller populations of large particles around 300-400 nm were also present in the sample, representing the population seen with flow cytometry. Thrombin-collagen stimulated platelets show a consistent fork around the main peak around the 100 nm region, which would be interesting to separate and investigate further for the presence of different subpopulations of small pEVs. A large majority of all particles seen with NTA were between 100 nm and 200 nm in all samples. These results are consistent with previous NTA analysis on pEVs produced with Ca^{2+} ionophore, thrombin and collagen and unstimulated platelets (Aatonen *et al.,* 2014). When overall trends in pEV sizes were compared, it was observed that unstimulated platelets and those stimulated with S100A8/A9 displayed smaller pEV size than those stimulated with Ca^{2+} ionophore or thrombin and collagen. However, it is necessary to note that a concentration of 40 particles per frame required for accurate NTA analysis was not reached in this sample batch, which may cause artefacts in statistical analysis. Lastly, the NTA as a system suffers from an inability to accurately detect particles below 70 nm (Gasecka *et al.,* 2019). Therefore, the possibility that, just like larger particle populations were present in the samples, smaller subpopulations of small EVs were also present but left undetected.

It has been shown that platelets secrete pEVs in the small EV size range (<100 nm) and that there are multiple subpopulations of small pEVs present in human plasma (Heijnen *et al.,* 1999, Multia *et al.,* 2019). This discovery was confirmed with an AF4 system set up for pEV separation in collaboration with the department of Chemistry at the University of Helsinki. Previously, AF4 was able to separate subpopulations of melanoma-derived EVs in the small EV size range (35-150 nm) (Zhang *et al.,* 2018). When Zhang and colleagues compared the separation achieved by the AF4 system to that with NTA, AF4 was able to achieve better resolution in the detection of EV subpopulations beyond the functional range of NTA. Therefore, to investigate whether different platelet agonists would produce different subpopulations of pEVs, a similar system to reliably detect small EVs below 100 nm was required for more in-depth characterization of their size profiles.

For this purpose, and AF4 system was set up at the faculty of Biological and Environmental sciences at the University of Helsinki for on-site study of pEVs. This system was equipped with a UV detector and therefore the study was later continued with the addition of a MALS detector at Wyatt Technology, Dernbach, Germany. Through method optimization based on previous AF4 parameters (Multia *et al., 2019,* Zhang *et al.,* 2018) for small EV separation and with the help of specialists at Wyatt Technology we were able to set up an AF4 method suitable for small pEV separation, where a linearly decaying V_c gradient was applied. When the system is accompanied with a UV detector, information on particle concentration and retention times can be obtained.

With an AF4 system equipped with a UV detector, very small particles were separated. Fractions around the most prominent subpopulation peaks were collected with a fraction collector and analysed with NTA to measure particle size. NTA revealed that almost no particles were present in the sample, suggesting that the fractionated peaks were contaminants. When BSA size standard was analysed with the same flow parameters, it was confirmed that proteins are eluted at the start of the run, whereas almost no particles in the EV size range were observed. A possible explanation for this finding is that EVs are simply not efficiently detected with the UV-detector. During this analysis, particles based on their absorbance at 280 nm were detected. In such measurements, a strong signal for tyrosine-containing proteins is detected which interfered with the weaker signal from EVs. Therefore, for samples rich in protein contaminants it has been suggested to measure EVs absorbance on lower wavelengths or with other methods (Jackson *et al.,* 2020).

When the same samples were analysed with a MALS detector, this protein interference is reduced and different sample size profiles are observed. The “protein peaks” are not present anymore, and possible subpopulations of small pEVs are revealed at the beginning of the analysis. From MALS scattering mean geometric radii can be calculated for each sample, the largest particles being produced with Ca^{2+} Ionophore and S100A8/A9, followed by pEVs from thrombin-and collagen stimulated platelets and lastly unstimulated platelets with mean diameters of 118.2 nm, 106.8 nm, 72.2 and 69.8 nm and 63.2 nm, respectively. The entire sample profiles fall within the small EV size range with variance between 30 and 165 nm. This is partially in accordance with NTA results, where the most particles settled around a peak at 110 nm, with Ca^{2+} Ionophore being larger than the others at approximately 130 nm. NTA results for the mean particle sizes are skewed towards larger particles, whereas the distribution obtained from AF4-MALS produces a smaller mean particle size due to the separation range of the optimized program. Simply put, both techniques provide a profile where a clear majority of all detected particles fall between 60 and 120 nm, but NTA has limitations in lower detection limit and AF4 in the upper separation limit with these particular flow parameters.

These results are similar to previously obtained results where agonist-dependent characterization of pEVs was carried out (Aatonen *et al.,* 2014). However, in the same study Ca^{2+} Ionophore was shown to produce smaller pEVs than thrombin-collagen co-stimulation and unstimulated platelets.

Yet in this study, Ca^{2+} ionophore produced larger particles than other agonists. Therefore, it is possible that Ca^{2+} ionophore may not always produce pEVs with a consistent size. In AF4-MALS, Ca^{2+} ionophore produced a uniform, bell-shaped distribution of particles, which is narrower than the particle distributions produced by other agonists. Ca^{2+} ionophore is not a physiological platelet activator and causes unspecific membrane vesiculation that produces small, protein poor and non-selectively packed EV-like particles (Hess & Siljander, 2001, Aatonen *et al.,* 2014). This distribution suggests that its nature of unspecific fragmentation of the plasma membrane extends to its effect on the resulting particle size distribution as well. Overall it can be concluded that the different activators produced pEVs with different size profiles. In the future, the reproducibility of the results should be investigated along with how they are tied to the different subpopulations of differently packed α-granules and other vesicle subtypes.

Because very small subpopulations of particles were seen at the low-end tail of the main peak for S100A8/A9- and unstimulated platelets, it is possible that weakly activated platelets secrete different small pEV subpopulations whereas strong activation creates a more homogenous population of small EVs. These vesicles were, however, close to the protein region and could be protein aggregates, lipoproteins or small lipid-poor nanoparticles called exomeres. Exomeres were discovered recently with AF4-MALS and are visible in the analysis around 30-50 nm (Zhang *et al.,* 2018).

It is noteworthy that the larger pEVs detected earlier with NTA and flow cytometry were absent from the AF4 fractograms. The flow parameters used in this study were developed to characterize particles in the small EV range in detail, and very large particles may elute in the void volume (V_0) or at the end of the run after V_c is stopped (Marioli & Kok, 2019). As sample material was seen to elute at both of these times, larger particles were not separated with our parameters. It is also possible that both V_0 and the area after separation contained protein aggregates that are too large to be separated. A residual peak after a linearly decaying V_c gradient has been shown to contain particles that had interacted with the membrane during the run and eluted abnormally when gold particles in the small EV size range were analysed with AF4 (Schmidt *et al.,* 2011). Therefore, it is not certain what kind of particles the residual peak contained in this study. Based on NTA results, where a subpopulation of larger particles was observed beyond 200 nm, it is likely that the residual peak consisted of them. In the future, fractions of these particles could be collected and their diameter measured with other methods such as NTA or electron microscopy. Large particles outside of the separation range may also elute from the channel after detection has been stopped altogether.

The aim of this project was to set up an AF4 protocol firstly for the characterization of small EVs in a way that would allow them to be collected for downstream analysis. A second aim with the AF4 setup was to investigate whether the operating range could be extended to characterize the entire pEV population produced by different agonists. Instrumental parameters such as channel size, spacer thickness, sample amount and focusing, V_c and V_{out} as well as runtime were all chosen with

these goals in mind and according to their availability in the used instruments. Good separation was achieved in the small EV size range below 200 nm. Additionally, differences in retention times and small variations in particle size profiles were observed. These differences may reflect previously undiscovered agonist-dependent differences in pEV subpopulations (Boilard & Brisson, 2015).

To modify the system to characterize the total EV population beyond just focusing on the small EV range, both V_c and V_{out} could be increased for fast separation over longer runtimes. However, even in studies where large particle ranges are claimed to have been characterized, the effective separation range in these runs is usually between 1-120 nm (Zhang *et al.,* 2018) or 1-200 nm with a runtime extended up to 70 minutes (Guyomarc'h *et al.,* 2010). If V_c gradient is extended over a longer time period, problems with peak broadening are encountered when sample retention occurs too far away from the void volume, giving poorer separation of larger particles and erroneous size estimates (Wahlund, 2013). By increasing the V_c/V_{out} ratio, better separation would be achieved, but it would come with the drawbacks of increased sample dilution and membrane-sample interactions (Kok & Qureshi, 2010, Eskelin *et al.,* 2019), which were already shown to be present in this study when no V_c was present. High V_c has also shown to cause permanent sample loss during the characterization of yeast microsomes between 20-200 nm (Giddings & Caldwell, 1984). If V_c is increased, the V_{out} can be adjusted to achieve a desired compromise between resolution and runtime (Kok & Qureshi, 2010). When sample amounts are small, like in the case of pEVs produced with limited amounts of S100A8/A9 which was able to only weakly induce pEV formation, sample dilution might become a serious limitation for particle detection. When sample availability is a major concern and the objective of the analysis is analytical rather than preparative, the use of a thinner channel spacer or a smaller channel may be applied to counter these problems (Kok & Qureshi, 2010).

Overall, for the purpose particle characterization and sample retrieval for further analysis with limited starting material, a lower V_c may be required when AF4 is used for EV separation as is proposed in this thesis. AF4 is a sensitive and versatile method for the separation of biological membrane-enclosed particles of a large size range. Viruses (Eskelin *et al.,* 2019), exomeres and exosomes (Zhang *et al.,* 2018), small pEVs (Multia *et al.,* 2019) and larger particles up to entire cell organelles several hundreds of nanometers in size (Yang *et al.,* 2015) have been separated with AF4, encompassing the entire EV size range from small EVs to apoptotic bodies. However, due to necessary compromises between sample recovery, detection and accurate characterization for both large and small particles, their simultaneous characterization in a single run may not a viable strategy. Therefore, for sensitive characterization of EV subpopulations, separate parameters and separate runs are the best tactic for the characterization of unknown polydisperse EV populations with a broad size range. A protocol for sensitive separation of small pEVs for their fractionation and downstream analysis is presented here. The instrumentation could be further complimented with a DLS detector to obtain the shape factor of the analysed particles together with a fraction

collector. This way EV fractions identified with AF4-MALS could be collected and pooled for downstream analysis of their surface markers or cargo with different omics techniques.

5.4 Nanoimaging as a method for pEV detection and characterization

Nanoimaging is an emerging technique that had not been previously set up at the Faculty of Biological and Environmental Sciences in the University of Helsinki for EV characterization and co-localization studies. The co-localization of pEV marker CD61 and CMDR can reveal information on the origin of pEVs. Due to the fact that almost all particles that absorbed the lipid dye were not positive for CD61, it is possible that the samples were not “pure” pEVs free of contaminants. An excess of lipid dye may also be due to aggegates of dye being indistinguishable from actual particles, despite the removal of unbound dye from the sample with SEC. Still, 66.8% of EVs stained with CD61 were also positive for the lipid dye. The P-value for the co-localization of fluorophores is 0.236, which indicates slight co-localization when P = 0 indicates no co-localization, P = 1 indicates perfect co-localization and P = -1 indicates negative correlation. From the work conducted in this study it appears that at least part of the particles isolated were pEVs, because there was some co-localization of a pEV marker and a lipid marker. However, this is not considered sufficient proof according to the newest guidelines (Théry et al 2018) that demand at least the confirmation of 3 markers, one of which is a cytosolic marker. Total pEV cargo could be analysed with proteomic techniques such as mass spectrometry or the presence of single markers verified with western blotting (for further list of methods, refer to table II - Conventional and emerging techniques in EV detection and characterization). However, if correctly optimized, dSTORM imaging can be a tool for future characterization of EV markers and their localization on EV surfaces, as shown previously by Chen and colleagueEV surface markers can be characterized s (Chen *et al.,* 2016). With an AF4 system equipped with a fraction collector, EVs could be separated, pooled and concentrated, and then further characterized with optimized dSTORM imaging as the preliminary results of this work demonstrate. Further optimization of the staining method will still be required for the imaging of multiple markers at the same time to avoid a scenario where bright and abundant signal is obstructing that from markers that are present in lower quantities.

Live imaging of stained particles comparable to NTA was not possible to perform in this study due to immediate bleaching of all tested fluorophores even when minimal laser power was employed. This was an unfortunate drawback, as a functional live imaging method similar to NTA would be able to provide information regarding particle size and concentration of pEVs generated with S100A8/A9 in comparison to other agonists. This would also allow for the simultaneous recording of different fluorescent markers on EV surfaces.As hopefully demonstrated in this thesis, a need for such a technique is great. To obtain similar information on EV samples, multiple techniques such as conventional NTA and dSTORM imaging must be employed. Other EV techniques that track the Brownian movement of particles together with their zeta potential are simultaneously able to estimate size and concentration as well as surface composition (Jamaludin *et al.,* 2019). In addition to further optimization of dSTORM imaging, they deserve further investigation.

6. FINAL CONCLUSIONS

Despite the promise of EVs in diagnostics, therapeutics and as sign posts towards biological insight, the young research field suffers from a lack of standardized techniques for their isolation and characterization. The new methods employed in this work – albeit not yet perfectly optimized – were advantageous in comparison to other approaches such as the use of NTA and nanoparticle flow cytometry. These latter methods have previously been used for the characterization of activator-dependent differences in pEV subpopulations, but difficulties in the precise isolation and characterization of pEV populations with potential subtle differences wre reported (Aatonen *et al.,* 2014). Later, it was shown that such subtle differences do exist within small pEVs below 100 nm, and they could be detected with AF4-MALS (Multia *et al.,* 2019). AF4 offers a gentle and tunable alternative for pEV characterization and is sensitive enough to separate small particle contaminants from possible pEV populations as shown in this study. The preparative potential of AF4 warrants further investigation, offering a less labor-intensive solution to a persisting problem with subpopulation loss during UC or a fast alternative for EV separation with SEC.

In this project several different new analysis methods and markers were used in conjunction with more conventional methods in an ambitious attempt to create a new procedure through which pEVs can be studied in a more complete fashion. AF4 and dSTORM imaging have not previously been used for EV study in our laboratory and both represent emerging methods in the global EV field. Here, they have been performed in conjunction with conventional NTA and nanoparticle flow-cytometry to obtain novel information the way platelets respond to different platelet agonists. The use of the emerging platelet activation marker, TLT-1, along with the other more widely used markers such as P-Selectin allowed for a much greater depth of analysis than with just a single marker, a critical advantage when studying novel, previously uncharacterized activators such as S100A8/A9. Through the use of these markers, a difference in the distribution of TLT-1 and P-selectin on platelet and pEV surfaces was discovered when the pro-inflammatory S100A8/A9 was used as a platelet agonist. This finding supports recent discovery that TLT-1 and P-selectin reside in differently packed α-granules (Larsen *et al.,* 2015) and platelet activation in conditions that mimic inflammation and hemostasis may affect their mobilization through different mechanisms. The small pEV populations secreted by platelets activated with thrombin-collagen and S100A8/A9 stimulation had different size profiles where the pEVs produced with S100A8/A9 stimulation were clearly larger. This study therefore confirmed previous understanding that platelets react differently to different agonists by producing different pEVs, and sometimes the difference in activation may be only detected in the pEV population. This study also highlighted the importance of the use of multiple and variable platelet activation markers for the studied agonist, as seen in the disparity of TLT-1 and P-selectin positive pEVs.

However, the study was not without its drawbacks, and the significant ambition of the study, using both novel proteins and processes, combined with restrictions in available equipment, meant that

certain issues could not be overcome during the period of this work. Limited resources with respect to AF4 instrumentation - especially the fact that the AF4 fraction collector and MALS detector were not available in the same place - presented the greatest issue making our original intention of obtaining fractionated pEVs impossible. To further develop the pipeline for fast EV enrichment and collection for downstream applications, a fraction collector combined with AF4-MALS is needed to confirm the suitability of the system for preparative EV studies. The further addition of a DLS detector to the system would provide data on the molecular weight and shape factor of the analyzed particles, making it possible to identify populations of protein contaminants and to obtain information on the shape and fullness of the analyzed EVs. With the lack of the use of conventional UC or SEC for pEV enrichment in this project is very likely that the EV samples were contaminated to some extent with lipoproteins, protein aggregates and debris from other blood cells. The presence of contamination was implicated by UV-AF4 and was suspected to be present based on results from dSTORM imaging where only a negligible population of the imaged lipid particles carried the pEV marker CD61 on their surfaces. However, further optimization of particle staining is required to assess the usefulness of dSTORM imaging for pEV research, as it currently requires large amounts of starting materials for anything to be imaged and suffers for the obstruction of weaker signals with more abundant ones. Material limitations are also a recurring problem in EV applications and therefore methods that demand high concentrations of EVs are generally labour-intensive and impractical.

Material limitations also provided further issues - best described with the volume of S100A8/A9 produced for the study. As each sample was created individually prior to this study within a narrow experimentation window, it was difficult to tell if lack of pEV production was due to real biological phenomena or just simply because a sub-optimal concentration of the agonist was used. As the highest tested concentration of the S100A8/A9 protein was determined by the availability of the protein, it is possible that higher concentrations would have produced more pEVs. For the sake of transparency, it has to be noted that occasionally the fact that the results were not statistically significant was also compounded by relative inexperience of the operator with the novel methods and equipment. A further limitation of this study is that the presence of contaminating blood cells was not excluded after alleged platelet isolation and the presence of pEVs was not confirmed. A good way to improve and expand the study in the future would be to repeat the flow cytometry experiment and to screen the effect of more platelet activators and activation markers related to platelet immunity responses.

Despite having clear shortcomings in regard to optimization, verification of results and lack of appropriate instrumentation, the combination of novel and industry standard methods allowed us to push the boundaries of convention in the field. This project tackled the hurdle of “climbing the mountain” of method development in order to reach the “valley” of novel biological understanding. We succeeded in providing new hints towards meaningful discoveries in platelet biology by characterizing the way platelets respond to inflammatory and hemostatic signals by shedding pEVs. We also tested novel methods to detect subtle differences in small EV population

sizes that are easily missed with conventional methods due to their technical limitations. These results extend their usefulness beyond just pEV research and can serve as reference for the separation and characterization of the heterogeneity of other EV types as a part of a collective effort to propel the field past methodological difficulties. Reliable methods in EV enrichment and characterization are necessary to tap into their true potential in diagnostics and therapeutics and will ultimately expand our knowledge in the fundamentals of how cells communicate and exchange biological material with each other.

7. ACKNOWLEDGEMENTS

From the bottom of my heart, I would like to thank my supervisors Pia Siljander and Mari Palviainen for taking me under your wing and letting me embark on this journey of lifelong learning with you. Thank you for introducing me to the hidden world of EVs and the versatility of platelets. Thank you, Pia, for the long chats about daring to put on the tin foil hat and go look for that which is not yet understood. Thank you, Mari, for being a pillar of calm support that I could always lean on in the lab. I am forever grateful for your guidance and patience and cannot wait for the years to come.

I would like to extend my thanks to Dr. Katri Eskelin for teaching me the secrets of AF4 and sharing her knowledge on the method optimisation. I also want thank Dr. Roger Scherrers for helping us individualise the AF4 method for our pEV samples and for taking the time to measure them on my behalf. Thank you everyone at Wyatt Technology for letting us use your cutting-edge instrumentation. I also thank Dr. Junichiro Futami for donating the plasmid for the expression of the S100A8/A9 construct used extensively in this project.

I also want to thank everyone in EV-Group for welcoming me into your team when I knew nothing about EVs and had nothing to bring but my enthusiasm and endless patience for protein purification. I will always remember your help, scientific insight and the laughs we shared when days in the lab turned into nights. Thank you Kata, Maija, KeKe, Sami, Zeynep, Iida and Rosabella for letting me learn by your side.

Finally, I want to thank my family, friends and my wonderful partner for encouraging me in my success and for holding my hand when I felt lost. Thank you everyone at Viikki-speksi, for providing a space where self-discovery and creativity will forever flourish. I thank the daring adventurers Johannes, Essi, Tero, Henrik, Otso, Elviira, Nick, Heli and Pontus for welcoming me at their table for exciting sessions of Dungeons & Dragons. You all inspire me in my ventures, both in the realms of imagination and the adventures of our daily lives.

8. REFERENCES

Ambrosio, A. L., & Di Pietro, S. M. (2017). Storage pool diseases illuminate platelet dense granule biogenesis. *Platelets*, 28(2), 138-146.

Arraud N., Linares R., Tan S., Gounou C., Pasquet J.-M., Mornet .S, Brisson A.R. (2014). Extracellular vesicles from blood plasma: determination of their morphology, size, phenotype and concentration. *Journal of Thrombosis and Haemostasis,* 12(5),614–27.

Atri, L. & Schattner, M. (2017). Platelet toll-like receptors in thromboinflammation. *Frontiers in bioscience (Landmark edition).* 22, 1867-1883.

Battinelli, E. M. & Loscalzo, J. (2020) Normal Mechanisms of Vascular Hemostasis. In (Ed.) Beckman, J. A., Creager, M. A. & Loscalzo, J. *Vascular medicine: A companion to Braunwald's heart disease.* (*3rd edition*., pp. 64-69). Elsevier.

Bennett J. S. (2005). Structure and function of the platelet integrin alphaIIbbeta3. *The Journal of clinical investigation*, 115(12), 3363–3369.

Boilard, E., Duchez, A. C., & Brisson, A. (2015). The diversity of platelet microparticles. Current opinion in hematology, 22(5), 437–444.

Boudreau L. H., Duchez A. C., Cloutier N., Soulet D., Martin N., Bollinger J., Paré A., Rousseau M., Naika G. S., Lévesque T., Laflamme C., Marcoux G., Lambeau G., Farndale R.W., Pouliot M., Hamzeh-Cognasse H., Cognasse F., Garraud O., Nigrovic P. A., Guderley H., Lacroix S., Thibault L., Semple J. W., Gelb M. H., Boilard E. (2014). Platelets release mitochondria serving as substrate for bactericidal group IIA-secreted phospholipase A2 to promote inflammation. *Blood*. 124(14),2173-83.

Brennan, K., Martin, K., Fitz, Gerald, S. P., O'Sullivan, J., Wu, Y., Blanco, A., Richardson, C., & Mc Gee, M. M. (2020). A comparison of methods for the isolation and separation of extracellular vesicles from protein and lipid particles in human serum. *Scientific reports*, 10(1), 1039.

Böing, A. N., van der Pol, E., Grootemaat, A. E., Coumans, F. A., Sturk, A., & Nieuwland, R. (2014). Single-step isolation of extracellular vesicles by size-exclusion chromatography. Journal of extracellular vesicles, 3, 10.3402/jev.v3.23430.

Castaman, G., Yu-Feng, L., & Rodeghiero, F. (1996). A bleeding disorder characterised by isolated deficiency of platelet microvesicle generation. *Lancet*, 347(9002),700–701.

Chargaff, E. & West, R. (1946). The biological significance of the thromboplastic protein of blood. *Journal of biological Chemistry*, 166, 189-97

Chen C, Zong S, Wang Z, Lu J, Zhu D, Zhang Y, Cui Y, (2016). Imaging and Intracellular Tracking of Cancer-Derived Exosomes Using Single-Molecule Localization-Based Super-Resolution Microscope. *ACS Applied Materials & Interfaces* 8(39),25825-25833.

Coumans F. A. W., Brisson A. R.,Buzas E. I. ,Dignat-George F., Drees E. E. E., El-Andaloussi S., Emanueli C., Gasecka A., Hendrix A., Hill A. F., Lacroix R., Lee Y., van Leeuwen T. G., Mackman N., Mager I., Nolan J. P., van der Pol E., Pegtel D. M., Sahoo S., Siljander P. R. M., Sturk G., de Wever

O., Nieuwland R. (2017). Methodological guidelines to study extracellular vesicles. *Circulation Research.* 120,1632–48.

de Witt, S. M., Swieringa, F., Cavill, R., Lamers, M. M., van Kruchten, R., Mastenbroek, T., Baaten, C., Coort, S., Pugh, N., Schulz, A., Scharrer, I., Jurk, K., Zieger, B., Clemetson, K. J., Farndale, R. W., Heemskerk, J. W., & Cosemans, J. M. (2014). Identification of platelet function defects by multi-parameter assessment of thrombus formation. *Nature communications,* 5, 4257.

Dean W. L. , Lee M. J., Cummins T. D., Schultz D. J., Powell D. W. (2009). Proteomic and functional characterisation of platelet microparti- cle size classes. *Thrombosis and Haemostasis*, 102,711–718.

Dovizio, M., Bruno, A., Contursi, A., Grande, R., & Patrignani, P. (2018). Platelets and extracellular vesicles in cancer: diagnostic and therapeutic implications. *Cancer metastasis reviews*, 37(2-3), 455–467.

Ed Rainger, G., Chimen, M., Harrison, M. J., Yates, C. M., Harrison, P., Watson, S. P., Lordkipanidzé, M., & Nash, G. B. (2015). The role of platelets in the recruitment of leukocytes during vascular disease. *Platelets,* 26(6), 507–520.

Eskelin, K., Lampi, M., Meier, F., Moldenhauer, E., Bamford, D. H., & Oksanen, H. M. (2016). Asymmetric flow field flow fractionation methods for virus purification. *Journal of chromatography*. 1469:108–119.

Garcia, B. A., Smalley, D. M., Cho, H., Shabanowitz, J., Ley, K., & Hunt, D. F. (2005). The platelet microparticle proteome. *Journal of proteome research*, 4(5):1516–1521.

Giebel, B., & Helmbrecht, C. (2017). Methods to Analyze EVs. *Methods in molecular biology*. 1545:1–20.

Gould, S. J., & Raposo, G. (2013). As we wait: coping with an imperfect nomenclature for extracellular vesicles. Journal of extracellular vesicles, 2, 10.3402/jev.v2i0.20389.

Guo, S., Tao, S., Yin, W., Qi, X., Yuan, T. & Zhang, C. (2017). Exosomes derived from platelet-rich plasma promote the re-epithelization of chronic cutaneous wounds via activation of YAP in a diabetic rat model. *Theranostics*, 7(1), p. 81-96.

Guyomarc'h F., Violleau F., Surel O., Famelart M. H. (2010). Characterization of heat-induced changes in skim milk using asymmetrical flow field-flow fractionation coupled with multiangle laser light scattering. *Journal of Agricultural and Food Chemistry*. 58(24), 12592-12601.

Hess, M. W., & Siljander, P. R. M. (2001). Procoagulant platelet balloons: evidence from cryopreparation and electron microscopy. *Histochemistry and cell biology*, 115(5), 439–443.

Hugel B., Socié G., Vu T., Toti F., Gluckman E., Freyssinet J. M., Scrobohaci M. L. (1999). Elevated levels of circulating procoagulant microparticles in patients with paroxysmal nocturnal hemoglobinuria and aplastic anemia. *Blood* 93,3451–3456.

Italiano J. E. Jr., Battinelli E. M. (2009). Selective sorting of alpha-granule proteins. *Journal of Thrombosis and Haemostasis.* 7(Suppl 1),173-176.

Jackson, K. K., Powell, R. R., Bruce, T. F., & Marcus, R. K. (2020). Solid-phase extraction of exosomes from diverse matrices via a polyester capillary-channeled polymer (C-CP) fiber stationary phase in a spin-down tip format. *Analytical and bioanalytical chemistry,* 10.1007/s00216-020-02728-z. [Advance online publication]

Jamaludin, N. A., Thurston, L. M., Witek, K. J., Meikle, A., Basatvat, S., Elliott, S., Hunt, S., Andronowska, A., & Fazeli, A. (2019). Efficient isolation, biophysical characterisation and molecular composition of extracellular vesicles secreted by primary and immortalised cells of reproductive origin. *Theriogenology*, 135, 121–137.

Kalluri, R., & LeBleu, V. S. (2020). The biology, function, and biomedical applications of exosomes. *Science*. 367(6478):eaau6977.

Koupenova, M., Clancy, L., Corkrey, H. A., & Freedman, J. E. (2018). Circulating Platelets as Mediators of Immunity, Inflammation, and Thrombosis. *Circulation research*, 122(2), 337–351.

Kreimer, S., Belov, A. M., Ghiran, I., Murthy, S. K., Frank, D. A., & Ivanov, A. R. (2015). Mass-spectrometry-based molecular characterization of extracellular vesicles: lipidomics and proteomics. Journal of proteome research, 14(6), 2367–2384.

Lannan, K. L., Sahler, J., Kim, N., Spinelli, S. L., Maggirwar, S. B., Garraud, O., Cognasse, F., Blumberg, N., & Phipps, R. P. (2015). Breaking the mold: transcription factors in the anucleate platelet and platelet-derived microparticles. *Frontiers in immunology,* 6, 48.

Larsen, S. B., Grove, E. L., Pareek, M., Kristensen, S. D., & Hvas, A. M. (2015). Calprotectin and platelet aggregation in patients with stable coronary artery disease. PloS one, 10(5), e0125992.

Lood C., Tydén H., Gullstrand B., Jönsen A., Källberg E., Mörgelin M., Kahn R., Gunnarsson I., Leanderson T., Ivars F., Svenungsson E., Bengtsson A. A.. (2016). Platelet-Derived S100A8/A9 and Cardiovascular Disease in Systemic Lupus Erythematosus. *Arthritis & Rheumatology*. 68(8), 1970-80.

Lopez E., Srivastava A. K., Burchfield J., Wang Y.-W., Cardenas J. C., Togarrati P. P., Miyazawa B., Gonzalez E., Holcomb J. B., Pati S. & Wade C. E., (2019). Platelet-derived- Extracellular Vesicles Promote Hemostasis and Prevent the Development of Hemorrhagic Shock. *Scientific Reports.* 9, 17676.

Lopes Pires, M. E., Clarke, S. R., Marcondes, S., & Gibbins, J. M. (2017). Lipopolysaccharide potentiates platelet responses via toll-like receptor 4-stimulated Akt-Erk-PLA2 signalling. PloS one, 12(11), e0186981.

Lu, Q., & Malinauskas, R. A. (2011). Comparison of two platelet activation markers using flow cytometry after in vitro shear stress exposure of whole human blood. *Artificial organs*, 35(2), 137–144.

Machlus, K. R., & Italiano, J. E., Jr (2013). The incredible journey: From megakaryocyte development to platelet formation. *The Journal of cell biology*, 201(6), 785–796.

Marioli, M., & Kok, W. T. (2019). Recovery, overloading, and protein interactions in asymmetrical flow field-flow fractionation. *Analytical and bioanalytical chemistry,* 411(11), 2327–2338.

Michelson, A. D., Barnard, M. R., Hechtman, H. B., MacGregor, H., Connolly, R. J., Loscalzo, J., & Valeri, C. R. (1996). In vivo tracking of platelets: circulating degranulated platelets rapidly lose surface P-selectin but continue to circulate and function. *Proceedings of the National Academy of Sciences of the United States of America*, 93(21), 11877–11882.

Michelson, A. D., Benoit, S. E., Kroll, M. H., Li, J. M., Rohrer, M. J., Kestin, A. S., & Barnard, M. R. (1994). The activation-induced decrease in the platelet surface expression of the glycoprotein Ib-IX complex is reversible. *Blood*, 83(12), 3562–3573.

Momen-Heravi, F., Balaj, L., Alian, S., Mantel, P. Y., Halleck, A. E., Trachtenberg, A. J., Soria, C. E., Oquin, S., Bonebreak, C. M., Saracoglu, E., Skog, J., & Kuo, W. P. (2013). Current methods for the isolation of extracellular vesicles. Biological chemistry, 394(10), 1253–1262.

Momen-Heravi, F., Getting, S. J., & Moschos, S. A. (2018). Extracellular vesicles and their nucleic acids for biomarker discovery. Pharmacology & therapeutics, 192, 170–187.

Moore BW, McGregor D. (1965) Chromatographic and electrophoretic fractionation of soluble proteins of brain and liver. *Journal of Biological Chemistry*. 240(1647),53–60.

Morel, A., Rywaniak, J., Bijak, M., Miller, E., Niwald, M., & Saluk, J. (2017). Flow cytometric analysis reveals the high levels of platelet activation parameters in circulation of multiple sclerosis patients. *Molecular and cellular biochemistry,* 430(1-2), 69–80.

Panagopoulou, M. S., Wark, A. W., Birch, D., & Gregory, C. D. (2020). Phenotypic analysis of extracellular vesicles: a review on the applications of fluorescence. *Journal of extracellular vesicles*. 9(1),1710020.

Plé, H., Landry, P., Benham, A., Coarfa, C., Gunaratne, P. H., & Provost, P. (2012). The repertoire and features of human platelet microRNAs. *PloS One*, 7(12):1.

Primavera R., Barbacane R., Congia M., Locatelli M. & Celia C. (2014). Laser diffraction and light scattering techniques for the analysis of food matrices. *Biomed International – Advances In Food Safety And Health*. 6: 40-60.

Raposo, G., & Stahl, P. D. (2019). Extracellular vesicles: a new communication paradigm?. Nature reviews. Molecular cell biology, 20(9), 509–510.

Rondina, M. & Zimmerman, G. (2019). The Role of Platelets in Inflammation. In (Ed.) Michaelson A. D., Cattaneo M., Frelinger A. L. & Newman P. J. *Platelets* (4th edition) pp. 505-522. Academic Press.

Sadallah, S., Eken, C., Martin, P. J., & Schifferli, J. A. (2011). Microparticles (ectosomes) shed by stored human platelets downregulate macrophages and modify the development of dendritic cells. Journal of immunology. 186(11), 6543–6552.

Saenz-Pipaon, G., San Martín, P., Planell, N., Maillo, A., Ravassa, S., Vilas-Zornoza, A., Martinez-Aguilar, E., Rodriguez, J. A., Alameda, D., Lara-Astiaso, D., Prosper, F., Paramo, J. A., Orbe, J., Gomez-Cabrero, D., & Roncal, C. (2020). Functional and transcriptomic analysis of extracellular vesicles identifies calprotectin as a new prognostic marker in peripheral arterial disease (PAD). *Journal of extracellular vesicles*, 9(1), 1729646.

Satta N, Toti F, Fressinaud E, Meyer D, Freyssinet JM. Scott syndrome: an inherited defect of the procoagulant activity of platelets. *Platelets*. 8(2-3),117-24

Scharf RE. (2018) Platelet Signaling in Primary Haemostasis and Arterial Thrombus Formation: Part 1. *Hamostaseologie*. 38(4), 203-210.

Schmidt, B., Loeschner, K., Hadrup, N., Mortensen, A., Sloth, J. J., Koch, C. B., & Larsen, E. H. (2011). Quantitative characterization of gold nanoparticles by field-flow fractionation coupled online with light scattering detection and inductively coupled plasma mass spectrometry. *Analytical chemistry*, 83(7), 2461–2468.

Schmoker, A. M., Perez Pearson, L. M., Cruz, C., Colon Flores, L. G., Branfeild, S., Pagán Torres, F. D., Fonseca, K., Cantres, Y. M., Salgado Ramirez, C. A., Melendez, L. M., Ballif, B. A., & Washington, A. V. (2020). Defining the TLT-1 interactome from resting and activated human platelets. *Journal of proteomics*, 215, 103638.

Selvadurai, M. V. & Hamilton, J. R. (2018). Structure and function of the open canalicular system - the platelet's specialized internal membrane network. *Platelets*, 29(4), 319-325.

Semple, J., Italiano, J. & Freedman, J. (2011) Platelets and the immune continuum. *Nature Reviews Immunology,* 11(4),264–274.

Semple, J. & Kapur, R. (2020). Platelet immunology from the inside out. *ISBT Science Series.* 0, 1–5

Shabani F, Farasat A, Mahdavi M, Gheibi N. (2018) Calprotectin (S100A8/S100A9): a key protein between inflammation and cancer. *Inflammation Research*. 67(10), 801-812.

Shao, H., Im, H., Castro, C. M., Breakefield, X., Weissleder, R., & Lee, H. (2018). New Technologies for Analysis of Extracellular Vesicles. Chemical reviews, 118(4), 1917–1950.

Swieringa, F., Spronk, H. M. H., Heemskerk, J. W. M. & van der Meijden, P. E. J. (2018). Integrating platelet and coagulation activation in fibrin clot formation. *Research and Practice in Thrombosis and Haemostasis*. 2, 450–460.

Théry, C., Witwer, K. W., Aikawa, E., Alcaraz, M. J., Anderson, J. D., Andriantsitohaina, R., Antoniou, A., Arab, T., Archer, F., Atkin-Smith, G. K., Ayre, D. C., Bach, J. M., Bachurski, D., Baharvand, H., Balaj, L., Baldacchino, S., Bauer, N. N., Baxter, A. A., Bebawy, M., Beckham, C., … Zuba-Surma, E. K. (2018). Minimal information for studies of extracellular vesicles 2018 (MISEV2018): a position statement of the International Society for Extracellular Vesicles and update of the MISEV2014 guidelines. *Journal of extracellular vesicles*, 7(1), 1535750.

Tomaiuolo, M., Brass, L. F., & Stalker, T. J. (2017). Regulation of Platelet Activation and Coagulation and Its Role in Vascular Injury and Arterial Thrombosis. Interventional cardiology clinics, 6(1), 1–12.

van der Meijden, P & Heemskerk, J. (2018). Platelet biology and functions: new concepts and clinical perspectives. *Nature Reviews Cardiology*. 16(3),1.

Vasina EM, Cauwenberghs S, Feijge MA, Heemskerk JW, Weber C, Koenen RR. (2011) Microparticles from apoptotic platelets promote resident macrophage differentiation. *Cell Death and Disease*. 2(9),e211.

Villa, F., Quarto, R., & Tasso, R. (2019). Extracellular vesicles as natural, safe and efficient drug delivery systems. Pharmaceutics, 11(11), 10.3390/pharmaceutics11110557. doi:E557

Vogl, T., Gharibyan, A. L., & Morozova-Roche, L. A. (2012). Pro-inflammatory S100A8 and S100A9 proteins: self-assembly into multifunctional native and amyloid complexes. *International journal of molecular sciences*, 13(3), 2893–2917.

Wei, H., Malcor, J.M. & Harper, M.T. (2018). Lipid rafts are essential for release of phosphatidylserine-exposing extracellular vesicles from platelets. *Scientific Reports.* 8, 9987.

Wahlund K. G. (2013). Flow field-flow fractionation: critical overview. *Journal of Chromatography*. 1287, 97–112.

Wahlund, K. G., & Giddings, J. C. (1987). Properties of an asymmetrical flow field-flow fractionation channel having one permeable wall. *Analytical chemistry*, 59(9), 1332–1339.

Yáñez-Mó, M., Siljander, P. R., Andreu, Z., Zavec, A. B., Borràs, F. E., Buzas, E. I., Buzas, K., Casal, E., Cappello, F., Carvalho, J., Colás, E., Cordeiro-da Silva, A., Fais, S., Falcon-Perez, J. M., Ghobrial, I. M., Giebel, B., Gimona, M., Graner, M., Gursel, I., Gursel, M., … De Wever, O. (2015). Biological properties of extracellular vesicles and their physiological functions. Journal of extracellular vesicles, 4, 27066. Yang, J. S., Lee, J. Y., & Moon, M. H. (2015). High Speed Size Sorting of Subcellular Organelles by Flow Field-Flow Fractionation. Analytical chemistry, 87(12), 6342–6348.

Chen, Y., Yuan, Y., & Li, W. (2018). Sorting machineries: how platelet-dense granules differ from α-granules. *Bioscience reports*, 38(5), BSR20180458.

Zaldivia, M., McFadyen, J. D., Lim, B., Wang, X., & Peter, K. (2017). Platelet-Derived Microvesicles in Cardiovascular Diseases. *Frontiers in cardiovascular medicine*, 4, 74.

Zhang, S., Axtell, R. C., Ju, S., Mu, J., Zhang, L., Steinman, L., Miller, D., & Zhang, H. G. (2011). Treatment of brain inflammatory diseases by delivering exosome encapsulated anti-inflammatory drugs from the nasal region to the brain. Molecular therapy : the journal of the American Society of Gene Therapy, 19(10), 1769–1779.

Zwaal, R. F., & Schroit, A. J. (1997). Pathophysiologic implications of membrane phospholipid asymmetry in blood cells. Blood, 89(4), 1121–1132.

S.1 Assesment of S100A8/A9 purity.

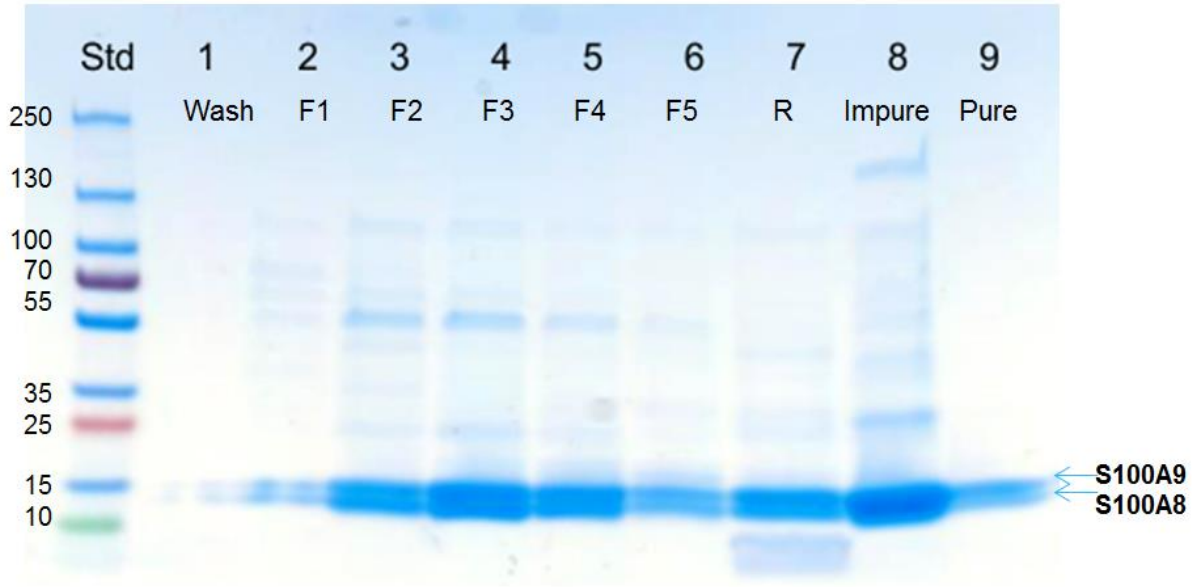

Supplemental figure S1. ***Assessment of S100A8/A9 protein purity for platelet activation with SDS-PAGE.*** *S100A8/A9 dimer was purified with cation exchange chromatography in a 0.5 M stepwise gradient ranging from 0.15 M to 6 M NaCl. The best fractions that contained the most protein with the least contaminants were selected, pooled and purified again with the same column with elution at 0.2 M NaCl (fractions F1-F5). Lane 8 represents a protein fraction that was only purified once as impure control. Lane 1 represents washing of the column with buffer after protein binding to the matrix whereas lane 7 shows the fraction that was removed from the column after regeneration with 1M NaCl. Lane 9 contains the final purified fraction of S100A8/A9 which was chosen for platelet activation experiments presented in this thesis. The pure fraction has undergone two IEX purification cycles and ultrafiltration with a 30 kDa cutoff membrane at 4000 RPM for 60 minutes to remove contaminants. Both the A8 (11 kDa) and A9 (13 kDa) monomers were detected on the gel in equal proportions. Commercial 4-20% Biorad Mini-PROTEAN TGX stain free gel was used for the separation of proteins with 170V and 400 mA current for 30 minutes, after which the gel was stained with 20 ml of PageBlue for 1h 45 min and destained 2 x with 100 ml of MQ water.*

S2. Gating of flow cytometry experiments.

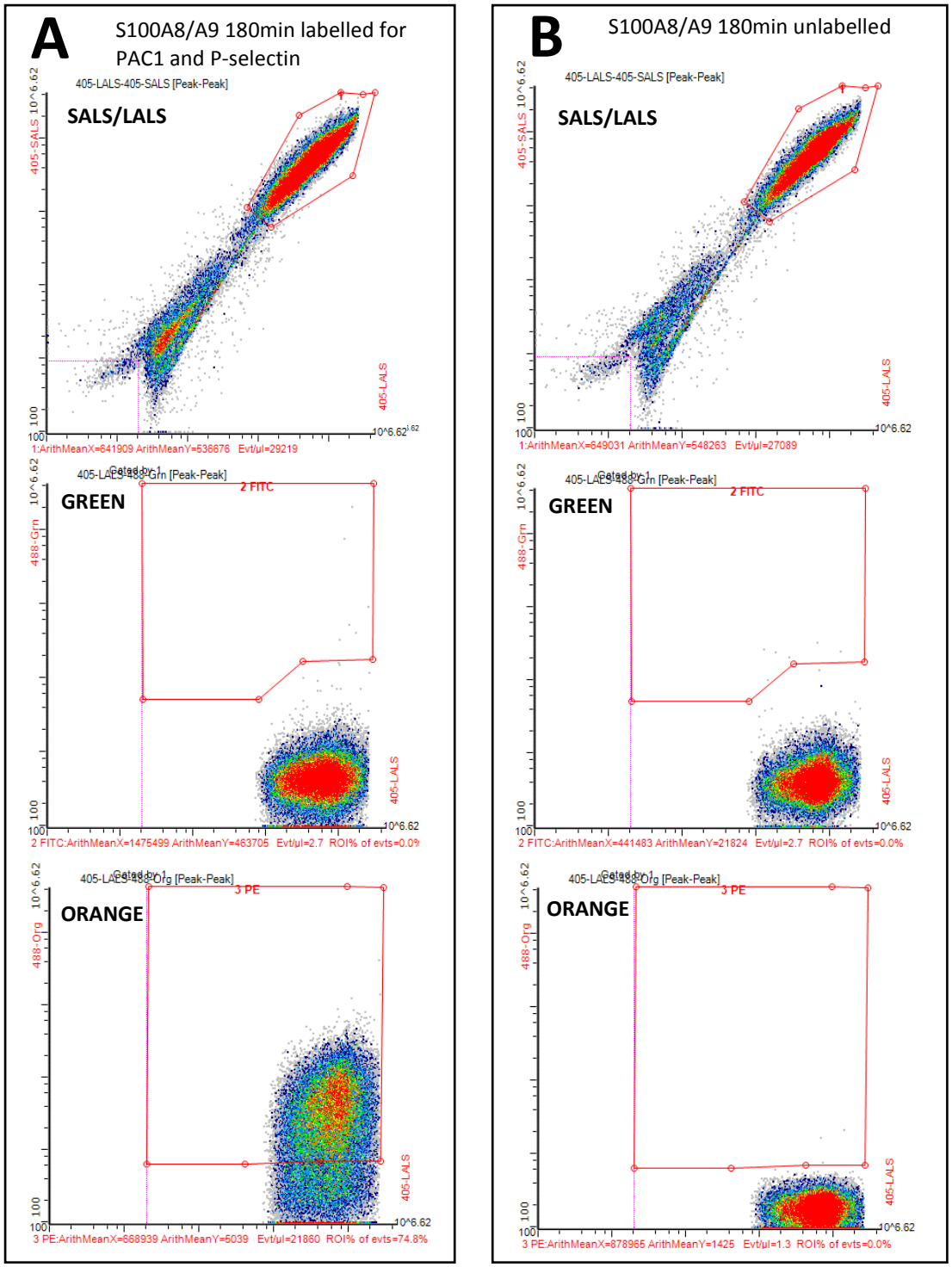

Supplemental figure S2. ***Typical representation of flow cytometry scattergrams from the assessment of platelet activation with the Apogee A50 Micro Flow Cytometer system.*** *Total platelet population is represented as SALS vs LALS scatter signal intensity and gated for all observed platelets. LALS signal was further filtered to capture fluorescence in the green and orange wavelengths and gated for PAC1 and P-Selectin, respectively. Samples that were typical representations of scatter signal data for this batch were chosen for this supplement for A) S100A8/A9 180 minute activation labelled with P-Selectin-PE and PAC1-FITC and B) an unlabelled control for the same activation.*

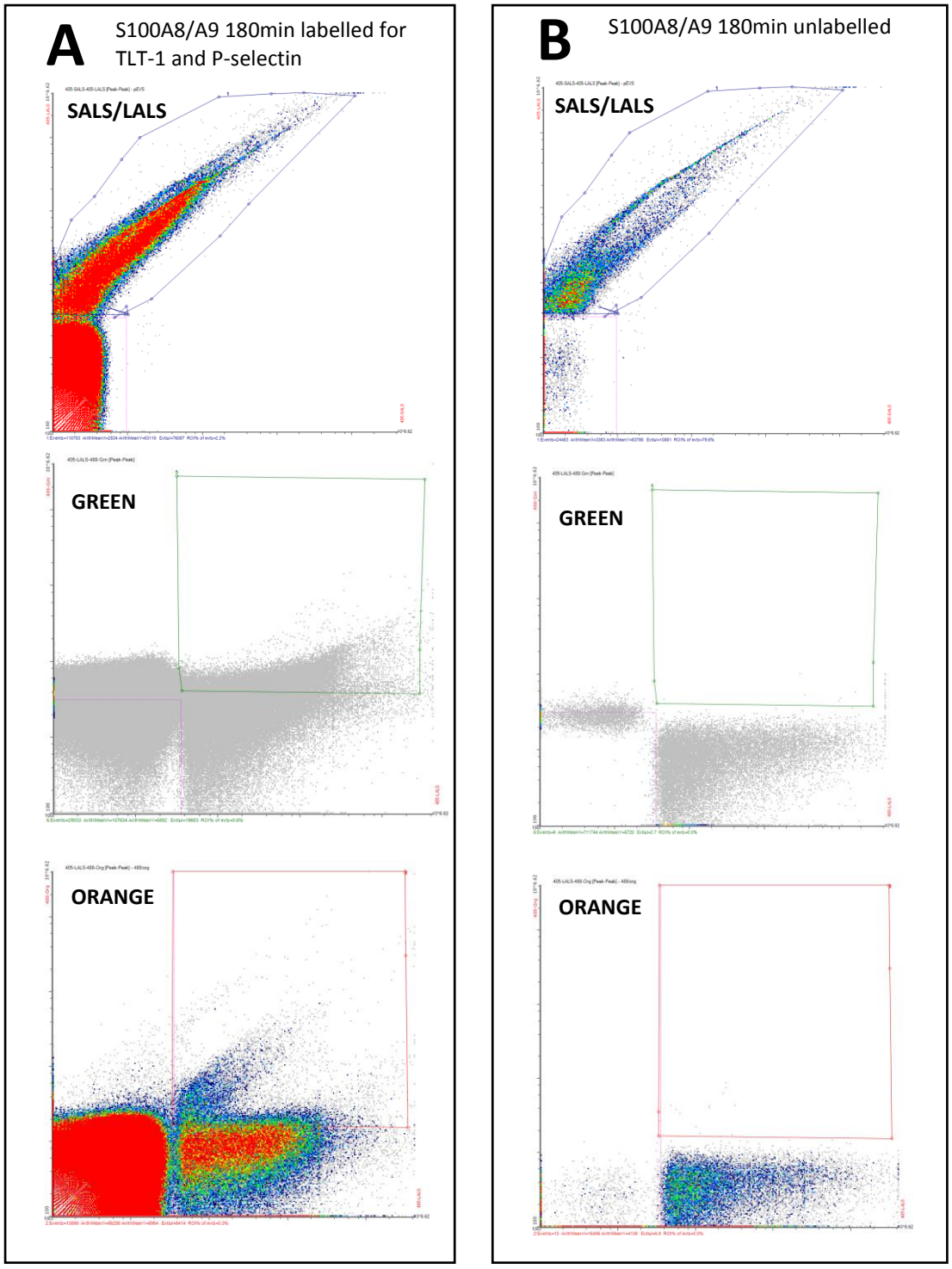

Supplemental figure S3. ***Typical representation of flow cytometry scattergrams from the assessment of pEV marker profiles with the Apogee A50 Micro Flow Cytometer system.*** *Total pEV population is represented as SALS vs LALS scatter signal intensity and gated for all observed pEVs. LALS signal was filtered for green and orange wavelengths and gated for TLT-1 and P-Selectin, respectively. Samples that were typical representations of scatter signal data for this batch were chosen for this supplement for A) S100A8/A9 180 minute activation labelled with P-Selectin-PE and TLT-1-Alexa-488 and B) an unlabelled control for the same activation.*